Identification of Novel Inhibitors of the Amino Acid Transporter B^0AT1 (SLC6A19), a Potential Target to Induce Protein Restriction and to Treat Type 2 Diabetes

By

QI CHENG

Australian National University

A thesis submitted for the degree of Doctor of Philosophy of The Australian National University

May, 2018

AUTHOR'S DECLARATION

The results presented in this thesis are, except where explicitly acknowledged, the original work of the author. I certify that the substance of this thesis has not previously been, or is currently being submitted for any other degree or diploma.

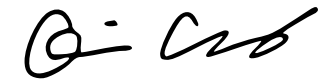

Qi Cheng (Author)

06/Mar/2019

Date

ACKNOWLEDGEMENTS

First and foremost, I would like to give my sincere thanks to my supervisor, Prof. Stefan Bröer, for his great support on my PhD research over the past four years. Stefan is always very kind to offer his help and provide his idea on my research plan, experimental design, and trouble shooting. I very much appreciate all the effort he has put into my PhD project and all the encouragements he has given to me. I would also like to thank my panels, A/Prof. Ben Corry and A/Prof. Kevin Saliba, for their helpful suggestions on my research proposals and plans.

I really had a wonderful time with everyone in Broer's Lab during my PhD. I would like to deeply thank Angelika Bröer, not only for her patience in guiding me in my experiments and teaching me those critical laboratory skills, but also for her huge support in my most difficult times. This compound screening project is based on a large-scale virtual screening done by Nishank Shah, who was co-authored with me to make our work published in a peer-reviewed journal. Many thanks to Yang Jiang and Kiran Javed for their help in mouse experiments. Kiran has also provided me with lots of help and suggestions on the GC-MS analysis based on her experience, which I really appreciate. I am also thankful for the help from Dr Steven Fairweather in my experiments on Xenopus oocytes. I would also like to thank Dr Emrah Tumer, Weidong Jing, Gregory Gauthier-Coles, and Aditya Yadav for their suggestions on my project.

Last, but definitely not the least, I would like to give a big thank you to my parents, for their love and support in my study and my life. I would like to thank my partner, Jianqun Gao, in particular. Without your accompanying and support, I wouldn't be where I am today.

This research is supported by an Australian Government Research Training Program (RTP) Scholarship.

ABSTRACT

Apical broad-spectrum neutral (0) amino acid transporter B^0AT1 (encoded by the SLC6A19 gene) is mainly expressed in small intestine and kidney, mediating the transport of all neutral amino acids in a Na^+-dependent manner. Its ancillary proteins, carboxypeptidase angiotensin-converting enzyme 2 (ACE2) and the homolog collectrin (TMEM27, transmembrane protein 27), are critical for the surface expression and catalytic transport function in small intestine and kidney, respectively. Slc6a19 nullizygous mice have improved insulin sensitivity and show reduced weight gain on a HFD (high fat diet) compared to wild-type mice. Moreover, reduced insulin secretion could protect β-cells from endoplasmic reticulum (ER) stress and long-term failure in insulin secretion. Hence, pharmacological inhibition of B^0AT1 using chemical compounds could lead to new drugs to treat type 2 diabetes (T2DM) and its related metabolic disorders. A CHO (Chinese Hamster Ovary) - based cell line was generated, stably expressing B^0AT1 and collectrin with the aid of a Flp-In™ transfection system. Using this cell line, a high-throughput screening (HTS) assay was developed, which uses a fluorescent dye to detect depolarisation of the cell membrane during amino acid uptake via B^0AT1. A radio-labelled substrate uptake assay was used to determine the potency (IC_{50}) and mechanism (competitive or non-competitive) of inhibition, as well as the specificity of B^0AT1 inhibitors. Potential novel inhibitors were derived from three sources, first commercially available substrate analogues, second medium-scale virtual screening, and third high-throughput screening of chemical libraries. Selected inhibitors were further tested in in-vitro (*Xenopus laevis* oocytes), ex-vivo (mouse small intestine) and in-vivo (C57BL/6NCrl wild-type mice) systems. I characterised a series of novel inhibitors of the B^0AT1 transporter in more detail. Benztropine (NSC63912) was identified as a competitive inhibitor showing an IC_{50} of 44±9μM; whereas 2-benzyl-1-(3-phenylpropyl)piperidine (NSC22789) was identified as a non-competitive inhibitor with an IC_{50} of 90±21μM. These two compounds were selective with regard to related transporters (system L, ASCT2), and they blocked substrate (leucine) uptake in both *Xenopus* oocytes overexpressing B^0AT1 and collectrin, and inverted mouse small intestine. Two more potent B^0AT1 inhibitors with IC_{50} below 10μM were further identified from the HTS of a small molecule compound library. The tools established in this study can be widely used to identify new transport inhibitors. Using these tools we were able to identify compounds that can be used to study epithelial transporters or be developed further through medicinal chemistry.

CONTENTS

LIST OF FIGURES

LIST OF TABLES

ABBREVIATIONS

ACE2	angiotensin-converting enzyme 2
ANG-2	Asante NaTRIUM Green-2
APN	aminopeptidase N/CD13
B^0AT1	broad-spectrum neutral (0) amino acid transporter 1
BCAAs	branched-chain amino acids
CHO	Chinese Hamster Ovarian
FGF21	fibroblast growth factor 21
FLIPR	Fluorescent (Fluorometric) Imaging Plate Reader
FRT	Flp Recombination Target
GCN2	general control non-derepressible 2
GIP	gastric inhibitory polypeptide
GLP-1	glucagon-like peptide 1
HTS	high-throughput screening
IR	insulin resistance
mTORC1	mammalian target of rapamycin complex 1
T2DM	type 2 diabetes mellitus
TMEM27	transmembrane protein 27, also known as collectrin

Chapter 1: General Introduction

1.1 The role of amino acids in the development of insulin resistance and type 2 diabetes; the benefits of protein restriction to improve metabolic health

Type 2 diabetes mellitus (T2DM) was formerly known as non-insulin-dependent diabetes mellitus (NIDDM), a disorder in which there is a chronically elevated blood glucose concentration resulting from both insufficient insulin secretion and insulin resistance (IR) usually associated with obesity. It is the main type of diabetes mellitus since it accounts for 90-95% of all diabetics, particularly in adultsDeshpande, Harris-Hayes [1]. Due to its acute and chronic complications such as cardiovascular disease and stroke, it results in increased morbidity and mortality and thus places a heavy burden on society. Obesity caused by over-nutrition and/or lack of physical activity is a key risk factor in the development of IR, which consequently causes increased demand for insulin. The majority of individuals with IR can remain normoglyceamic in the early stage due to a compensatory increase in insulin secretion supported by an increase in β-cell mass and function. However, such compensation may fail due to a progressive decrease in β-cell mass and function, ultimately resulting in T2DM [2].

Elevated levels of neutral amino acids, especially branched-chain amino acids (BCAAs), have been reported to be linked to the development of IR or even T2DM [3]. It was reported that in a Chinese and Asian-Indian male population, IR was correlated with increased levels of alanine, proline, valine, leucine/isoleucine, phenylalanine, tyrosine, glutamate/glutamine and ornithine. These changes were not due to increased protein intake [4]. Similar in an American population, five branched-chain and aromatic amino acids had highly-significant associations with future diabetes, namely isoleucine, leucine, valine, tyrosine, and phenylalanine. Meanwhile, a combination of three amino acids (isoleucine, phenylalanine, tyrosine) were found to be good predictors of future diabetes, suggesting that amino acid profiles could help in diabetes risk assessment [5]. Therefore, significant efforts have been made to understand how these amino acids affect the metabolic balance in our bodies.

The mammalian target of rapamycin complex 1 (mTORC1) signalling pathway is the most widely-studied and well-known amino acid sensing pathway, regulating protein translation through the phosphorylation and activation of mTORC1's downstream target p70S6 kinase (p60S6K) and 4E-binding protein 1 (4E-BP1) [6-11]. This signalling pathway also regulates autophagy through the interaction between mTORC1 and the ulk1 (UNC51-like kinase 1)/atg13 (autophagy 13)/FIP200 (focal adhesion kinase-interacting protein 200kDa) complex [12]. In general, when amino acids become abundant, mTORC1 is recruited to the lysosomal

surface where it is activated by Ras homologue enriched in brain (Rheb) to enhance protein biosynthesis, while under amino acid depletion, the inactive mTORC1 is dispersed throughout the cytoplasm, leading to the progressively increased association between mTORC1 and ulk1 complex to induce protein degradation; thus, this amino acid sensing pathway is critical for maintaining cellular amino acid homeostasis [12, 13]. The general control non-derepressable 2 (GCN2)/activating transcription factor 4 (ATF4) pathway is activated in addition to the suppression of mTORC1 signalling during amino acid restriction. Unlike the mTORC1-dependent sensing of amino acids, the protein kinase GCN2 is stimulated by binding to uncharged tRNAs, which are accumulated during amino acid restriction. The upregulation of the GCN2/ATF4 pathway results in a reduction of global translation through phosphorylation of the eukaryotic initiation factor 2α (eIF2α) and an increase of the intracellular amino acid pool by promoting amino acid biosynthesis and/or transport [12]. In addition to the mTORC1- and GCN2- dependent signalling pathways, G protein-coupled receptors (GPCRs) and the Cxcl10 transcriptional/Dusp16 posttranscriptional responses were reported to be involved in sensing of amino acid excess and limitation, respectively [14]. However, their molecular mechanisms still remain to be elucidated [14]. Systemic amino acid homeostasis is also tightly modulated in a mTORC1-dependent manner. Elevated levels of circulating amino acids after food intake contribute to the release of insulin, which in turn up-regulates the transport of amino acids, particularly BCAAs, into muscles where they incorporate into proteins through the activation of mTORC1 and its downstream targets p70S6K and 4E-BP1 as mentioned above. Meanwhile, insulin itself is also capable of stimulating mTORC1 by binding to and activating insulin receptor substrate proteins to trigger a signalling cascade of PI3K (phosphoinositide 3-kinase) /PKB (protein kinase B)/mTORC1. Muscle protein can be degraded to refill the amino acid pool during fasting [12]. The amino acid sensing pathways are summarized in figure 1.1. The understanding of amino acid sensing pathways under physiological conditions is essential to understand why BCAAs correlate with IR or T2DM, and different mechanisms have been suggested. Previous studies have provided evidence that insulin responses are attenuated due to BCAA-mediated mTORC1 activation (see review [15]). However, the causative role of BCAAs has been challenged by another work [15]. For example, middle-aged mice showed a dissociation between mTORC1 activation and change of insulin sensitivity after feeding with BCAAs for 3 months [16]. As a result, BCAAs may rather be considered biomarkers or predictors for IR or T2DM, than the cause of the disease [3]. Currently, a more widely accepted hypothesis invokes mitochondrial dysfunction in pancreatic β-cells and stress signalling, caused by the accumulation of toxic metabolites resulting from BCAA dysmetabolism

(branched chain α-keto acids and branched chain acyl-coenzyme A), as the mechanism underlying IR [17].

Caloric restriction protects against age-related diseases in a wide range of species, although to a variable extent. Restriction of protein showed the best protective effects compared to the restriction of carbohydrates and fat [14]. Restriction of the intake of proteins or of specific amino acids (e.g. tryptophan, methionine) proved to be beneficial to the extension of lifespan and healthspan in rodent models, as well as being associated with lower risks of cancer, obesity, insulin resistance, diabetes, cardiovascular disease and overall mortality in humans [18, 19]. Furthermore, low-protein diet proved to be beneficial for kidney function in diabetic nephropathy [20]. On the contrary, when providing mice with high-protein diets, even with restriction on total calorie intake, there was no beneficial effect on lifespan, which correlated with the activation of hepatic mTORC1 signalling by elevated circulating levels of BCAAs [21]. In contrast to long-term activation, short-term activation of mTORC1 protects against insulin resistance, because it up-regulates the secretion of satiety hormone leptin in brain, leading to a decrease in food intake [22]. However, the persistent hyperactivation of mTORC1 can be harmful for health by inducing endoplasmic reticulum (ER) stress due to enhanced protein translation [15, 23-29].

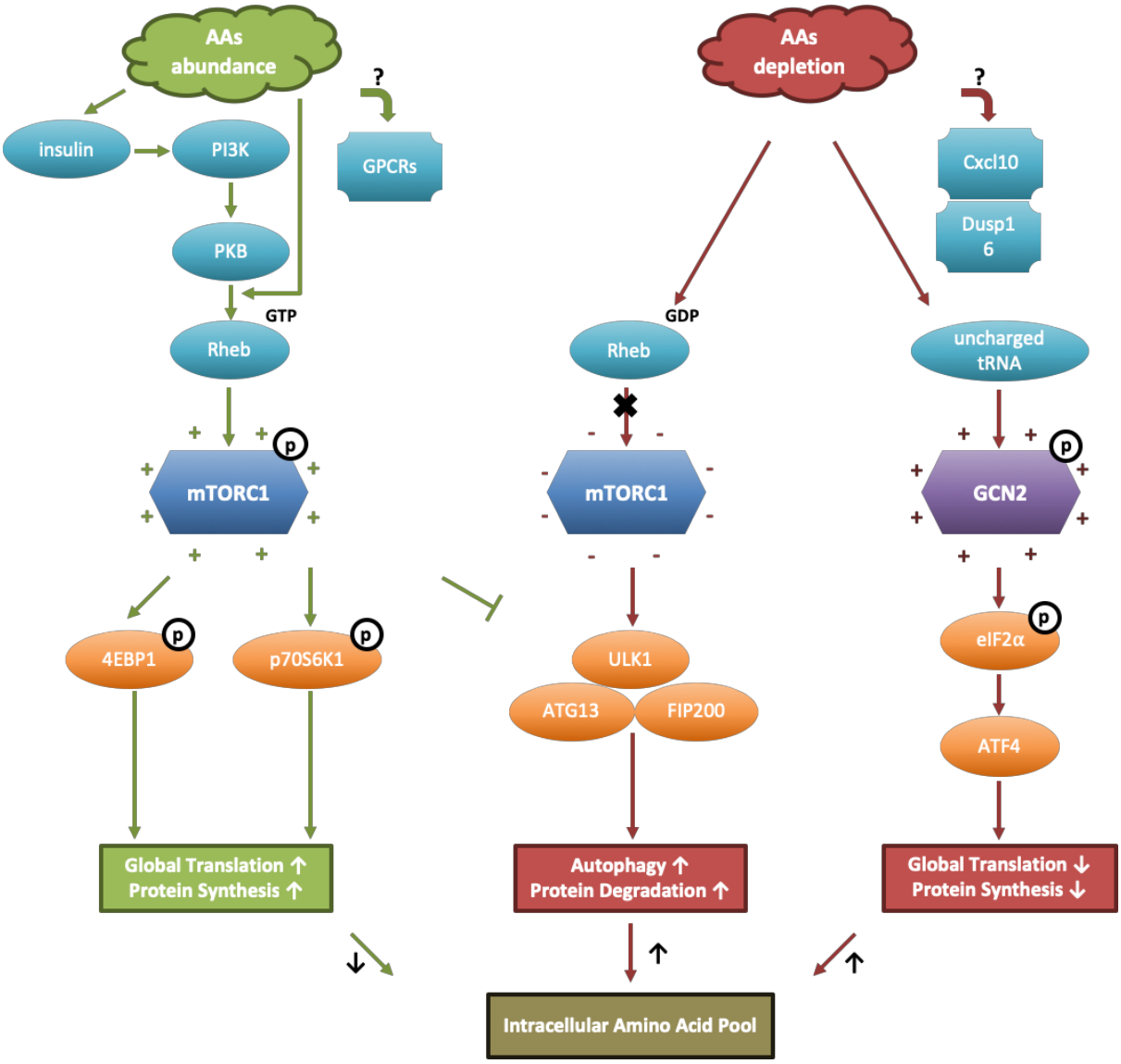

Figure 1.1: Amino acid sensing pathways. When amino acids become abundant, mTORC1 is activated by GTP-bound Rheb, which potentiates global translation and protein synthesis by the phosphorylation and activation of p60S6K and 4E-BP1, whereas the activated mTORC1 down-regulates autophagy by suppressing the ulk1/atg13/FIP200 complex. Meanwhile, insulin released post the elevation of circulating amino acid levels also stimulates mTORC1 by a signaling cascade of PI3K/PKB/mTORC1. Under amino acids depletion, the inactivated mTORC1 associates the ulk1/atg13/FIP200 complex to induce autophagy-mediated protein degradation. In addition, the amino acid restriction leads to the accumulation of uncharged tRNAs, which stimulates the protein kinase GCN2 and subsequently results in ATF4-mediated suppression of global translation and protein synthesis [12, 13]. In addition, the amino acid abundance and depletion can also be sensed by GPCRs and Cxcl10 transcriptional/Dusp16 posttranscriptional responses, respectively, via unknown mechanisms [14].

1.2 Intestinal protein absorption and renal transport

Approximately 30% of our nutrition stems from proteins, which are critical sources of energy and building blocks for human beings. Upon dietary intake, proteins are digested and enzymatically hydrolysed into large peptides in stomach under the action of protease pepsin, then further degraded into smaller peptides in the presence of a variety of pancreatic proteases (e.g. trypsin, chymotrypsin, elastase and carboxypeptidases) entering into the small intestine. Finally, individual amino acids, di- and tri-peptides are generated by brush-border peptidases in the apical membranes of small intestine enterocytes [30]. The hydrolysed small peptides and amino acids are transported into the small intestinal epithelial cells by specific peptide transporters (PEPT1 [31] and amino acid transporters (figure 1.2), respectively, all of which are located in the apical membrane of intestinal enterocytes. The majority of absorbed small peptides are further digested into amino acids by cytoplasmic peptidases before the release by another set of transporters located in the basolateral membrane of intestinal enterocytes. These amino acids are subsequently collected by the hepatic portal vein (figure 1.2).

To maintain systemic amino acid homeostasis, amino acids are reabsorbed by the kidney before they are wasted through urine, and such reabsorption is mediated by the epithelial cells of the proximal convoluted and straight tubules [32]. Notably, low-affinity amino acid transporters were identified in the proximal convoluted tubule; whereas high-affinity ones were found in the proximal straight tubule [33]. A wide variety of amino acid transporters are involved in the transcellular amino acid reabsorption by the proximal tubule cells, which are shown in figure 1.2, whereas the di-and tri- peptides are transported by PEPT2 in kidney [34]. Eventually, the reabsorbed amino acids return to the circulatory system through the renal vein.

Generally, similar transport systems are expressed in both intestinal enterocytes and kidney epithelial cells. There are four major transport systems on the apical side of the membrane in both small intestine and kidney. The term “system” indicates a type of transport activity identified in various cells, whereas the term “solute carrier (SLC)” indicates the molecular identification of a particular transporter.

1. System X^-_{AG}: facilitating the transport of anionic amino acids (aspartate, glutamate) in a Na^+- and H^+- dependent manner, the transporter was identified as EAAT3 (SLC1A1) [35] in kidney and intestine;

2. System $b^{0,+}$: facilitating the uptake of cationic amino acids (lysine, arginine) and cystine in exchange with neutral amino acids, the correlated transporter (SLC7A9) forms a heterodimer with the heavy subunit rBAT (SLC3A1) [36] in kidney and intestine;

3. The IMINO/glycine System Comprised of PAT1 (SLC36A1) (intestine) and PAT2 (SLC36A2) (kidney), which are proton symporters participating in the absorption of proline and glycine in kidney with lower affinities compared to SIT1 and XT2 [37]. The $2Na^+$, $1Cl^-$ and proline cotransporter SIT1 (SLC6A20) [38] in kidney and intestine; The Na^+- and Cl^--dependent glycine transporter XT2 [39], later called B^0AT3 (SLC6A18) [40]. This transporter is only relevant in mouse, in humans the transporter is replaced by PAT2.

4. System B^0: facilitating neutral amino acid transport in a Na^+-dependent manner. Three transporters were identified in this system, including B^0AT1 (SLC6A19) expressed in kidney and small intestine, B^0AT2 (SLC6A15) expressed in brain [41], and B^0AT3 (SLC6A18) expressed in kidney [40]. B^0AT1 is introduced in detail in later sections.

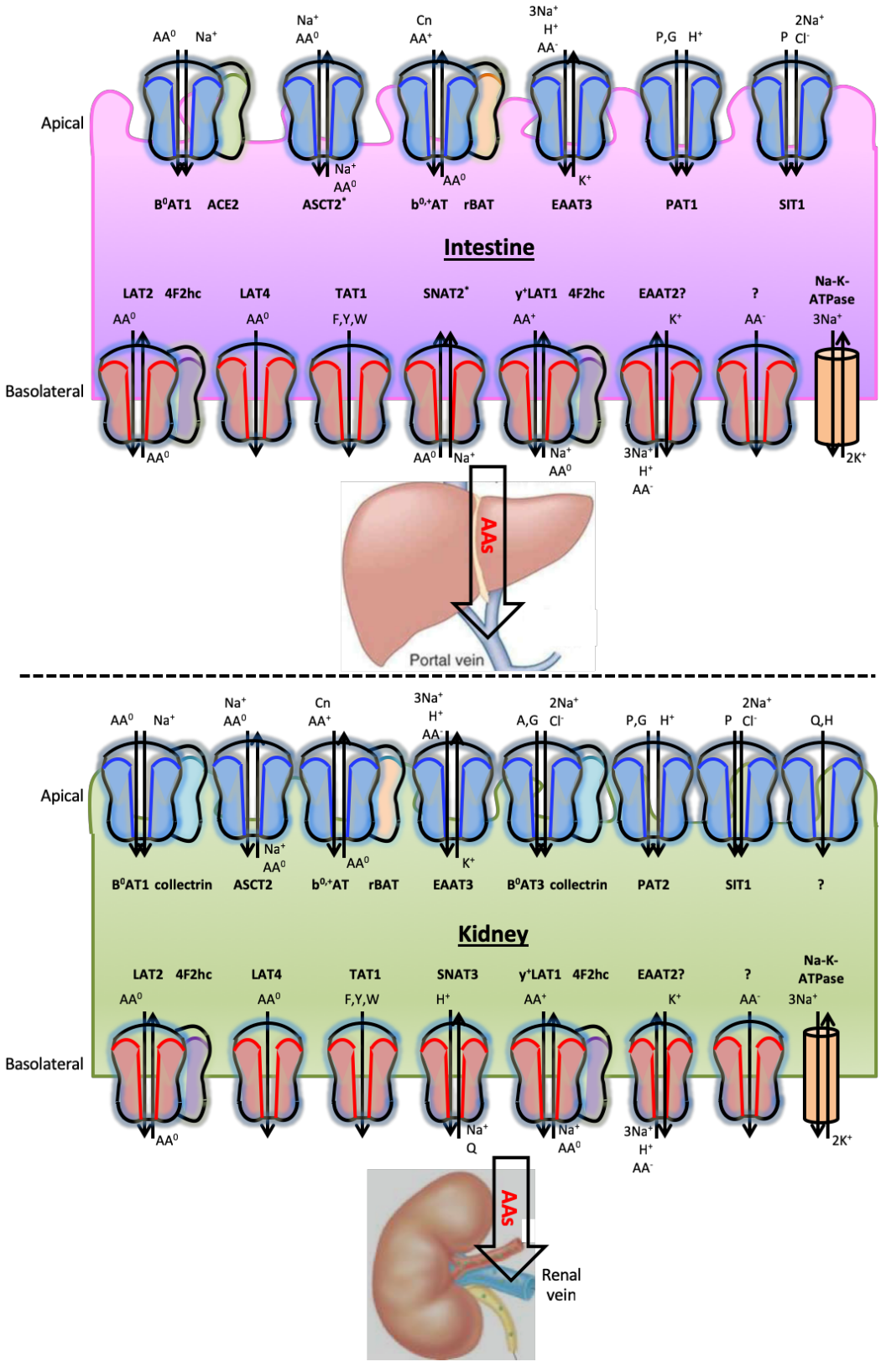

Figure 1.2: Amino acid transporters on apical and basolateral sides of intestine and kidney. *ASCT2 on the apical side and SNATs on the basolateral side are only detected in distal intestine. The net efflux of anionic amino acids across the basolateral membrane remains to be elucidated. AA, amino acid; Cn, cystine [12, 42-44].

1.3 Amino acid transporter pharmacology

Amino acids are essential for protein synthesis and serve as important energy sources for all living cells. Amino acids are absorbed or reabsorbed through various transporters in different organs, and these transporters belong to different SLC families, namely SLC1, SLC3, SLC6, SLC7, SLC16, SLC17, SLC25, SLC32, SLC36, SLC38 and SLC43 families [12]. Importantly, suppression of single/multiple specific transporter(s) could cause beneficial effects in humans under pathological conditions, thus, amino acid transporters are investigated as pharmacological targets in a variety of areas, such as cancer, nervous system disorders and metabolic disorders.

Cancer: Amino acid transporters are highly expressed in tumour cells to support rapid replication, hence, being investigated as targets for treating various cancers. For example, system L amino acid transporter 1 (LAT1, SLC7A5) was shown to be highly expressed in human tumour cell lines [45]. Initially, substrate analogues were used as transporter inhibitors, for example, the nonmetabolizable amino acid analogues, 2-aminobicyclo-(2,2,1)-heptane-2-carboxylic acid (BCH) and N-Methylaminoisobutyric acid (MeAIB), were used as inhibitors of system L and system A transporters, respectively [46]. However, due to poor selectivity of these inhibitors to the targets, they are unlikely to be developed as drug candidates. BCH, for instance, was found to inhibit transporters other than LAT1 [47, 48], so significant efforts have been put into synthetic chemistry and in vitro screening to identify more specific LAT1 inhibitor, such as JPH203 (previously known as KYT0353) [49]. As a proof of principle, 2-aminobicyclo-(2,2,1)-heptane-2-carboxylic acid (BCH) showed inhibitory effects on cancer cell proliferation in a non-small cell lung cancer cell line [50], and silencing of LAT1 suppressed cell invasion and migration in a cholangiocarcinoma cell line [51]. The novel LAT1 specific inhibitor, JPH203, has demonstrated therapeutic potential in treating cholangiocarcinoma [52] and thymic carcinoma [53]. Occasionally, approved drugs can be repurposed as transport inhibitors. For instance, the anti-inflammatory drug Sulfasalazine (initially approved to treat arthritis) was identified as an effective antagonist of the cystine/glutamate antiporter SLC7A11 (also known as xCT) potentially useful for the treatment of small-cell lung cancer [54]. As another example, alanine/serine/cysteine transporter 2 (ASCT2, SLC1A5) mediates glutamine uptake as a harmonizer in many cancer cells. Glutamine is essential for many cancer cell lines to support glutaminolysis, which is critical for cancer cell growth and protein translation [55]. It was reported that pharmacological inhibitors of ASCT2 or shRNA-mediated ASCT2 knockdown suppressed cell growth and proliferation of triple-negative basal-like breast cancer cells, but not for luminal breast cancer

cells [56]. A novel ASCT2 inhibitor, 2-amino-4-bis(aryloxybenzyl)aminobutanoic acids was synthesized on the basis of previously reported ASCT2 inhibitors, which were glutamine or serine analogues, but with much higher potency, shedding light on cancer treatment when ASCT2 is a target [57]. However, inhibition of ASCT2 alone may not be sufficient to suppress cancer cell growth because it is compensated by an up-regulation of sodium-coupled neutral amino acid transporter 1 (SNAT1, SLC38A1), whereas combined inhibition of GCN2 and ASCT2 could overcome this compensation [58].

Nervous system disorders: The high-affinity, Na^+-dependent excitatory amino acid transporters (EAATs) are widely-known as the main mediators of L-glutamate removal in mammalian central nervous system (CNS), and at least five distinct EAAT subtypes have been identified in humans as well as in rodents [59]. As a dominant excitatory neurotransmitter, L-glutamate participates in many key physiological events in the CNS, such as fast synaptic communications, regulation of synaptic plasticity, learning and memory. However, excessive levels of L-glutamate can trigger excitotoxicity and cause neuronal damage in both acute CNS injuries or chronic neurodegenerative diseases [60, 61]. Therefore, the removal of L-glutamate from the synaptic cleft into glial cells and neurons via the symport with $3Na^+$ and $1H^+$ in exchange for $1K^+$ by EAATs is critical to avoid excitotoxicity [62]. EAAT2 is responsible for up to 80-90% of the total extracellular glutamate reabsorption within the CNS, so its translational activators (ceftriaxone and LDN/OSU-0212320) or pharmacological activators (parawixin 1 and GT949/GT951) have been reported to be neuroprotective in animal models of ischemic stroke, brain trauma and neurodegenerations [63, 64]. Another sodium-coupled amino acid transporter, B^0AT2 (SLC6A15), is widely expressed at the plasma membrane of neurons across the cerebral cortex, hippocampus, cerebellum, midbrain and olfactory bulb, and plays an important role in leucine and proline homeostasis in the brain [65]. Based on a genome-wide association study (GWAS), SLC6A15 was identified as a susceptibility gene for major depression disorder (MDD). Interestingly, SLC6A15 knock-out mice showed lower levels of anxiety and depression after chronic social stress. Thus, B^0AT2 inhibitors could potentially be used as novel antidepressant drugs [65-67]. Glycine is an inhibitory neurotransmitter, whose receptors are predominantly found in inhibitory synapses in the spinal cord, brainstem and retina. Moreover, glycine can be excitatory when acting as a co-agonist at NMDA (N-methyl-D-aspartate) receptors, whereby their association at the glycine-B site is required for the activation of NMDA receptors by L-glutamate. On the one hand, inhibitors of glycine transporter 1 (GlyT1) can be used to increase glycine availability for NMDA receptors, leading to an up-regulation of NMDA receptor excitability, which is beneficial in treating

schizophrenia. On the other hand, inhibition of GlyT2 has therapeutical potential in pain treatment because it reduces the reuptake of glycine from glycinergic synapses in the spinal cord, resulting in the blocking of pain signal transmission to the thalamus [68]. A highly-selective and potent GlyT1 (SLC6A9) inhibitor bitopertin was tested in Phase III clinical trials in patients with schizophrenia [69], whereas GlyT2 (SLC6A5) inhibitors are explored to reduce chronic pain [70].

Metabolic disorders: Amino acids are also contributing to metabolic syndromes in various ways, allowing their transporters to be potential targets in treating these diseases. For example, it was reported that the active form of vitamin A (all-trans retinoic acid) suppressed up-regulation of ASCT2 in 3T3-L1 cells (an adipogenesis cell model), which was required for lipid accumulation as ascertained by inhibition of ASCT2 with l-γ-glutamyl-p-nitroanilide (GPNA), hence providing a potential target for obesity [71].

1.4 B^0AT1 (SLC6A19)

Apical broad-spectrum neutral (0) amino acid transporter B^0AT1 (SLC6A19) belongs to the solute carrier family 6, which has 20 family members in four major branches [72]. They are (i) the GABA transporter branch composed of GABA transporters GAT1-4, the taurine transporter TauT and creatine transporter CT1; (ii) the monoamine transporter branch containing the dopamine transporter DAT, the noradrenaline transporter NET and serotonin transporter SERT; (iii) the amino acid transporter branch (I) consisting of the general amino acid transporter $ATB^{0,+}$, glycine transporters GlyT1-2 and the proline transporter PROT; and (iv) the amino acid transporter branch (II) containing the neutral amino acid transporters B^0AT1-3, NTT4, the proline transporter SIT1 and NTT5, a transporter of unknown function.

B^0AT1 is a Na^+-dependent neutral amino acid transporter mainly expressed in small intestine and kidney and localized at the apical side of the brush-border membrane (BBM), showing increasing expression from the crypts towards the tip of the villi [73]. Its expression in small intestine increases from duodenum to ileum, whereas its expression in kidney is mainly in the proximal convoluted tubule (S1 and S2 segment) rather than proximal straight tubule (S3 segment), as shown by immunohistochemical analysis [74]. Although B^0AT1 was detected in pancreas at mRNA level [42], its expression in pancreatic β-cells remained uncertain, whereas its trafficking subunit collectrin was detected in β-cells [75, 76]. Lower, but significant expression of B^0AT1 mRNA was also detected in skin [73], prostate [77], stomach and liver [78]. Expression of B^0AT1 protein has not been verified in these tissues. Mouse B^0AT1 has 634 amino acids, with 12 transmembrane domains and a larger loop between helix 7 and 8

compared with other SLC6 family members [73]. The mouse Slc6a19 gene is localised on chromosome 13 in cytoband C1, in a region syntenic to human chromosome 5p15 [73]. Co-expression of B^0AT1 with the carboxypeptidase angiotensin-converting enzyme 2 (ACE2) in the intestine or its homolog collectrin (TMEM27, transmembrane protein 27) in the kidney is critical for the activity of the transporter mainly by affecting its trafficking to the apical membrane surface [79-81]. Apart from trafficking the transporter, collectrin is essential for the catalytic activity of B^0AT1 and B^0AT3, acting as an essential subunit of a heterodimeric secondary active transporter. Site-directed mutagenesis suggested that collectrin occupies a groove between TM5 and -7 of the transporter [40]. In mouse kidney collectrin expression develops late but eventually replaces ACE2. Low expression levels of B^0AT1 and collectrin cause aminoaciduria during the first week of life, a situation that resolves during the second week of life due to increased B^0AT1 and collectrin expression [82].

In addition, B^0AT1 was reported to form a complex with another peptidase, namely APN (aminopeptidase N/CD13), whose major role was to increase transport activity by increasing the local substrate concentration through a proximal binding site. Compared to ACE2 and collectrin, its role in increasing the surface expression of B^0AT1 was minimal [83]. The uptake of amino acid substrate leucine by B^0AT1, when expressed in *Xenopus laevis* oocytes was characterised as Na^+ -dependent, Cl^- -independent, membrane potential-driven, refractory to osmolarity change, and pH-dependent [73]. Later studies proved that the transport activity was electrogenic, substrate was co-transported with Na^+ in a 1:1 stoichiometry. Increased Na^+ concentration decreases the Km of substrate without affecting its Vmax, and vice versa, increased concentration of substrate decrease the Km for $Na^{+.}$ Although there is no strict binding order, amino acid preferentially binds to the transporter before Na^+ [84]. B^0AT1 transports substrates with similar V_{max} values but quite different affinities [44]. It shows a preference for branched-chain amino acids (leucine, isoleucine, valine) and methionine (K_m ~1mM), over large polar neutral amino acids glutamine, alanine, phenylalanine, asparagine and cysteine (K_m ~4mM), over smaller polar amino acids such as serine, glycine, threonine, proline and aromatic amino acids such as tyrosine, histidine, and tryptophan (K_m ~11mM). Anionic amino acids (aspartate and glutamate) and cationic amino acids (lysine and arginine) are not transported by B^0AT1. It is noteworthy that B^0AT1 is the only transporter for large neutral amino acids in the small intestine, whereas smaller amino acids are also transported by PAT1 [85].

Several regulators of B^0AT1 have been reported in different studies. Serum- & glucocorticoid-inducible kinase (SGK) isoforms SGK1-3 [86] and protein kinase B (PKB) [87] were reported

as stimulators of B^0AT1, by stabilizing the transporter at the plasma membrane to increase its surface abundance, further revealing the regulation of this transporter in intestinal and renal epithelial cells. Moreover, B^0AT1 was also found being stimulated by JAK2 (Janus kinase-2), a protein critical for the proliferation and survival of a variety of cancer cells in the development of many myeloproliferative diseases, hence, the upregulation of B^0AT1 was thought to provide an important source of amino acid nutrients to these JAK2 expressing cells [88].

1.5 ACE2 and collectrin

As mentioned above, ACE2 and collectrin are auxiliary proteins of B^0AT1 in intestine and kidney, respectively. In addition, these two proteins are co-expressing with B^0AT3 (SLC6A18) at the cell surface [89]. The angiotensin-converting enzyme 2 (ACE2) is a carboxypeptidase that catalyses the conversion of angiotensin I to angiotensin 1-9, and more importantly, the conversion of angiotensin II to angiotensin 1-7, which is a critical regulator of cardiovascular function [90, 91]. In addition, ACE2 also contributes to glucose homeostasis in obese C57BL/6 mice by regulating β-cell mass and function in response to hyperinsulinemia [92]. In another study, ACE2-deficient mice showed a β-cell defect with low insulin and collectrin levels. ACE-2 knock-out mice also demonstrated a shift of energy consumption towards glucose utilization in an angiotensin II-dependent manner [93-95]. In confirmation of its role as an ancillary protein for B^0AT1, immunofluorescent staining and immunoprecipitation experiment demonstrated that ACE2 knockout mice lack B^0AT1 expression in the intestine [96], leading to reduced plasma concentration of neutral amino acids (10-25%) because of their malabsorption in the intestine [97]. By contrast, the expression and function of B^0AT1 was barely affected in kidney [89]. The study of ACE2 deficient mice revealed its influence on gut microbiota composition, which might provide an explanation for diarrhea and intestinal inflammation seen in SLC6A19 mutated humans (Hartnup disorder patients) (see below) [98]. Even so, the ACE2 knockout mice did not manifest any symptoms of Hartnup disorder, such as skin rash or niacin deficiency, even under a low-protein and low-niacin diet [94]. In fact, these ACE2 null mice showed a variety of symptoms unrelated to the lack of neutral amino acid transport in the intestine but related to its role as a negative regulator of the renin-angiotensin system, including accelerated diabetic renal injury, acute respiratory stress syndrome and impaired cardiac contractility [95]. Apart from B^0AT1, ACE2 was also reported to be co-expressed with SIT1 (SLC6A20) in proximal tubule kidney cells both at protein level observed by immunofluorescence staining and at transcript level detected by RT-PCR [99].

Collectrin, also known as transmembrane protein 27 (TMEM27), is a type I transmembrane glycoprotein sharing 47.8% homology with C-terminal end of ACE2 [100] in its homologous domain. The N-terminal dipeptidylcarboxypeptidase catalytic domain of ACE2 is absent in collectrin, resulting in a larger size of ACE2 and a loss of enzymatic activity in collectrin [101]. Collectrin is most abundantly expressed in kidney, but is also observed in vascular endothelium [102] and pancreatic β-cells [103] in humans. Similar to ACE2, collectrin has a vascular protective effect, so the depletion of collectrin could cause hypertension, probably by uncoupling endothelial nitric oxide synthase [102]. In pancreas, it interacts with SNAPIN, a protein involved in the fusion of insulin-containing vesicles with the plasma membrane during exocytosis, resulting in reduced insulin secretion in collectrin-deficient mice [75]. Malakauskas et al. [104], by contrast, saw no change in pancreatic morphology (β-cell mass and proliferation) or function (acute-phase insulin response and glucose-stimulated insulin-release) in collectrin-deficient mice compared to wild-type mice. In this study collectrin-deficient mice demonstrated increased peripheral insulin sensitivity and decreased adiposity at 6 months of age, indicating protective effects on age-induced insulin resistance and obesity. Similar observations were made in Slc6a19 knockout mice [105].

1.6 Hartnup disorder

Mutations in different amino acid transporters cause various aminoacidurias, which are described in the Online Mendelian Inheritance in Man (OMIM) database. For example, mutations in either rBAT (SLC3A1) or $b^{0,+}$AT lead to cystinuria (OMIM220100 and OMIM600918) [106]; mutations in PAT2 (SLC36A2) and IMINO (SLC6A20) [107] result in iminoglycinuria (OMIM242600).

Inactivating mutations in SLC6A19 in humans are known to cause an autosomal recessive inherited disorder named Hartnup disorder (OMIM234500) [77, 78]. The frequency of its occurrence is about 1:30,000 in European populations [108]. It is characterised by a reduced uptake of branched-chain and other neutral amino acids in the intestine and by their loss through the urine. Thus, very high levels of neutral amino acids are found in urine, with the exception of proline [109]. Hartnup disorder was first described on two siblings in the Hartnup family of British ancestry in 1956 [110]. Its clinical symptoms, pellagra-like skin rash, cerebellar ataxia, and psychotic behaviour [111], are generally rare and only observed in younger patients. Individuals with Hartnup disorder tend to have lower body weight relative to their healthy siblings [112]. A large proportion of patients remain asymptomatic except for the hyperaminoaciduria [112, 113]. It has been argued that the skin rash is a consequence of

tryptophan depletion, as it is similar to that observed in niacin deficiency. Both tryptophan and niacin are major precursors of NAD(P)H biosynthesis. In agreement with this notion, the skin rash in Hartnup disorder responds to nicotinic acid supplementation [114], and also to supplementation of tryptophan-ethyl ester [115]. It appears likely that tryptophan malabsorption in Hartnup disorder can be compensated by peptide uptake and also by amino acid absorption in distal sections of the intestine [116]. In the two initial studies, nine mutations and two aberrant splicing in SLC6A19 were described [77, 78], in two subsequent studies, another ten mutations were identified [79, 96, 113]. Most mutations are rare occurring at a frequency of below 0.1% [111]. D173N was identified as the major mutation of SLC6A19 in the Australian population, with a frequency of 1 in 140 people (0.007) [77].

1.7 Slc6a19 knockout mice

Our lab previously reported that Slc6a19 nullizygous mice had neutral aminoaciduria, a reduction in body size and body weight, and decreased insulin secretion in response to food ingestion after fasting [42]. More importantly, Slc6a19 nullizygous mice showed improved glycaemic control, indicating that inhibition of the transporter might lead to improved insulin sensitivity. Moreover, glucose transport in the intestine was also decreased by more than 50% possibly due to the formation of a complex between the apical glucose transporter SGLT1 (sodium-dependent glucose transporter 1) and B^0AT1. Reduced amino acid absorption in the intestine resulted in reduced activation of mTOR (mammalian target of rapamycin) as indicated by reduced ribosomal protein S6 phosphorylation and the activation of the GCN2 (general control non-derepressible 2) /ATF4 (activating transcription factor 4) stress response pathway resulting in eIF2α (eukaryotic initiation factor 2α) phosphorylation [42]. Further characterisation of Slc6a19 knockout mice revealed that the reduced uptake of neutral amino acids in the intestine causes an increased amino acid load in the lumen of the intestine, which triggered the release of the two incretins glucagon-like peptide 1 (GLP-1) and gastric inhibitory polypeptide (GIP) from the intestine. Delayed amino acid absorption in addition results in the release of the hormone fibroblast growth factor 21 (FGF21) by a starvation response in the liver. The combination of these hormones caused a series of beneficial phenotypes including efficient glucose removal particularly by heart, reduced adipose tissue mass, browning of white adipose tissue, stimulation of ketone body production, reduced hepatic glucose output and reduced liver triglycerides. These results provided new evidence for B^0AT1 as a novel target to treat type 2 diabetes [105]. GLP-1 and GIP are two incretins that prepare the body for nutrient intake by enhancing insulin secretion and reducing appetite. GLP-1 has also been reported to increase glucose consumption in heart, thus, dual agonists of these two hormones are being

developed as drugs to treat T2DM [117]. FGF21 was reported to inhibit liver fatty acid synthesis and to stimulate white adipose tissue browning via the activation of GCN2 signalling. FGF21 expression can be stimulated by the restriction of methionine [118] or leucine [119]. Clinical trials using FGF21 mimetics showed significant improvements of the plasma lipid profile in obese patients, however, body weight and glucose homeostasis was not affected by the drug. Moreover, hypersensitivity reactions caused by subcutaneous injection are significant side-effects of the drug [120].

1.8 Hypothesis

We hypothesized that the pharmacological inhibition of B^0AT1 using small molecule chemical compounds could be able to replicate the metabolic phenotype of Slc6a19 knockout mice, thus providing new lead compounds to treat type 2 diabetes.

Chapter 2: Cell Line Generation and Method Validation

2.1 Introduction

In this chapter I shall introduce tools and methods that are used for drug and inhibitor screening that can be scaled up for the use in high-throughput screening (HTS) using B^0AT1 as an example.

Previously, B^0AT1 and its interaction with ancillary proteins ACE2 and collectrin has been studied in *Xenopus laevis* oocytes [73]. This expression system is superior for the study of transporter kinetics and structure-activity relationships. However, for the efficient screening and characterisation of novel inhibitors, a system that is more suitable for rapid data generation had to be developed. Using cell lines as *in vitro* models for drug screening, particularly HTS, is widely accepted due to its standard tissue culture procedures, fast cell proliferation, well understood culture medium requirements, high transfection efficiency, as compared to primary cells and stem cells [121]. As mentioned above, amino acid transporters are highly expressed in many human cancer cell lines for the demand of tumour growth. In this case, an oncology microarray database called Oncomine is potentially useful for identifying cell models with high expression levels of the desired transporter. Oncomine is a web-based data-mining platform with standardized microarray datasets (currently 715 in total) derived from published data or authors' correspondence by Compendia Bioscience. It comprises a total of 86,733 samples including gene expression data from over 500 cancer types and a wide range of human cancer cell lines [122]. Oncomine has been used widely for gene target or cell model selection [123, 124], biomarker development [125, 126] and anticancer drug screening studies [127, 128]. Moreover, Oncomine was also used in studies related to amino acid transporters [58, 129, 130].

If the endogenous expression of a transporter is sufficient, the selected cell line can directly be used for inhibitor screening. However, more often the target protein needs to be expressed heterologously. Stable transfection [131] is used to integrate the gene of interest into the genome of suitable cells, avoiding the loss of transfected material. It is accomplished by introducing a marker gene as a selectable tool together with the gene of interest. The Flp-In™ stable transfection system is a Saccharomyces cerevisiae-derived DNA recombination system, allowing the integration of a gene of interest into the genome of mammalian cells at a particular location called the Flp Recombination Target (FRT) site [132]. The FRT site is first introduced into the genome of a mammalian cell line of choice using a Flp-In™ target site vector, pFRT/*lac*Zeo, to generate a host cell line. Subsequently, an expression vector containing any gene of interest can be integrated into the genome via Flp recombinase-mediated DNA

recombination at the FRT site. Successfully transfected clones expressing the gene of interest can be selected using hygromycin resistance and Zeocin sensitivity (Flp-In™ System User Manual, Invitrogen). In detail, the Flp-In™ host cell line contains an SV40 early promoter, an ATG initiation codon, a single integrated FRT site acting as the binding and cleavage site for Flp recombinase, and a Zeocin resistance gene for selection. Then the pcDNA/FRT expression vector containing the gene of interest is co-transfected with pOG44 into the Flp-In™ host cell line. The pOG44 plasmid expresses Flp recombinase constitutively under the control of the human CMV promoter, catalysing the insertion of the pcDNA5/FRT construct into the genome at the FRT site. The insertion inactivates the lacZ-Zeocine fusion gene and at the same time introduces a hygromycin resistance gene in frame with the SV40 promoter and ATG initiation codon. As a result, the transfected cells become hygromycin resistant but Zeocine sensitive, which allows the selection of stable Flp-In expression cell lines by using hygromycin as an antibiotic. This Flp-In transfection system has been used routinely to generate highly reproducible stable transgenic cells for the expression of cytosolic or membrane proteins in various parental cell lines, including HEK293 (human embryonic kidney) cell line [133], CV-1 (African Green monkey kidney) cells line [134], CHO-K1 (Chinese Hamster Ovary cells) [135], BHK (Baby hamster kidney cells) [136], NIH/3T3 (mouse embryonic fibroblast) [137] and Jurkat (human T-cell leukemia) [138].

The Chinese hamster ovary (CHO) cell line was one of the first hosts to be used in stable transfection, and has become one of the most popular cell line for recombinant protein production [139]. It was first isolated by T.T. Puck in 1957 [140], and requires proline in the culture medium because of a defect in proline synthesis [141]. Three CHO cell lines are commonly used: the CHO-K1 line, the CHO-DXB11 line and the CHO-DG44 line, among which CHO-K1 is the only cell line still having a functional DHFR (dihydofolate reductase) gene. DHFR-deficient cell lines can be used for introducing the gene of interest (GOI) by a DHFR selection system [142]. The genome of CHO-K1 was sequenced for the first time by Xu et al. in 2011, which accelerated the application of this cell line [143]. CHO cells have become a popular mammalian expression system, particularly for the overexpression of recombinant proteins due to their rapid growth and high protein production [142]. Due to their epithelial-like property, CHO cells were also used to study membrane proteins, such as ion channels (KCNQ potassium channel and epithelial sodium channels) [144], α2β adrenergic receptor by transient transfection [145] or β2 adrenergic receptor by stable transfection [146] in structural studies. CHO cells are also useful for the expression of amino acid transporters, because their endogenous transporters have been studied in some detail [147]. System L-like transport

(including LAT1 and LAT2) was reported to mediate the Na^+-independent pregabalin (PGB) uptake in CHO cells [148]. Both of these transporters are functional in a heteromeric complex with the heavy subunit 4F2hc (SLC3A2) to act as exchangers and harmonizers of large neutral amino acids [12]. LAT1 substrate selectivity for neutral amino acids is more narrow compared to LAT2; and only LAT1, but not LAT2, interacts with D-amino acids [149]. A LAT1-like activity was detected in CHO cells also by Shikano et al. [150].

Apart from choosing an appropriate *in-vitro* cell model, selection of appropriate assays is critical for compound screening studies. Membrane potential based assays including Fluorescent (Fluorometric) Imaging Plate Reader (FLIPR) assays and Fluorescence Resonance Energy Transfer (FRET) assays are widely used to monitor the function of ion channels and electrogenic transporters [151]. FLIPR assays were designed to quantitively analyse changes in membrane potential, elicited by activation of ion permeable receptors, ion channels or transporters [152]. They have been used in a variety of drug discovery applications including HTS of chemical compound libraries at the initial stage [153, 154], and analysis of compound potency, selectivity and specificity at the follow-up stage [155, 156]. The major advantages of this system include real-time recording and rapid measurement of membrane potential changes in either a 96-well or 384-well format, which are essential for the HTS [157]. Bis-(1,3-dibutylbarbituric acid)trimethine oxonol [$DiBAC_4(3)$] is a traditional membrane potential sensitive dye also used in fluorescence resonance energy transfer (FRET) assays. Membrane depolarization causes it to partition into the membrane, which in turn increases its fluorescence. It is extruded out of the membrane following hyperpolarization, resulting in a decrease in fluorescence [157]. Because of its slow response, $DiBAC_4(3)$ is not well suited for fast screening applications [151]. Moreover, this dye is temperature sensitivity and works only at 37°C. A faster responding and temperature-flexible dye has been developed as the FLIPR membrane potential assay kit by Molecular Devices (FMP) (figure 2.1.1). In addition, the fluorescent sensor is pre-combined with impermeable quenchers (either a blue quencher or a red quencher) in the kit to reduce the background fluorescence signal and to improve the signal-to-noise ratio. This is necessary because the dye-loaded cells cannot be washed. Last but not the least, the FMP dye has higher temperature stability compared to the traditional dyes, e.g. dye loading and plate reading can occur at room temperature. In addition to FLIPR assays, FRET is also a popular technique used for the detection of membrane potential changes [158, 159] and the characterization of amino acid transport [160, 161]. The principle of FRET is to have a donor dye (e.g. coumarin-linked phospholipid (CC2-DMPE) in the Pan Vera system) outside the cell coupled with an oxonol dye (e.g. $DiSBAC_2(3)$ in the Pan Vera system) acting

as a mobile voltage sensor and FRET acceptor [162]. Upon depolarization, the negatively-charged hydrophobic oxonol dye partitions into the plasma membrane, whereas the FRET donor only binds to the exterior side of the cell membrane, consequently resulting in an increased emission ratio of donor's blue fluorescence signal (@460nm) over acceptor's red fluorescence signal (@570nm) (BMG Labtech). When using two FRET acceptors [$DiSBAC_1(5)$ and $DiSBAC_1(3)$] in the Axiom system, it increases the sensitivity of the assay (Axiom Biotecnologies Inc.). Wolff et al. systematically compared ion channel screening assays using the above two FLIPR systems and two FRET systems. The study showed a good correlation among these 4 systems when determining IC_{50} values. The FLIPR dye from Molecular Devices showed the highest signal over background ratio and the FRET system from Pan Vera had the fastest response [151]. Although no obvious improvement in signal stability or Z' parameter was seen when comparing to the traditional oxonol dye $DiBAC_4(3)$, the author still found a few benefits of using these novel dye systems in the large-scale HTS, such as reduced temperature sensitivity, faster responses and simplified assay procedures. The Z' parameter, also known as Z' assay sensitivity factor, is a measurement of statistical effect size that considers the average and standard deviation of both positive and negative controls, when Z'>0.8, it is ideal for HTS, although Z'>0.5 is also acceptable [163].

As outlined above, the electrogenicity of B^0AT1 transport is due to the symport of sodium ion with amino acid substrate at the ratio of 1:1, hence, the detection of sodium ion crossing the membrane by ion-sensitive fluorescent dyes is another option to measure transport function. One of the most commonly used Na^+-indicators is sodium-binding benzofuran isophthalate (SBFI), which was first designed and characterized in 1989 [164]. The applications of this indicator in the quantification of intracellular free sodium ion is flexible, allowing fluorescence ratiometric analysis, fluorescence lifetime imaging microscopy (FLIM) [165, 166], and it can be adapted to microplate readers as well [167]. However, SBFI requires UV excitation and is difficult to load. Attempts were made to find alternatives excitable in the visible range, including Sodium Green [168], CoroNa Red [169] and CoroNa Green [170]. Unfortunately, they are not ideal for various problems, such as inaccurate measurements of sodium ion due to the association with cell proteins [171], incapability to detect small $[Na^+]_i$ changes [172], and fast leakage from cells after loading [173]. An improved efficient and sensitive sodium dye, namely Asante NaTRIUM Green (ANG), has been developed recently. It enables accurate measurements of intracellular Na^+ dynamics in situ with a bright fluorescent signal during physiological responses [174]. When comparing with SBFI, it displays a range of desirable characteristics, including high sensitivity and loading efficiency, resistance to photobleaching,

as well as good fluorescent brightness and dynamic range (TEFLABs). Acetoxymethyl (AM) ester are used to improve loading efficiency by increasing the permeability of the sodium dye (figure 2.1.2). In addition, Pluronic F-127 is always used as a surfactant polyol to disperse the AM esters of fluorescent ion indicators [175]. Lower concentrations of Pluronic F-127 dissolved in DMSO proved to yield a better loading and staining efficiency of an AM ester calcium dye [176]. Both the FLIPR assay and the sodium indicator assay were used in HTS because of their adaptability to multi-well plate readers. One lab has previously evaluated the ANG-2 sodium sensing dye (TEFLABs) in a 1536-well format assay by comparing with the FMP blue dye (Molecular Devices), identifying a large amount of unique hits from each assay. The author suggested to use both assays in an HTS strategy to increase the likelihood of recognition of true positives [177].

To reduce false positive rates, a secondary assay is usually required in the drug screening, especially after HTS. For example, a radio-labelled substrate uptake assay is a reliable direct measurement of the transport activity. ^{14}C and ^{3}H are beta-particle emitting radioisotopes generally used for labelling due to safety issues, however, ^{14}C is employed more often because of its higher energy and higher efficiency in liquid scintillation counting (LSC), in which the beta particle transfers energy to the scintillator, which in turn emits light. The number of light flashes generated by a beta-particle is a direct measure of its energy and is detected by a scintillation counter. The assay has been used in numerous studies. A recent example from our lab is the analysis of amino acid fluxes in 143B osteosarcoma cells using ^{14}C-labelled glutamine revealed the essential role of two system A amino acid transporters in glutaminolysis in cancer cell lines with depletion of ASCT2 [58].

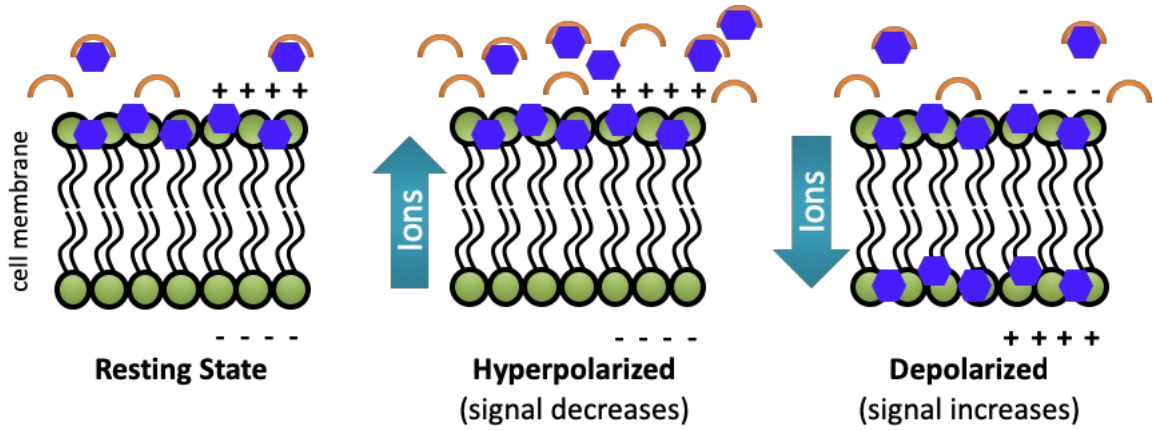

Figure 2.1.1: Principle of membrane potential (FLIPR) assay (Molecular Devices): the voltage-sensitive dye allows the detection of membrane potential changes in the following way. During membrane hyperpolarization, fluorescent signal decreases in intensity as the negatively charged blue dye accumulates outside the membrane (middle). During membrane depolarization, the fluorophore penetrates into the membrane bilayer, increasing in intensity as the dye accumulates inside the membrane (right). Fluorescence is quenched by specific dyes outside the cell (orange half circles).

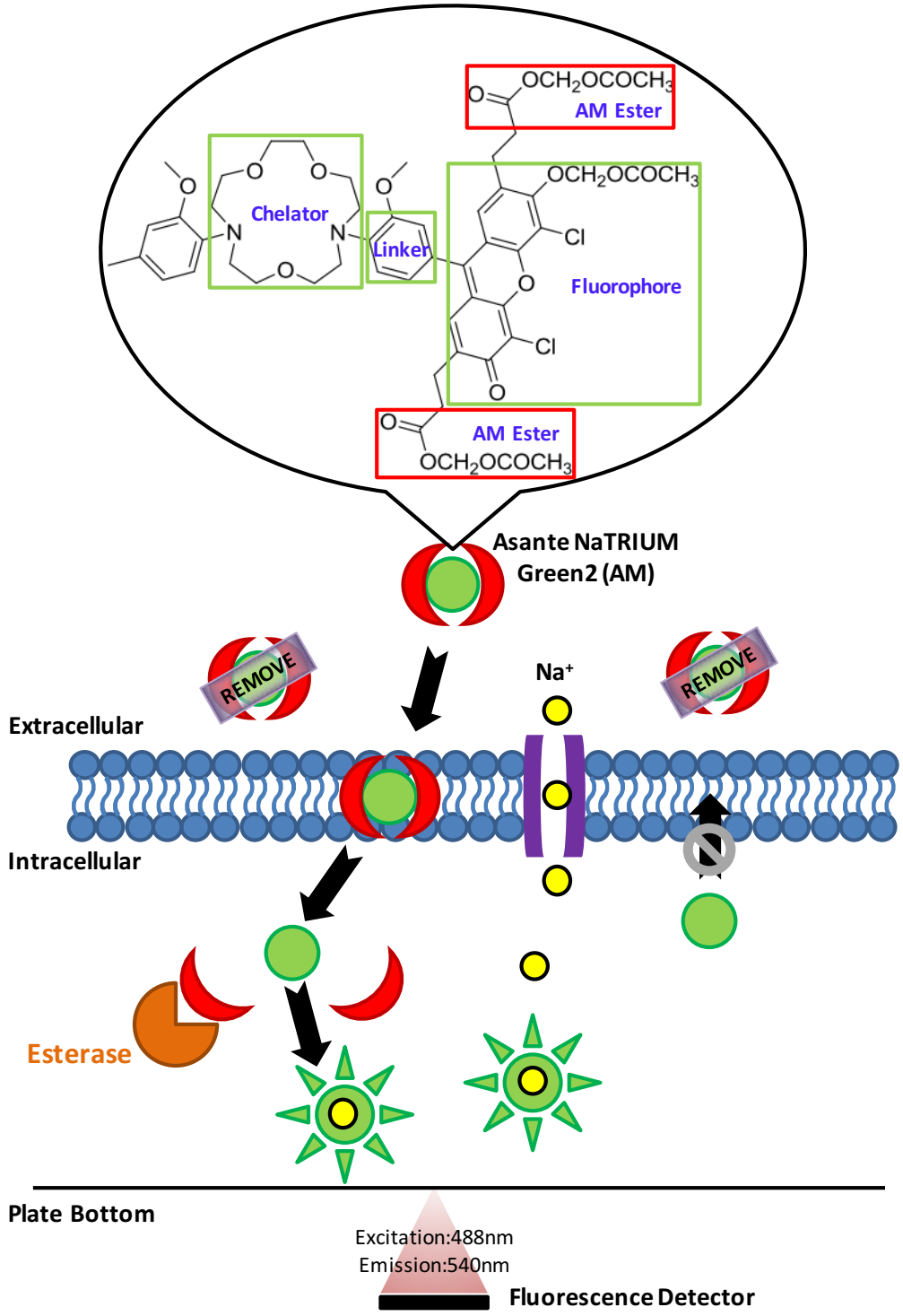

Figure 2.1.2: Principle of sodium dye assay. The acetoxymethyl ester (AM)-ester of Asante NaTRIUM Green 2 (ANG-2) is used to increase the permeability of the dye to the plasma membrane. Once the dye permeates into the cytosol, its acetoxymethyl group is cleaved by intracellular esterases to allow the interaction between the dye and Na^+. Meanwhile, cleavage of the acetoxymethyl group dramatically increases the hydrophilicity of the dye to prevent its leaking out of the cell. The extracellular unloaded dye will be washed away, and the intracellular sodium-bound dye can be detected by a fluorescence detector with the excitation wavelength of 488nm and the emission wavelength of 540nm.

2.2 Materials and Methods

2.2.1 Cell lines and media

A CHO (Chinese Hamster Ovary) Flp-In™ host cell line (CHO parental) and a CHO cell line stably expressing human B^0AT1 (hB^0AT1) and human collectrin (hcollectrin) using a Flp-In™ transfection system (Invitrogen) (CHO-BC) were provided by Sanofi-Aventis Pharmaceutical Company. CHO parental cells were cultured in Ham's F-12 Nutrient Mix GlutaMAX™ medium (Gibco® GlutaMAX™ supplement L-alanyl-L-glutamine dipeptide was used as a replacement of L-glutamine due to higher stability and minimal levels of toxic ammonia) (Invitrogen, #31765035) supplemented with 10% (v/v) heat-inactivated fetal bovine serum (FBS) (Invitrogen, #10082147) and 100µg/mL Zeocin selection antibiotic (Invitrogen, #R250-01), while CHO-BC cells were maintained in the same medium supplemented with 10% (v/v) FBS, and selection antibiotics Hygromycin B (0.33mg/mL, Invitrogen, #10687010) and Geneticin (G418 sulfate) (0.275mg/mL, Invitrogen, #10131035). The Ham's F-12 GlutaMAX™ medium could be replaced by Ham's F-12 medium (Sigma, #N4888) supplemented with 1mM L-alanyl-L-glutamine dipeptide (Sigma, #A8185). CHO-BC cells were not used for radio-labelled substrate uptake assays after passage 10 or in membrane potential assays after passage 15 due to the gradual loss of transport activity.

GP2d (human colon adenocarcinoma cell line), LLC-PK1 (pig kidney epithelial cell line) and MCF-7 (human breast adenocarcinoma cell line) cells were maintained in Dulbecco's Modified Eagle's Medium (DMEM) / Ham's Nutrient Mixture F12 (Sigma, #D8437) supplemented with 10% (v/v) FBS, 1X non-essential amino acids (NEAAs, 1:100 dilution of the original stock solution) (Gibco, #11140) and 2mM L-glutamine. 143B TK^- (human osteosarcoma cell line) cells were cultured in the same medium without the addition of NEAAs. HuH7 (human hepatoma cell line) cells were cultured in MEM GlutaMAX™ (Invitrogen, #41090036), supplemented with 10% (v/v) FBS, 1X NEAAs, as well as 5mM glucose (glucose final concentration was 10mM). HuH7 cells were seeded onto collagen (Sigma, #c4243) – coated dishes to enhance attachment. MDCK (Madin-Daby canine kidney cell line) and Li-7 (human hepatoma cell line) cells were maintained in DMEM / F-12 Ham medium (Sigma, #D8437) supplemented with 10% (v/v) FBS. Li-7 cells were purchased from the Riken BRC Cell Bank (RCB1941), other cell lines were from stocks available in the laboratory.

All cells were maintained in 75cm^2 flasks containing 20mL culture media in a 95% air, 5% CO_2, 37°C humidified incubator. The medium was changed every 3-4 days. Cells were passaged and subcultured once reaching 80-90% confluence. After removing old culture

medium from the flask, cells were detached by addition of 5mL of 0.05% trypsin-EDTA solution (Invitrogen, #25300054) for 3-4min at 37°C. After trypsinization, the detached cells were resuspended in 15mL culture medium, and a total volume of 20mL cell suspension was transferred to a 50mL falcon tube for centrifugation. For cell counting, 100µL cell suspension at this stage was taken out and mixed with same volume of 0.4% (w/v) Trypan Blue solution (Invitrogen, #15250061). After thoroughly mixing the cell suspension with Trypan Blue solution, 20µL of the mixture was added under the cover-slip of a hemocytometer. Four fields were counted under 100x microscope magnification and the total cell number was calculated by the average count per field x 2 (dilution factor of cells in trypan blue mixture) x 10^4 x 20 (total volume of cell suspension). The remaining cell suspension was spun down at 1500rpm for 5min and the supernatant was completely removed. The cell pellet was resuspended in 1mL culture medium, with about $2x10^5$ cells added back to the $75cm^2$ flask for maintenance, while the rest of the cells were seeded out for experiments. For future use, cell pellets were resuspended in freezing medium (90% FBS and 10% DMSO) and gradually chilled to -80°C. After 24hr, cells were transferred to liquid nitrogen for long-term storage.

2.2.2 Transient transfection using Lipofectamine

Before transfection, the cells were seeded in 35mm dishes at a density of $0.5x10^6$ cells/dish and maintained in full culture medium overnight so that cell density reached 70-90% confluence at the time of transfection. The transient transfection with constructs of hB^0AT1, hcollectrin or hHNF1α were conducted in the presence of Lipofectamine™ 2000 (Invitrogen, #11668019), Lipofectamine™ LTX (Invitrogen, #15338100) or Lipofectamine™ 3000 (Invitrogen, #L3000001) according to the manufacturer's instructions. The plasmid constructs were generated previously in our lab [40]. On the day of transfection, the culture medium in each dish was replaced by fresh medium without antibiotics. The transfection reagent was prepared in microtubes as follows:

Tube 1: 10µL Lipofectamine™ 2000 + 240µL Opti-MEM™ medium (Invitrogen, #31985062), or 9µL Lipofectamine™ LTX + 241µL Opti-MEM™ medium;
Tube 2: 2.5µg plasmid DNA + Opti-MEMTM medium, total volume 250µL;

For Lipofectamine 3000:

Tube 1: 5µL Lipofectamine™ 3000 + 120µL Opti-MEM™ medium;
Tube 2: 2.5µg plasmid DNA + Opti-MEMTM medium + 5µL P3000™ Reagent (from the Lipofectamine™ 3000 kit), total volume 125µL;

The mixtures were incubated at room temperature for 5min, followed by adding the content of tube 2 to tube 1. The transfection reagent (500µL, 250µL for Lipofectamine^{TM} 3000) was further incubated at room temperature for 20min, then added drop-by-drop to the 35mm dish with cells and 1.5mL medium (1.75mL for Lipofectamine^{TM} 3000). The transfection medium was replaced by full culture medium at 6hr post-transfection. The cells were incubated for 48hr before further testing or subculture. Maps of constructs used in transient transfection are shown in figure 2.2.1. The map of pcDNA3.1/hB^{0}AT1 is shown in figure 2.2.2C, the expression plasmid of mouse HNF1α integrated in a pCMV6 vector was purchased from Origene (#MC202766).

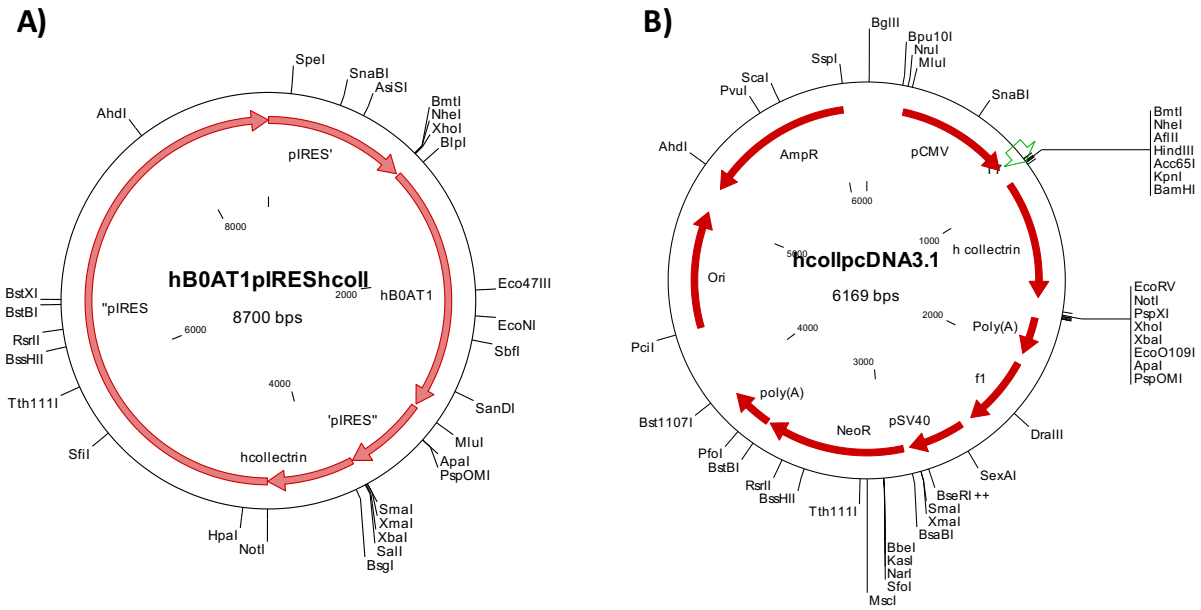

Figure 2.2.1: Maps of constructs. A) pIRES/hB^{0}AT1/hcollectrin; B) pcDNA3.1/hcollectrin.

2.2.3 Generation of pcDNA5/FRT/hB^{0}AT1 construct

The principle of Flp-mediated recombination and the procedures of generating pcDNA5/FRT/hB^{0}AT1 construct is illustrated in figure 2.2.2, while the confirmation of each step by electrophoresis in the generation of the construct is shown in figure 2.2.3. The orientation of the insert (B^{0}AT1) was confirmed by electrophoresis (figure 2.2.3E) and the insertion was confirmed by sequencing (data not shown) using the T7 priming site (bases 863-882) and BGH reverse priming site (bases 1022-1039).

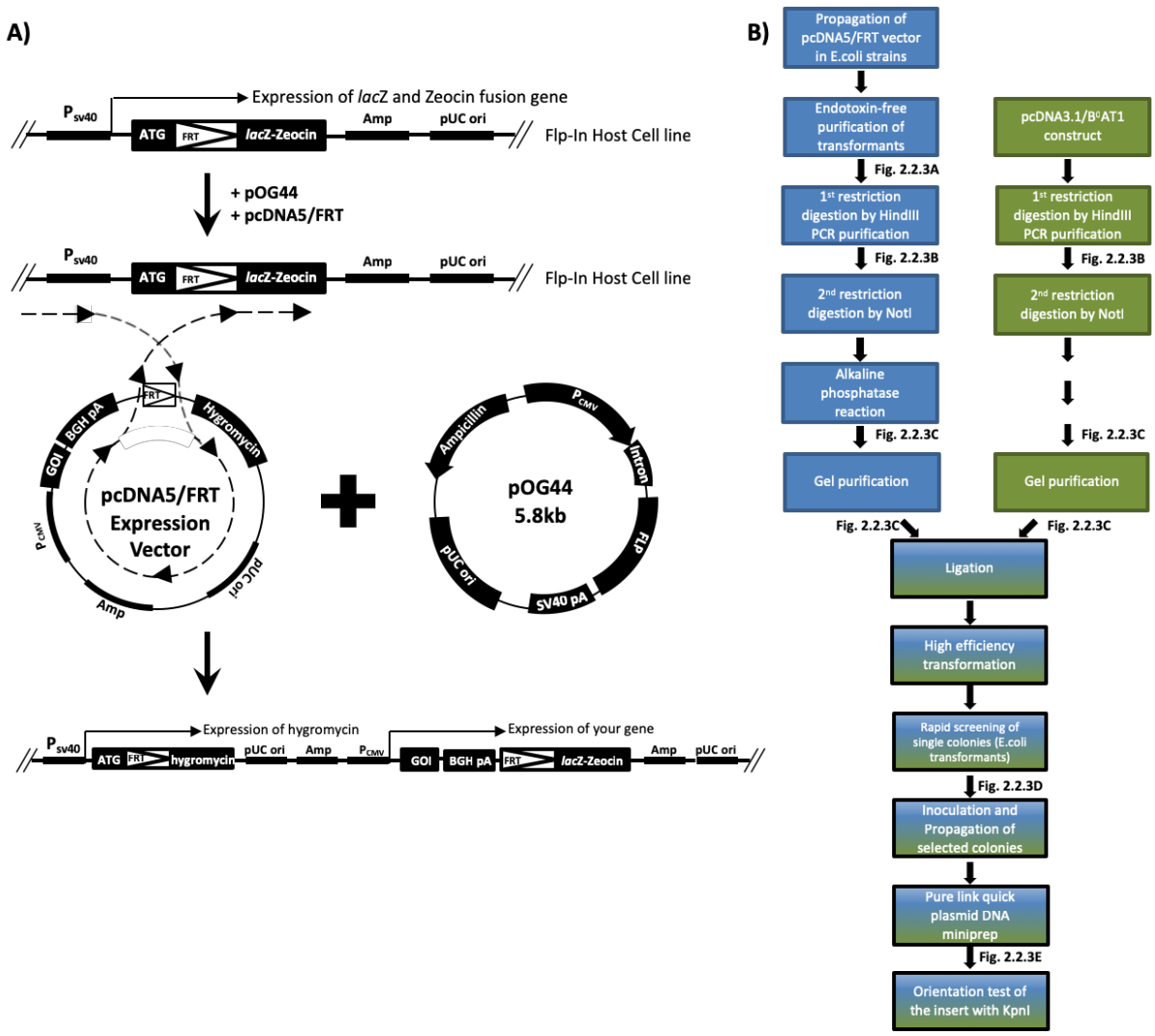
A)
Expression of lacZ and Zeocin fusion gene
Psv40
ATG
FRT
lacZ-Zeocin
Amp
pUC ori
Flp-In Host Cell line
+ pOG44
+ pcDNA5/FRT
pcDNA5/FRT Expression Vector
pOG44 5.8kb
Hygromycin
BGH pA
GOI
Ampicillin
Intron
FLP
SV40 pA
Expression of hygromycin
Expression of your gene
hygromycin
B)
Propagation of pcDNA5/FRT vector in E.coli strains
Endotoxin-free purification of transformants
Fig. 2.2.3A
1st restriction digestion by HindIII PCR purification
Fig. 2.2.3B
2nd restriction digestion by NotI
Alkaline phosphatase reaction
Fig. 2.2.3C
Gel purification
pcDNA3.1/BGAT1 construct
Ligation
High efficiency transformation
Rapid screening of single colonies (E.coli transformants)
Fig. 2.2.3D
Inoculation and Propagation of selected colonies
Pure link quick plasmid DNA miniprep
Fig. 2.2.3E
Orientation test of the insert with KpnI

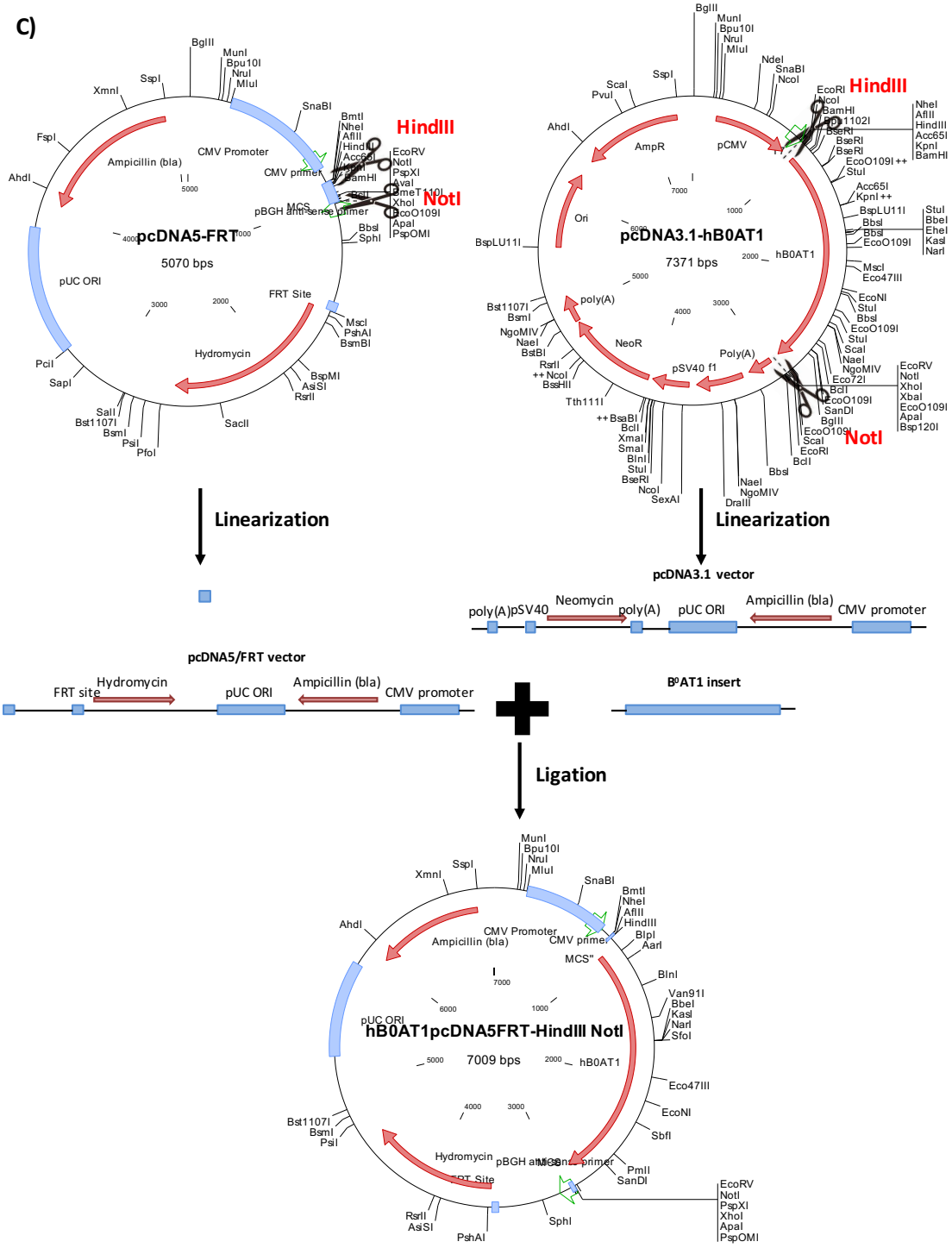

Figure 2.2.2: The principle of Flp-mediated recombination and the procedures of generating the pcDNA5/FRT/hB^{0}AT1 construct. A) The Zeocin-resistant Flp-In™ host cell line has a FRT site inserted just downstream of its SV40 promoter and ATG initiation codon. Co-transfection with plasmids pOG44 and pcDNA5/FRT facilitates recombination of the gene of interest into the FRT site of the host cell line. The pcDNA5/FRT vector carries a hygromycin resistance gene with a FRT site embedded in the 5' coding region but without a promoter and the ATG initiation codon. Meanwhile, the pOG44 plasmid expresses the Flp recombinase, which catalyses a homologous recombination event between the FRT sites both in the genome of the host cell line and in the expression vector. The insertion of the expression vector into the genome at the FRT site results in the relocation of the hygromycin resistance gene behind the SV40 promoter and in frame with the ATG initiation codon and at the same time

relocates the lacZ-Zeocin fusion gene to a site without promoter. Therefore, the successfully transfected clones could be selected by hygromycin resistance. B) The flow diagram of the generation of pcDNA5/FRT/hB^{0}AT1 construct. C) The ligation of the target vector (pcDNA5/FRT) and the insert (hB^{0}AT1) to form the final construct.

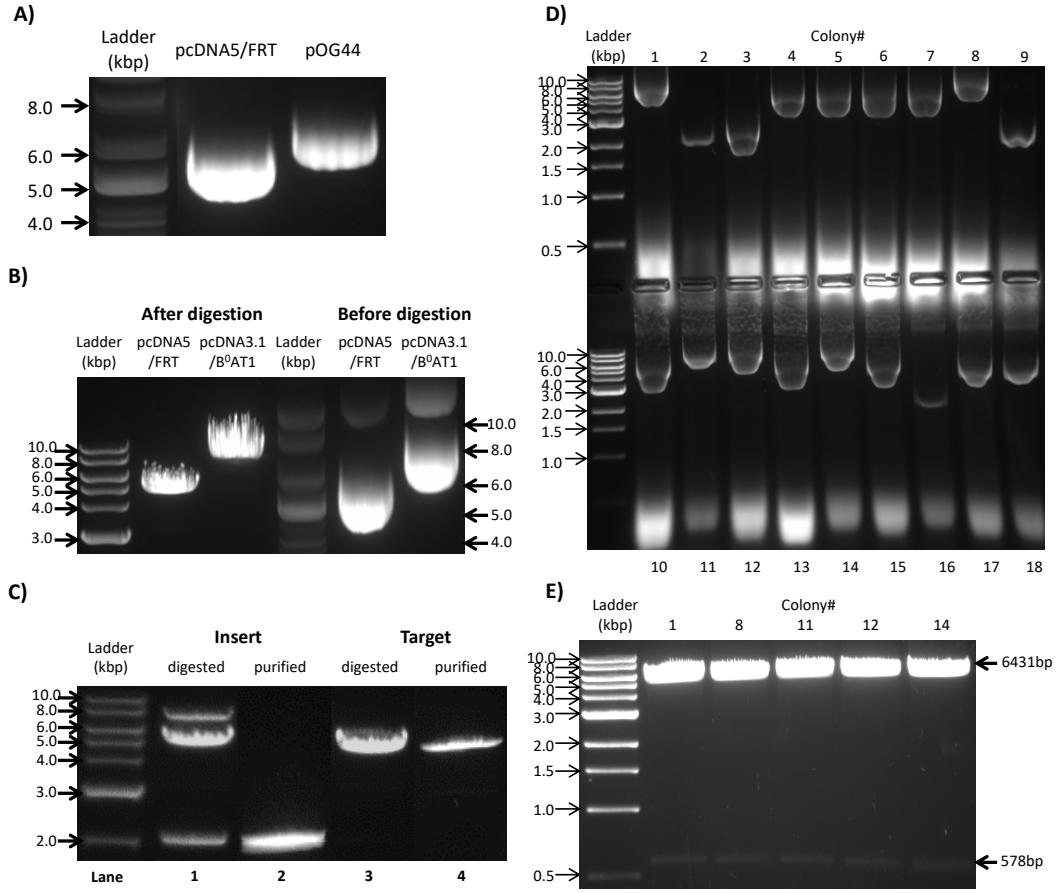

Figure 2.2.3 Generation of pcDNA5/FRT/hB^{0}AT1 construct. A) The purity and integrity of propagated vectors was checked by electrophoresis. 1µg of plasmid DNA was loaded onto a 1% agarose gel. From left to right: supercoiled NEB DNA ladder (BioLabs, N0472s), pcDNA5/FRT vector (5070bp), pOG44 vector (5785bp). B) First restriction digestion of pcDNA5/FRT vector and pcDNA3.1/B^{0}AT1 plasmid by HindIII. The digested products as well as undigested plasmid DNA were run on a 1% agarose gel. The left ladder is a 1kB DNA ladder (BioLabs, N3232), the right ladder is supercoiled NEB DNA ladder. C) Second restriction digestion by NotI. The NotI-digested products were run on a 1% agarose gel, with a small amount for size checking (Lane 1 for pcDNA5/FRT, Lane 3 for pcDNA3.1/B^{0}AT1) and a large amount for gel cutting. The digested products with correct sizes were cut out of the gel, purified and checked on a 1% agarose gel (Lane 2 for pcDNA5/FRT target vector, Lane 4 for B^{0}AT1 insert). D) Rapid screening of E. coli transformants containing the ligated vector and insert on a 1% agarose gel. Expected sizes of the bands: pcDNA5/FRT target vector (5002bp), hB^{0}AT1 insert (2007bp), pcDNA5/FRT/hB^{0}AT1 construct (7009bp). Colony #1, 8, 11, 12, 14 were regarded as complete constructs, whereas colony #2, 3, 9, 16 contained the insert only and colony #4, 5, 6, 7, 10, 13, 15, 17, 18 were vector only. E) Orientation check for the insert by restriction digestion using KpnI. The location of the insert (hB^{0}AT1) in the pcDNA5/FRT/B^{0}AT1 construct is between 969 and 2873 bps. KpnI cuts at 917bp and 1495bp, so the expected sizes of bands are 6431bp and 578bp if the orientation is correct.

The pcDNA5/FRT expression vector and the pOG44 vector were provided with the Flp-In™ transfection system kit (Invitrogen, #K601001). Both vectors were first propagated in a recA1-reduced, endA1-eliminated E.coli strain (NEB 5-alpha Competent E. coli) following NEB C2987H/C2987I high efficiency transformation protocol. To this end, 100ng plasmid DNA was mixed with a tube of thawed competent E.coli cells and incubated on ice for 30min. Then the mixture was heat-shocked at 42°C for 30sec, followed by an incubation on ice for another 5min. To improve recovery of E. coli after transformation, 950µL of SOC medium (Invitrogen, #15544034) was added into the cell-plasmid mixture and mixed thoroughly by shaking at 250rpm and 37°C for 90min. Different volumes (2µL, 5µL, 15µL) of the mixture were spread onto pre-warmed selection LB agar plates and incubated at 37°C overnight. On the following day, single colonies on LB agar plates were picked and propagated by shaking in 5ml LB broth (25g/L) containing 100µg/mL ampicillin selective antibiotic at 37°C for 8hr. For plasmid isolation the starter culture was diluted 1/1000 into 100mL LB broth containing 100µg/mL ampicillin and propagated by shaking at 300rpm and 37°C overnight.

For transfection, the plasmid DNA was purified to Endotoxin-free standard using a Nucleobond Xtra Midi EF kit (Macherey-Nagel, #740420.10) according to the manufacturer's instructions. After overnight incubation, plasmid containing cells were first spun down by centrifugation in two 50mL falcon tubes at 3270 x g and 4°C for 20min. The supernatant was discarded and the pellet was resuspended completely in Resuspension Buffer. The cells were lysed by gently mixing Lysis Buffer into the suspension and incubating at room temperature for 5min. The cell lysate was then neutralized in Neutralization Buffer and incubated on ice for 5min before loading onto the pre-equilibrated NucleoBond Xtra column filter for clarification by gravity flow. After three washes of the column, the plasmid DNA was detached with Elution Buffer and the yield was determined by measuring A_{260} with a NanoDrop™ 1000 microvolume spectrophotometer (Invitrogen). The eluted plasmid DNA was precipitated with isopropanol and collected by centrifugation at 15,000 x g for 30min in a benchtop centrifuge. The precipitates were washed with 70% endotoxin-free ethanol and air-dried at room temperature for 10-15min to remove all ethanol. Finally, the DNA pellet was dissolved in endotoxin-free buffer or water to a final concentration of 0.5-1µg/µL. The final yield was determined with a NanoDrop™ 1000, and the purity and integrity of plasmid DNA was confirmed by electrophoresis using 1% agarose gel.

The Endotoxin-free pcDNA3.1/hB^{0}AT1 construct was generated in our lab previously. The hB^{0}AT1 insert of this construct was cut out and subcloned into the pcDNA5/FRT expression vector from the Flp-In™ transfection system kit using the following strategy. Two restriction

digestions were applied on both pcDNA5/FRT vector and pcDNA3.1/hB^{0}AT1 construct. The first digestion was conducted with HindIII (BioLabs, R0104s) in 50µL 1X NEB buffer2 (BioLabs, R7002s) containing 6µg of pcDNA5/FRT vector or pcDNA3.1/hB^{0}AT1 construct and 40 units of HindIII. The mixture was incubated at 37°C for 4hr and the digested products were checked on a 1% agarose gel to ensure complete digestion. Then the digested products were heat-inactivated at 65°C for 20min and purified using Wizard SV gel and a PCR clean-up system (Promega, A9281). The second digestion was done with NotI (BioLabs, R0189s). The digestion reaction was assembled in a total volume of 50µL 1X NEB Buffer3.1 (BioLabs, B7203s), containing the products from the first digestion, and 40 units of NotI. The mixture was incubated at 37°C for 4hr and the digested products were heat-inactivated at 65°C for 20min. After digestion was completed, Antarctic Phosphatase (BioLabs, M0289s) was used on the target vector (pcDNA5/FRT) to remove 5' phosphoryl groups and prevent its self-ligation. The alkaline phosphatase reaction was conducted by adding 5µL of 10X Antarctic Phosphatase Reaction Buffer and 1.5µL (7.5 units) of Antarctic Phosphatase (BioLabs, M0289s) into the second digestion reaction and incubating at 37°C for 1hr, followed by heat-inactivation at 65°C for 5min. Then the target vector and the insert were run on a 1% agarose gel, with a small amount (about 500ng) used to determine the size and the remaining digestion products used for gel purification. The cut gel was melted by heating at 65°C for 10-20min in chaotropic buffer. The plasmid fragment was purified using a Wizard SV gel and PCR clean-up system (Promega A9281) and checked on a 1% agarose gel. Ligation of the target vector (pcDNA5/FRT) and the insert (hB^{0}AT1) was performed using a Quick Ligation Kit (BioLabs, M2200s). To this end, 50ng of the vector was combined with a 3-fold molar excess of insert, together with 1X Quick Ligation Reaction Buffer and 2µL of Quick T4 DNA Ligase to make a total volume of 20µL. After mixing and collecting the reagents at the bottom of a microcentrifuge tube, the ligation reaction was incubated at room temperature for 30min. The high-efficiency transformation of E.coli was conducted immediately after the completion of ligation using NEB protocol C2987H/C2987I as described above. On the next day, single colonies were selected and spread on agar plates. Plasmid-containing colonies were selected by a rapid screening process as follows. The smears of the colonies were first collected in microcentrifuge tubes and resuspended in 40µL of 10mM EDTA (pH8.0). The suspension was then incubated at room temperature for 5min in the presence of 50µL of 2X cracking buffer (1mL of 2X cracking buffer contained 0.2g sucrose, 50µL of 10% SDS, 40µL of 5M NaOH), followed by incubation on ice for 5min in the presence of marker mix (1.5µL of 4M KCl, 1µL of 0.4% Bromophenol blue, and 10µL of 10mM EDTA). The samples were spun down in a benchtop centrifuge at top speed (13,200rpm) for 3min and 25-50µL of supernatant was loaded on a 1% agarose gel. The

selected colonies were propagated in LB broth (25g/L) containing 100 µg/ml ampicillin by shaking at 300rpm and 37°C overnight and the plasmids purified using a PureLink Quick Plasmid DNA miniprep kit (Invitrogen, K2100-10) according to the manual. Finally, the orientation of the insert was tested by cutting the construct with KpnI (BioLabs, R0142s). The restriction digestion was done in 50µL 1X NEB Buffer I containing 1µg of the plasmid DNA and 2µL of KpnI (20 units) at 37°C for 1.5hr. The final digestion products were run on a 1% agarose gel.

Five pre-selected colonies were sequenced to confirm the insertion of B^0AT1. The purified plasmid DNA was used as a template in the cycle sequencing reaction containing 2µL Big Dye Terminator (BDT), 3µL of 5x sequencing buffer, 3.2pmol T7 primer (5'-TAATACGACTCACTATAGGG-3') or BGH reverse primer (5'-TAGAAGGCACAGTCGAGG-3'), 300ng template, ddH_2O to a final volume of 20µL. The sequencing reaction was performed under the following conditions:

1. Incubate at 94°C for 5 min---Initialization
2. Incubate at 96°C for 10 sec---Denaturation
3. Incubate at 50°C for 10 sec---Annealing
4. Incubate at 60°C for 4 min---Extention/Elongation
   Repeat step 2-4 for 30 cycles
5. Incubate at 60°C for 4 min ---Final Elongation
6. Hold at 22°C

For purification, the 20µL cycle sequencing reaction was mixed with 2µL of 3M NaAcetate (pH4.6 or pH5.2), 50µL of Ethanol (100%), and incubated at room temperature for 15min. The products were then pelleted by centrifugation at maximum speed (16,000 x g) for 20min in a benchtop centrifuge. The pellets were washed twice with 70% Ethanol, 250µL/time. After removing the ethanol, the pellets were air-dried and stored in a -20°C freezer until being delivered to Biomolecular Resource Facility (BRF) in the Australian National University for sequencing.

2.2.4 Generation of CHO cell line stably expressing hB^0AT1 and hcollectrin

The CHO Flp-In™ host cell line with a single integrated FRT (Flp Recombination Target) site was purchased from Invitrogen (R758-07). The host cell line was maintained in Ham's F-12 medium (Sigma, #N4888) supplemented with 1mM Ala-Gln peptide (Sigma, #A8185), 10% (v/v) FBS and 100µg/ml Zeocin. The sensitivity of the host cell line to Hygromycin B

(Invitrogen, #10687010) was measured by IncuCyte Live Cell Analysis (Essen BioScience, Inc.) to determine the concentration of the antibiotic used for selecting successfully transfected colonies. To this end, the host cells were seeded at a density of 2000 cells/well in 200µL suspension in a 96-well plate. The cells were allowed to settle down in full culture medium for 6hr before exposing them to different concentrations of Hygromycin B (0, 50, 100, 200, 400, 600, 800µg/ml), 12 wells/concentration. The confluence of each well was scanned by IncuCyte every 3hr, and the medium was refreshed every 2-3 days to ensure sustained pressure from the antibiotics in the medium. The growth curve, depicted as percentage of confluence over time, was generated at the end of the incubation and the concentration for selection was determined as the minimal concentration (400µg/ml) that prevented growth within the timeframe required for the control cells to reach confluence. The Flp-In host cells were then transfected with pcDNA5/FRT/hB^{0}AT1 construct using Lipofectamine^{TM} 2000 in the way described above. The pOG44 plasmid was co-transfected with the expression construct at a ratio of 9:1 (w/w), i.e. a total of 22.5µg pOG44 and 2.5µg pcDNA5/FRT/hB^{0}AT1 was transfected together. 6hr post transfection, the transfection medium was replaced with culture medium without any antibiotics, and 48hr after transfection, the cells were split and seeded onto 10cm plates at a density of 8.8x10^5 cells per plate (10% confluence) containing medium with the preselected concentration (400µg/ml) of Hygromycin B. The medium with Hygromycin B was changed once every 2-3days until clones of hygromycin-resistant cells were identified. Then the hygromycin-resistant foci were picked from the 10cm plates and transferred to 24-well plates. The foci were first located and marked under a microscope. After removing the culture medium, the foci were enclosed by cloning cylinders (Sigma, c1059), detached by addition of 100µl of 0.05% trypsin-EDTA inside the cylinders for couple of minutes, and then transferred into sterilized microcentrifuge tubes containing 200µl culture medium. The cells were pelleted by centrifugation at 500 x g for 5min in a benchtop centrifuge, and transferred into 24-well plates with full culture medium containing Hygromycin B for propagation. When confluent in 24-well plates, the cells were transferred to 25cm^2 or 75 cm^2 flasks for further propagation. Once growing to a larger cell number, B^{0}AT1 expression was checked at protein and mRNA level before performing the co-transfection with collectrin.

After successful transfection with B^{0}AT1, CHO cells were tested for their sensitivity to Geneticin (G418 sulfate, Invitrogen, #10131035) by IncuCyte technology to determine the concentration (800µg/ml) to be used for selection of collectrin-transfected cells. Collectrin was subcloned into pcDNA3.1 which carries a Geneticin resistance gene. The pcDNA5/B^{0}AT1 transfected cells were seeded into 35mm dishes and maintained overnight in full medium

containing 400µg/ml Hygromycin B. The transfection with 2.5µg pcDNA3.1/hcollectrin construct was performed in the presence of Lipofectamine™ 2000 in the way described above. Transfection medium was replaced with full medium containing 400µg/ml Hygromycin B 6hrs after transfection, and $8.8x10^5$ cells were seeded into 10cm plates with culture medium containing the preselected concentration (800µg/ml) of G418 48hrs post transfection. The medium was refreshed once every 2-3days until clones formed. Hygromycin-and G418-resistant foci were further propagated for testing expression of B^0AT1 and collectrin by western blot as well as the function of the transporter by radioactive uptake assays.

To select cells with the highest transport activity of B^0AT1 in co-transfected CHO cells, cells were subcloned by limiting dilution and propagated from single clones as outlined in the following. After trypsinization, cells were pelleted by centrifugation at 500 x g for 5min, and the total number was counted by hemocytometer. The cells were first diluted to $1x10^6$cells/mL in the suspension, and were further diluted with full culture medium to 0.5 cell/200µL. Then 200µL cell suspension was distributed into each well of a 96-well plate to maximize the likelihood of single clones in the wells. When seeing a single colony growing in the well, the cells were transferred to 6-well plates, then to 25cm^2 and 75 cm^2 flasks for further propagation until the cell number was high enough for testing.

2.2.5 Radioactive Uptake Assay

Hank's buffer with or without sodium was prepared beforehand using the following recipe:

Hank's buffer + Na^+ (*pH 7.5) containing:

Compound	Final concentration (mM)	Powder concentration (g/L)
NaCl	136.6	8
KCl	5.4	0.4
KH_2PO_4	0.44	0.06
$MgCl_2$.6H2O	0.5	0.1
$MgSO_4$.7H2O	0.4	0.1
HEPES	10	2.38
$Na_2HPO_4.2H_2O$	2.7	0.48
#$CaCl_2$	1	100mM stock solution prepared
#D-glucose	5	1M stock solution prepared

Hank's buffer - Na^+ (*pH 7.5) containing:

Compound	Final concentration (mM)	Powder concentration (g/L)
N-Methyl-D-Glucamine (NMDG)	137	26.7
KCl	5.4	0.4
KH_2PO_4	0.44	0.06
$MgCl_2$.6H2O	0.5	0.1
$MgSO_4$.7H2O	0.4	0.1
K_2HPO4	2.7	0.47
HEPES	5	1.23
#$CaCl_2$	1	100mM stock solution prepared
#D-glucose	5	1M stock solution prepared

*The pH value was adjusted to 7.5 by 5M NaOH for Hank's + Na^+ buffer, and by 5M HCl for Hank's - Na^+ buffer. After adjusting the pH, the buffer was autoclaved for storage.
#Before using the buffer for experiments, 1mM $CaCl_2$ and 5mM D-glucose was added.

For uptake experiments the cells were seeded at a density of 1-2x10^5 cells/dish in 35mm dishes and grown in culture medium for 2-3days until reaching 80-90% confluence. To initiate the assay, the medium was removed and the cells were pre-washed with 2mL Hank's +/- Na^+ buffer for 3 times. The cells were then incubated with 1mL Hank's +/- Na^+ buffer containing radio-labelled substrates (L-[U-^{14}C]leucine (11.1 GBq/mmol), L-[U-^{14}C]isoleucine (11.1 GBq/mmol) or L-[U-^{14}C]glutamine (10 GBq/mmol) at a final concentration of 100 µM in a 37°C water bath for 6min. For pharmacological tests, substrate analogues and related chemical compounds were added to the transport buffer before the experiment at the concentration indicated in figures or tables. All radioisotopes were all purchased from Perkin Elmer. After the incubation, the buffer was immediately removed and the transport was terminated by 3 washes with 2mL ice-cold Hank's + Na^+ buffer. The cells were then harvested with 500µL of 0.1M HCl and scraped off the dishes using a scraper. An aliquot of 400µL cell lysate was added into a vial and mixed with 2.5-3mL scintillation fluid for counting of radioactivity in a scintillation counter, while the rest of the lysate was used for Bradford assay to measure the protein amount.

2.2.6 Membrane Potential Assay

Membrane Potential Assay was performed with the FLIPR® kit ordered from Molecular Devices (R8042 BLUE DYE). Before the assay, the voltage-sensitive blue dye in each vial was dissolved in 10mL of 1X assay buffer provided in the kit to make the dye-loading buffer.

Aliquots of the loading buffer could be stored at -20°C for up to 5 days. The cells were first seeded in black-wall 96-well plates (Corning, #3603) at a density of 60,000 cells/well and grown overnight. On the following day, the culture medium was removed and the cells were washed three times with 200µL/well of Hank's + Na^+ buffer before the addition of 100µl Hank's + Na^+ buffer containing test compounds and 100µl dye-loading buffer into each well. The cells were then incubated at room temperature for 30min and the fluorescence signal was detected by a TECAN INFINITE M1000 PRO Plate Reader. The fluorescence signal was read every 10sec for each cycle, with three cycles occurring before the addition of substrate and 10 cycles after the addition. The substrates were dissolved in Hank's +Na^+ buffer as stock solutions and 50µL was injected either manually or automatically to yield the final concentration as indicated in the figures. 50µL Hank's +Na^+ buffer without substrates was injected as a negative control. After injection, the plate was shaken in the machine for mixing. The signal was detected from the bottom of the plate, with an excitation wavelength of 530nm and an emission wavelength of 565nm (bandwidth 10nm). The program was set up in iControl as follows:

- ✓ Choose kinetic---kinetic cycle---kinetic condition: Execute at cycle 4; Number of cycles: 13; kinetic interval: 10sec
- ✓ Choose Actions---Injection. Injector A/B, volume 50µl, speed 100µl/sec, tick 'refill speed equals to injection speed'. Refill mode: standard
- ✓ Shaking after injection
- ✓ Choose Measurements---Fluorescence Intensity (well-wise):
- Wavelength/Excitation: 530nm; bandwidth: 10nm
- Wavelength/Emission: 565nm; bandwidth: 10nm
- Mode: BOTTOM
- Gain: Manual 70
- Flashes: Mode 1 [400Hz]: 50
- Settle time: 10ms

2.2.7 Sodium Dye Assay

Sodium dye assay was performed with the Na^+-sensitive fluorescent dye Asante NaTRIUM Green-2 (ANG-2) AM (Abcam, ab142802), and the protocol of the assay was downloaded from TEFLabs [178]. The stock solution of the dye was prepared by adding 460µL of anhydrous dimethylsulfoxide (DMSO) to 500µg of the powder to yield a final concentration of 1mM. The stock solution was divided into aliquots of 50µL and stored at -20°C for future use.

For the experiment, an aliquot of the stock was brought to room temperature, and then diluted to twice the original volume with 20% (w/v) Pluronic F-127 in DMSO (Invitrogen, P3000MP) to generate a working solution. The cells were seeded in a black-wall 96-well plate (Corning, #3603) at a density of 60,000 cells/well and grown in full culture medium overnight. For the sodium titration experiment, conditions were used as provided by TEFLabs [179] as follows. After removing the medium, the cells in each well were pre-loaded with 200µL fresh culture medium without antibiotics, supplemented with 2µM ANG-2 and 0.0075% (w/v) Pluoronic F-127 in the 37°C incubator for 60min. After removing the dye-loading solution, cells were washed three times with Hank's -Na^+ buffer and incubated in the same buffer during the assay. After recording the baseline readings by a TECAN INFINITE M1000 PRO Plate Reader, Monensin or Gramicidin A were added from a 1mM stock solution to generate a final concentration of 5µM and 2.5µM, respectively. This manipulation depletes cells of Na^+. When the fluorescent signal became stable, the extracellular Na^+ concentration was raised by the addition of NaCl to various levels (5, 15, 45, 145mM), with 145mM KCl added in the end. The assay was varied to optimise it for compound screening using CHO-BC cells as follows. After overnight growth in 96-well plates, the culture medium was removed and the cells were washed with Hank's buffer for three times before the addition of 200µL Hank's buffer containing 0.2-1% ANG-2/Pluronic F-127 working solution into each well. The cells were then incubated in dye loading buffer at room temperature or in the 37°C incubator for 10-30min. After the incubation, the cells were washed twice with Hank's buffer to remove the extracellular unloaded dye. Then 200µL Hanks's buffer was applied to each well, and the fluorescent signal was read by a TECAN INFINITE M1000 PRO Plate Reader before and after the manual addition of Na^+ and amino acid substrates. The optimized condition is highlighted in table 2.3.2 and was used in the subsequent experiments. The signal was detected from the bottom of the plate, with an excitation wavelength 488nm and an emission wavelength 540nm (bandwidth 10nm).

2.2.8 Whole Membrane Preparation of proteins from adherent cell culture

Cells cultured in a 60mm dish were washed 3 times with ice-cold 5mL pre-lysis PBS buffer (137mM NaCl; 2.7mM KCl; 5mM Na_2HPO4; 0.9mM $CaCl_2$; 0.5mM $MgCl_2$; pH7.4). The cells were then scrapped off the bottom of the culture dish with 1mL pre-lysis PBS buffer and transferred into a microcentrifuge tube. After centrifugation at 500 X g (2300rpm) in a benchtop centrifuge for 5min, the supernatant was discarded and the cell pellet was resuspended with 1mL hypotonic buffer (10mM HEPES pH8.0; 15mM KCl; 2mM $MgCl_2$; 0.1mM EDTA) and incubated on ice for 5min. The cells were homogenised by 30-35 strokes

using a 1mL syringe and needle (25 Gauge x 5/8”), followed by centrifugation at 600 X g (2500rpm) for 10min to remove the cell nuclei. Aliquots (800-900µL) of the supernatant from each sample were transferred to an ultra-centrifuge tube and spun down at 150,000 X g (65,000rpm) and 6°C for 60min to isolate the membranes. The pellet was resuspended in 50µl of 5mM L-glycine and vortexed vigorously until completely dissolved. Total protein amount was quantified via Bradford assay using a 1:10 dilution of the sample, and equal amounts of protein were loaded for SDS-PAGE.

2.2.9 Surface Biotinylation

The cells of a 60mm dish were washed 3 times with ice-cold pre-lysis PBS buffer (137mM NaCl; 2.7mM KCl; 5mM Na_2HPO4; 0.9mM $CaCl_2$; 0.5mM $MgCl_2$; pH 8). The cells were then biotinylated by incubating with 2ml pre-lysis PBS buffer supplemented with 0.5mg/mL Sulfo-NHS-LC-Biotin (Invitrogen, #B6353) at room temperature on a slow shaker for 30 min. After incubation, the cells were washed 3 times with ice-cold pre-lysis PBS containing 100mM glycine to quench the unbound reagent, and were then collected in 1mL lysis buffer (150mM NaCl; 20mM Tris-HCl, pH7.6; 1% Triton X-100) by scraping and transferring into a microcentrifuge tube. The cell lysate was incubated on ice for 1.5hr with occasional inversions, followed by a centrifugation at 11000rpm for 10min in a benchtop centrifuge. The supernatant was transferred to another microcentrifuge tube. The protein amount was determined by Bradford assay using a 1:10 dilution of the sample, and the same volume of protein sample (approximately 75µg) was added to 50µL streptavidin beads (high capacity streptavidin agarose Resin, Invitrogen, #20357). The sample-beads mixture was incubated at 4°C on a rotator overnight. On the following day, the mixture was washed with 1mL lysis buffer for 5 times, and then resuspended in 4x sample buffer for SDS-PAGE.

2.2.10 Bradford assay

Different concentrations (50, 75, 100, 200, 300, 400, 500µg/mL) of bovine serum albumin (BSA, Sigma, #A4612) were used to generate a standard curve. An assembly of 30µL protein sample or BSA standard and 270µL of Bradford assay reagent was added into each well of a 96-well plate. After 5 minutes, the absorbance was measured at 595nm with a TECAN INFINITE M1000 PRO Plate Reader and the protein amount was calculated based on the standard curve.

2.2.11 SDS-Polyacrylamide Gel Electrophoresis (SDS-PAGE) and Western Blot Analysis

The protein samples were mixed with (4x) NuPAGE LDS sample buffer (Invitrogen, #NP0008) and (10x) NuPAGE Reducing Agent (Invitrogen, #NP0004) to give a 1x final concentration. Cell homogenate or whole membrane preparation samples were incubated at 70°C for 10min and surface biotinylation samples were heated to 95°C for 5min, before separating by 4-12% SDS-PAGE (Invitrogen, #NP0321). SeeBlue^{TM} Plus2 pre-stained protein standard (Invitrogen, #LC5925) was used to estimate molecular weights. The electrophoresis took about 45min at 150-180 volts.

The separated proteins on the gel were transferred onto a 0.45μm nitrocellulose membrane (GE Healthcare, #10600003) at 100 volts for 120min using a wet transfer system (Bio-Rad) with transfer buffer (25mM Tris Base, 192mM glycine, 20% methanol). After transfer, the membrane was soaked in 5% (w/v) skimmed milk dissolved in 1x PBST (137mM NaCl, 2.7mM KCl, 5mM Na_2HPO4, PH7.4, 0.1% Tween 20) at room temperature for 1hr on an orbital shaker to block non-specific binding sites, and then stored at 4°C overnight. On the following morning, the membrane was washed three times with 1xPBST buffer and incubated with a primary antibody solution at room temperature for 2hr, followed by an incubation with the secondary antibody solution at room temperature for 1hr. Both primary and secondary antibodies were diluted in a PBST buffer containing 2% membrane blocking agent (GE Healthcare, #RPV2125V). Three washing steps with 1xPBST buffer were applied after the incubation with each antibody. To visualize the bands of interest, the blot was evenly covered by western HRP substrate (Millipore HRP substrates Luminata Forte) and luminescence was imaged using a Fusion SL Gel Chemiluminescence Documentation System 2012(Vilber Lourmat/Peqlab).

Table 2.2.1: Antibodies used in western blot

Primary Antibody	**Source**	**Dilution**	**HRP-conjugated secondary antibody**	**Band Size**
Anti-mouse B^0AT1	Customized, Pineda Antibody Service	1/2000-1/3000	donkey anti-rabbit IgG	64kDa
Anti-mouse collectrin	R&D Systems, AF4965	1/3000-1/5000	donkey anti-sheep IgG	43kDa
Anti-human β-actin	Abcam, ab8227	1/2000-1/3000	donkey anti-rabbit IgG	47kDa

Anti-human ACE2	Abcam, ab15348	1/500- 1/2000	donkey anti-rabbit IgG	97kDa

2.2.12 RT-PCR

Total RNA Isolation NucleoSpin RNA II Kit (Machery-Nagel) was used to extract RNA for RT-PCR according to the manufacturer's protocol. In brief, the cells were maintained in full culture medium in 60mm dishes until 80-90% confluent. After removing the culture medium, the cells were lysed by thoroughly mixing with 700µL Buffer RA1 and 7µL β-mercaptoethanol. The lysate was then pushed through a NucleoSpin Filter into a collection tube by centrifugation at 11,000 x g for 1min in a benchtop centrifuge. After adding an equal amount of 70% Ethanol to the sample, the RNA was bound to a NucleoSpin RNA II column. Then 350µl Membrane Desalting Buffer was added to desalt the silica membrane, and the flow-through was discarded after centrifugation at 11,000 X g for 1min. DNA was digested by a mixture of 10µL reconstituted rDNase and 90µl Reaction Buffer directly added onto the centre of the silica membrane of the RNA column, followed by an incubation for 20 min at room temperature. The membrane was then washed with buffer RA2 once and buffer RA3 twice, and dried completely. Finally, RNA was eluted in 60ul RNase-free water and RNA concentration was measured by NanoDrop™ 1000 microvolume spectrophotometry.

The SuperScript™ II Reverse Transcriptase (RT) (Invitrogen, #18064014) was used for cDNA synthesis. An amount of 2µg total RNA from each extraction was used as the template for reverse-transcription in a 20µL reaction. The RNA template was first mixed with 1µL random primers (Invitrogen, #48190011), 1µL of 10mM dNTPs (a mixture of dATP, dCTP, dGTP and dTTP from a dNTP set, Invitrogen, #10297018) as well as DNase-free RNase-free H_2O to generate a total volume of 12µL. The mixture was heated to 65°C for 5min and then quickly chilled on ice. After adding 4µL of 5x First-strand buffer, 2µL of 100mM DTT provided with the RT kit, together with 1µL of RNaseOUT™ Recombinant Ribonuclease Inhibitor (Invitrogen, #10777019), the mixture was incubated at 25°C for 2min. Finally, 1µL (200 units) of the SuperScript™ II Reverse Transcriptase was added into the reaction, then the mixture was incubated at 25°C for 10min, followed by an incubation at 42°C for 50min. The reaction was terminated by heating at 70°C for 15min.

The PCR reaction was set up to a final volume of 50µL by assembling 5µL of 10x PCR buffer (containing $MgCl_2$), 1.5 Unit Taq DNA polymerase provided in a DNA polymerase kit (Invitrogen), 1µL of 10mM dNTPs, 0.5µL Forward Primer (10µM stock), 0.5µL Reverse

Primer (10µM stock), 1µL cDNA template and ddH_2O to complete the volume in a PCR tube. Sequence of primers for human B^0AT1 and human collectrin (Proligo) are listed in the appendix. Actin (Gibco) and Clathrin (Sigma) were used as housekeeping genes.

The PCR program was set as follows:

1. Incubate at 94°C for 3 min---Initialization
2. Incubate at 94°C for 30 sec---Denaturation
3. Incubate at 55°C for 1 min---Annealing
4. Incubate at 72°C for 1 min---Extention/Elongation
   Repeat step 2-4 for 30 cycles
5. Incubate at 72°C for 1 min---Final Elongation
6. Hold at 20°C

2.2.13 TAE-Agarose gel electrophoresis

For agarose gel electrophoresis, 1.5% (w/v) Agarose (Melford) was dissolved either in 1x TAE buffer (40mM Tris-acetate, 1mM EDTA, pH 8) or in SYBR™ Safe DNA Gel Stain in 1x TAE (Invitrogen, #S33111) by heating in the microwave oven for approximately 2min. The melted agarose solution was poured onto the casting tray and allowed to set. RT-PCR products were mixed with 6x sample loading buffer (50% (v/v) glycerol, 0.1M EDTA (pH 8), 1% (w/v) SDS, 1mg/mL bromophenol blue, 1mg/mL xylene cyanol) at a ratio of 5:1, and loaded alongside a 100bp DNA ladder (New England Biolabs). Agarose gels were run horizontally in 1x TAE buffer at 100 volts for 40-50 minutes. After running, if not prepared in SYBR™ Safe DNA Gel Stain, the gel was stained in Ethidium Bromide (0.5µg/mL in 1X TAE buffer) for 15-30min and DNA was detected under UV light.

2.2.14 Statistical Analysis

Results are expressed as means ± standard deviations. Data were analysed by one-way analysis of variance, ANOVA, followed by Bonferroni correction for pair-wise comparisons in larger samples, or by two-tailed paired T-test using GraphPad Prism 6.0. Significance was assigned at $p< 0.05$. In figure legends, n indicates the number of replicates in each experiment, whereas e indicates the number of independent repeats of the experiments.

2.3 Results

The following sections describe several strategies and attempts to generate a cell line that expresses B^0AT1 plus one of its ancillary protein either heterologously or endogenously, as a tool to identify new inhibitors for the transporter and to develop high-throughput screening assays.

2.3.1 CHO-cells expressing B^0AT1 and collectrin

Sanofi Aventis provided us with six clones of CHO cells stably expressing B^0AT1 and collectrin using the Flp-In™ transfection system, as well as their parental cells for functional testing and characterisation. The best performing clone (Clone #1), will be called CHO-BC (B^0AT1+collectrin) from now on. Clone #1 was chosen based on the following reasons: 1) B^0AT1 and collectrin were abundantly and simultaneously detected at the surface of the membrane of CHO-BC cells, but not of CHO parental cells (figure 2.3.1A), using whole membrane preparation and surface biotinylation. Notably, in the surface biotinylation sample of CHO-BC cells, an additional B^0AT1 immunoreactive band just above the 98kDa protein marker was observed. It may represent an SDS resistant B^0AT1 dimer, or more likely an SDS resistant heterodimer formed between B^0AT1 (64kDa) and collectrin (43kDa). 2) B^0AT1 was detectable in all 6 clones of CHO Flp-In B^0AT1 + collectrin cells, however, collectrin was only detectable in membrane preparations of CHO-BC, clone #2 and #4 (figure 2.3.1A, B). Above all, CHO-BC was the best clone with regard to the protein level of B^0AT1 and collectrin at the cell surface (figure 2.3.1 B/C). 3) The uptake of radio-labelled substrate by transporter-expressing cells is the most robust way to measure transport activity, and the BCAA isoleucine is a preferred substrate of the B^0AT1 transporter. Hence, I measured the uptake of 100µM ^{14}C-labelled isoleucine by CHO-BC, CHO parental, clone #2 and #4 cells over a 6-minute time frame (figure 2.3.1D). In the parental cells, uptake of isoleucine was entirely Na^+-independent, thus, any functional expression of B^0AT1 should induce Na^+-dependent isoleucine uptake. CHO-BC cells had the highest sodium-dependent isoleucine uptake, which was incidentally a similar level to the sodium-independent isoleucine uptake by the endogenous transporters (most likely by the hamster isoform of LAT2 in CHO cells). Clone #2 also had some sodium-dependent isoleucine uptake, but its level was much lower as compared to CHO-BC cells, whereas there was nil net uptake in CHO parental cells and clone #4. The abundance of B^0AT1 expression at the membrane was positively correlated to the transport activity, i.e. less sodium-dependent isoleucine uptake was seen in clones (#2 and #4) with less B^0AT1 in whole membrane proteins. 4) As a symporter of amino acid and one sodium ion, the transport of

amino acid substrate by B^0AT1 is electrogenic and will cause membrane depolarization due the simultaneous intake of Na^+, which could be recorded by the fluorescence-based membrane potential assay. Figure 2.3.1E showed a large depolarization peak in CHO-BC cells induced by the addition of 1.5mM isoleucine to the buffer, while depolarization was neither observed in CHO parental cells, suggesting that the endogenous transport activity was electroneutral, nor in CHO-BC cells without isoleucine added, consistent with the co-transport of AA substrate and one sodium ion. This was further confirmed by a similar response to 1.5mM leucine, another preferred substrate of B^0AT1 (figure 2.3.1F). It is noteworthy that a small peak was induced by leucine, but not by isoleucine, in CHO parental cells, suggesting that isoleucine might be a more selective substrate for B^0AT1 in CHO cells. The functional assays also indicated that CHO-BC was the preferred cell line for the study of B^0AT1.

However, one major problem of CHO-BC cells was the gradual decrease of B^0AT1 activity after passaging. Radioactive substrate uptake assays demonstrated a steady drop of Na^+-dependent isoleucine uptake after passage 3, whereas the endogenous Na^+-independent isoleucine uptake was unaffected by passaging (figure 2.3.2). Hence, we only used CHO-BC cells of passage numbers < 10 in the uptake assay. One possibility for the decline of B^0AT1 transport activity over time is the osmotic load that the transporter imposes on the cells. The cotransport of sodium may increase internal osmotic pressure and subsequently down-regulate sodium transport via B^0AT1 (Na^+ feedback inhibition), as previously shown by the epithelial Na^+ channel ENaC [180]. Moreover, the osmotic imbalance has been shown to cause cell viability change, which could be improved by the inclusion of extracellular osmotic regulator such as sucrose, which is mostly membrane impermeable [181]. To test this hypothesis, we added sucrose to the media and measured B^0AT1 activity and cell growth. However, addition of sucrose resulted in the deterioration rather than improvement of the transport activity or cell growth (figure 2.3.3A&B).

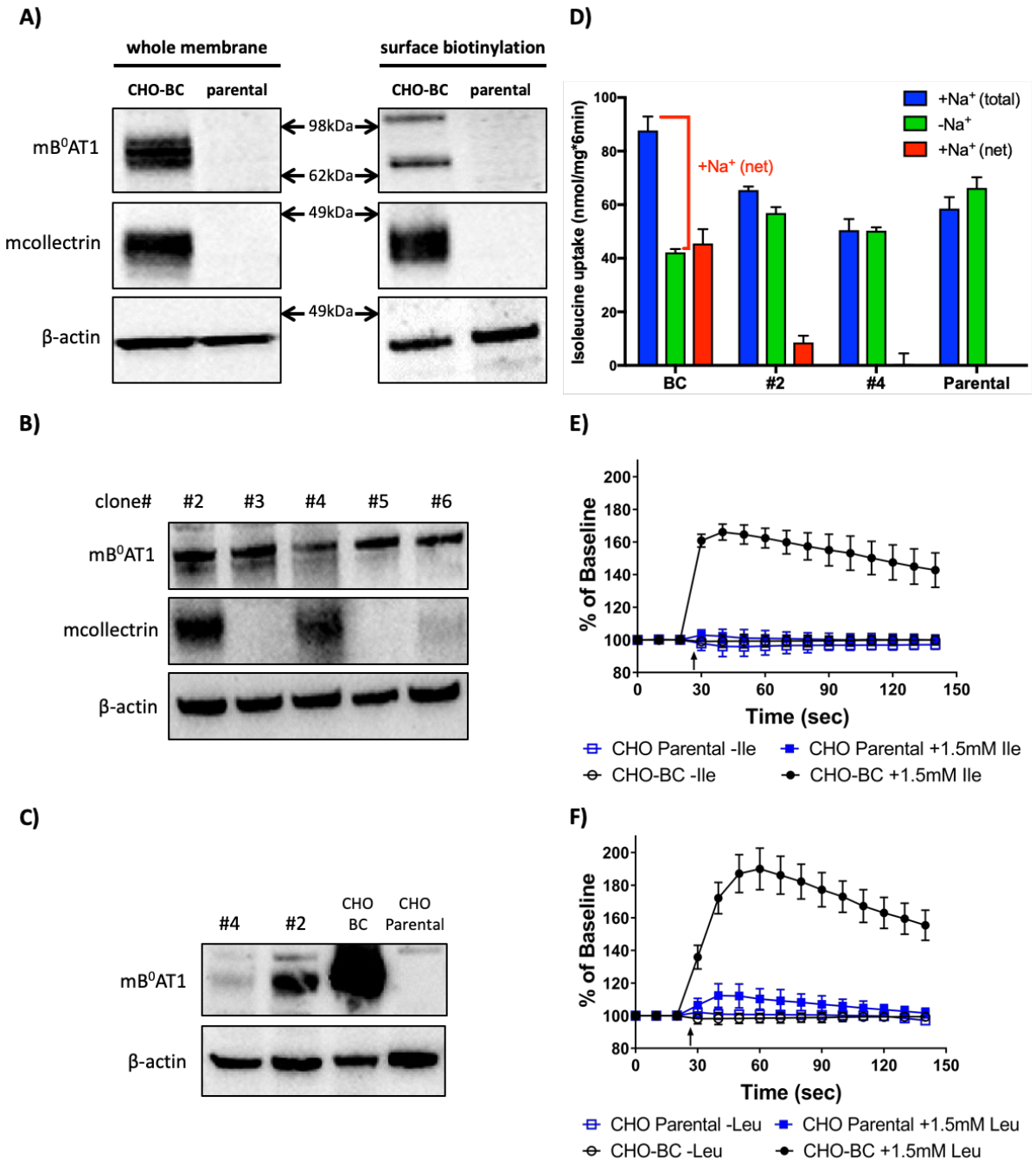

Figure 2.3.1: Characterisation of B^0AT1 expressing CHO cell lines. A) Whole membrane preparation and surface biotinylation were used to isolate membrane proteins from CHO-BC (aka clone #1) and CHO parental cells for immunoblotting to detect B^0AT1 and collectrin protein expression. Both proteins were only detectable in CHO-BC cells, but not in CHO parental cells. β-actin was used as a loading control. Protein markers are indicated beside the blots (n=1, e=5). B) Whole membrane protein samples were prepared for another 5 clones of CHO Flp-In B^0AT1+collectrin cells to test the protein expression of B^0AT1 and collectrin by immunoblotting. B^0AT1 was detectable in all five clones, whereas collectrin was only detected in clone #2, #4 and weakly in #6 (n=1, e=1). C) Clone #2 and #4 were compared with CHO-BC by immunoblotting using whole membrane protein samples. B^0AT1 expression level was lower in these two clones. CHO parental cells were used as a negative control (n=1, e=1). D) ^{14}C-labelled isoleucine uptake assay on CHO-BC, CHO parental, and clone #2 and #4 cells. The cells were exposed to 100µM [^{14}C]isoleucine in Hank's buffer with and without Na^+ buffer

for 6min. Subsequently, the radioactivity of cell lysates was measured. The result is shown as nmol isoleucine uptake ± std (n=3, e=5). The Na^+ (net) uptake level (red columns) was calculated by subtraction of -Na^+ uptake activity (green columns) from the total uptake activity (blue columns). E) Membrane potential assay on CHO-BC (n=3, e=10) and CHO parental (n=3, e=5) cells. The fluorescent signal was induced by the addition of 1.5mM isoleucine into the buffer, as indicated by the arrow in the figure. F) Membrane potential assay on CHO-BC (n=3, e=35) and CHO parental (n=3, e=5) cells. The fluorescent signal was induced by the addition of 1.5mM leucine into the buffer, as indicated by an arrow in the figure. The result is shown as average percentage of baseline readings (before the addition of substrate) ± std. (n indicates number of replicates in each experiment, e indicates number of independent experiments.)

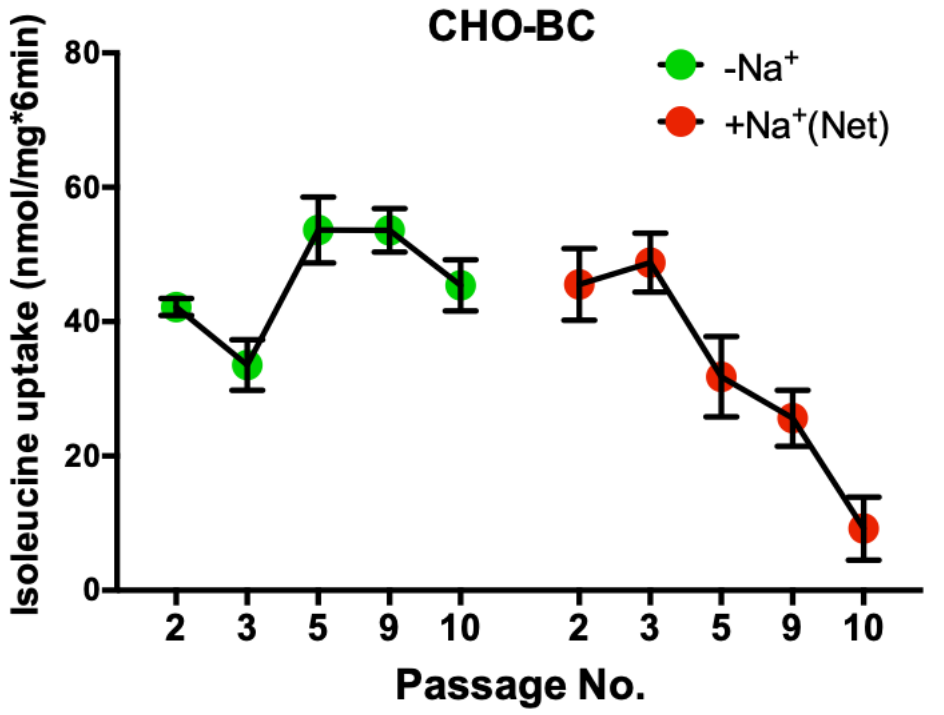

Figure 2.3.2: Passaging CHO-BC cells caused a gradual decrease in heterologous expression. The uptake of 100µM [^{14}C]isoleucine was measured over a period of 6 min using CHO-BC cells at different passages (2 to 10). The sodium-dependent isoleucine uptake level (red dots) decreased steadily after passage 3, while endogenously expressed sodium-independent isoleucine uptake activity (green dots) was not influenced by passaging (n=3, e=10).

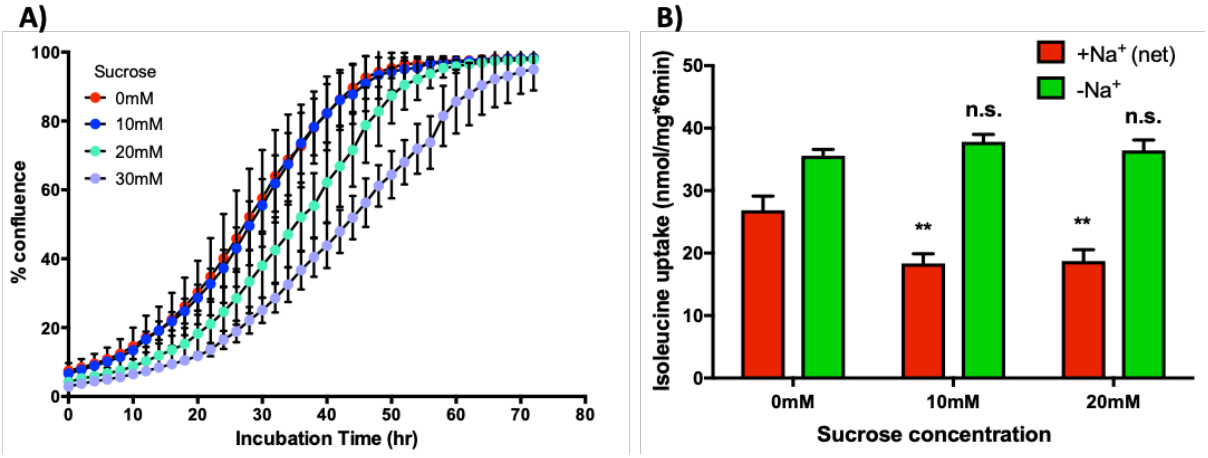

Figure 2.3.3: Effect of osmolarity on B^0AT1 expression. Sucrose slowed down the growth of CHO-BC cells and affected B^0AT1 activity. A) CHO-BC cells were seeded in a 96-well plate and incubated in medium containing different concentrations of sucrose for 72hr. Cell density in each well was monitored every 2hr by IncuCyte technology and the growth curve was generated by the averaged confluence of 12 wells under each condition (n=12, e=1). B) CHO-BC cells were incubated in medium containing sucrose for 72hr before measuring the uptake of 100µM [^{14}C]isoleucine over 6min (n=3, e=1). **, $p<0.01$; n.s. not significant; as compared to control (0mM sucrose).

2.3.2 Characterization of B^0AT1 using CHO-BC cells

The first series of experiments showed that CHO-BC had the highest B^0AT1-like transport activity. In the next series of experiments, I wanted to verify that the transporter expressed in CHO-BC cells has indeed the properties of B^0AT1 as published before [73, 84, 182]. Firstly, the transport of AA substrates was sodium dependent. The sodium dependence was evidenced by the disappearance of depolarization peaks in the absence of either sodium ions or AA substrate leucine or both in the membrane potential assay (figure 2.3.4A). Secondly, the selectivity of amino acid substrates was also determined by membrane potential assay (figure 2.3.4B). Methionine seemed to be the preferred substrate of B^0AT1, followed by BCAAs leucine and isoleucine. Cysteine, phenylalanine, alanine, valine and glutamine induced similar depolarisation, but less than the top three substrates. As expected, anionic (aspartate and glutamate) and cationic (lysine and arginine) amino acids were not transported by B^0AT1. Thirdly, a competition experiment was conducted by measuring the uptake of 100μM [^{14}C]isoleucine in the presence of a 100-fold excess (10mM) of unlabelled amino acids including arginine, phenylalanine, serine and glycine in CHO parental (figure 2.3.4C) and CHO-BC cells (figure 2.3.4D). The sodium-dependent isoleucine uptake in CHO-BC cells was abolished by B^0AT1 substrates phenylalanine and serine, and slightly decreased by the less-preferred substrate glycine. However, arginine, which was not transported by B^0AT1, did not influence the uptake of isoleucine by the transporter (figure 2.3.4D). A similar inhibitory pattern was shown by sodium-independent isoleucine uptake in both CHO parental (figure 2.3.4C) and CHO-BC cells (figure 2.3.4D), indicating a similar substrate preference of the endogenous transporter to B^0AT1. Finally, the Km values of two preferred substrates, leucine and isoleucine, were determined by both membrane potential (FLIPR) assay and radioactive uptake assay. Based on FLIPR assay (figure 2.3.4E&F), the Km values of leucine and isoleucine were determined as 0.5 ± 0.1mM and 0.8 ± 0.1mM, respectively, whereas by uptake assay (figure 2.3.4G&H), the Km values of leucine and isoleucine were 1.05 ± 0.05mM and 1.4 ± 0.1mM, respectively. These characteristics of B^0AT1 observed in CHO-BC cells were consistent with the published features, confirming that CHO-BC was a good cell model to study B^0AT1.

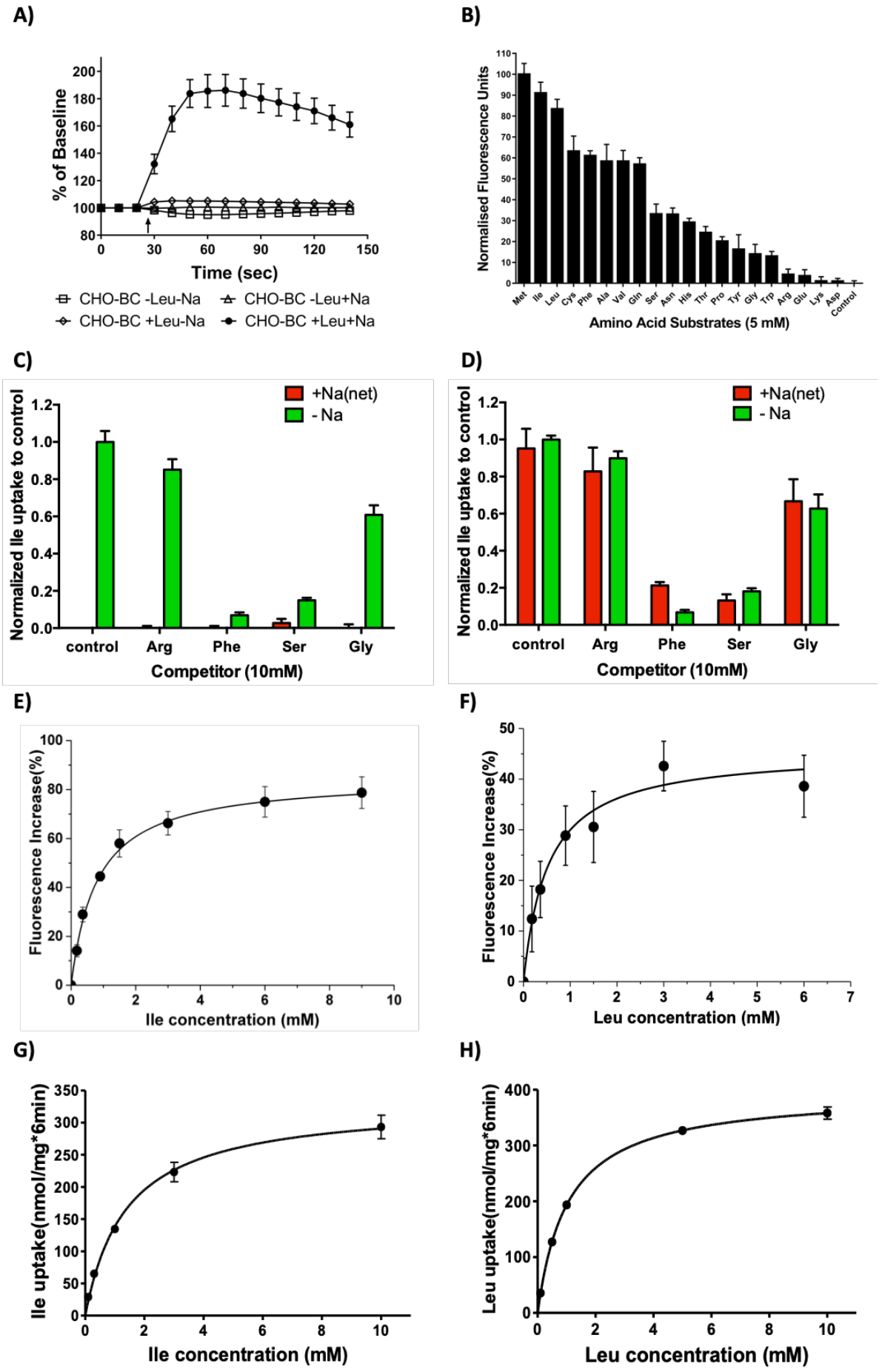
A)
% of Baseline
Time (sec)
CHO-BC -Leu-Na
CHO-BC -Leu+Na
CHO-BC +Leu-Na
CHO-BC +Leu+Na
B)
Normalised Fluorescence Units
Met Ile Leu Cys Phe Ala Val Gln Ser Asn His Thr Pro Tyr Gly Trp Arg Glu Lys Asp Control
Amino Acid Substrates (5 mM)
C)
+Na(net)
- Na
Normalized Ile uptake to control
control Arg Phe Ser Gly
Competitor (10mM)
D)
+Na(net)
- Na
Normalized Ile uptake to control
control Arg Phe Ser Gly
Competitor (10mM)
E)
Fluorescence Increase(%)
Ile concentration (mM)
F)
Fluorescence Increase(%)
Leu concentration (mM)
G)
Ile uptake(nmol/mg*6min)
Ile concentration (mM)
H)
Leu uptake(nmol/mg*6min)
Leu concentration (mM)

Figure 2.3.4: Characterization of B^0AT1 using CHO-BC cells. A) Sodium dependence tested by membrane potential assay on CHO-BC cells. The blue dye was dissolved in ddH_2O instead of the assay buffer provided in the kit to exclude Na^+ in the solution. Half of the cells were washed with Hank's -Na^+ buffer and pre-loaded with 100µL of blue dye in ddH2O plus 100µL of 2x Hank's -Na^+ buffer, whereas another half of the cells were washed with Hank's +Na^+ buffer and pre-loaded with 100µL of blue dye in ddH2O plus 100µL of 2x Hank's +Na^+ buffer. After the baseline readings, the -Na^+- treated wells were injected with 50µL leucine dissolved in Hank's -Na^+ buffer to a final concentration of 1.5mM or with Hank's -Na^+ buffer only. The +Na^+- treated wells were injected with 50µL leucine dissolved in Hank's +Na^+ buffer to a final concentration of 1.5mM or with Hank's +Na^+ buffer only (n=3, e=5). B) Amino acid selectivity of B^0AT1 measured by membrane potential assay in CHO-BC cells. After the baseline readings, 50µL Hank's +Na^+ solution containing each indicated amino acid was manually injected into each well at a final concentration of 5mM. Substrate-induced changes of fluorescence were normalized to the fluorescent increase level induced by methionine (n=3, e=5). C) and D) [^{14}C]isoleucine uptake assay with competitors in CHO parental cells (C) and CHO-BC cells (D). After washing, CHO cells were exposed to Hanks' buffer containing 100µM [^{14}C]isoleucine as well as 10mM Arg, Phe, Ser or Gly for 6min. The data was normalized to the uptake level of control cells, which were only treated with isoleucine (n=3, e=5). E) and F) Km values of isoleucine (E) (n=3, e=5) and leucine (F) (n=3, e=1) determined by membrane potential assay. The depolarization signals were induced by various concentrations of the substrates, and the data points in the figure indicate the peak value of the increase of the signal at each substrate concentration. G) and H) Km values of isoleucine (G) and leucine (H) determined by radioactive substrate uptake assay (n=3, e=1). The cells were treated with various concentrations of the substrates in the presence of sodium, and the data points in the figure indicate the average uptake level at each substrate concentration.

2.3.3 Cell lines that express B^0AT1 endogenously

As outlined above, CHO-BC cells were a suitable model to study the pharmacology of B^0AT1. However, the significant decline of transport activity after several passages suggested that heterologous expression was stressful for the cells resulting in active down-regulation. As a result, I investigated whether cell lines existed that express collectrin/ace2 and B^0AT1 endogenously.

After searching through Oncomine, three human cancer cell lines were selected as potential candidates based on their endogenous expression of SLC6A19 (B^0AT1) or TMEM27 (collectrin) (table 2.3.1). All data shown in the table were log2-transformed, median-centred per array, and the standard deviation was normalized to one per array [183]. Because kidney is one of the major organs expressing B^0AT1, two renal cell lines were also investigated, namely LLC-PK1 (pig kidney epithelial) and MDCK (Madin-Daby canine kidney).

Table 2.3.1: Expression of B^0AT1 (SLC6A19) and collectrin (TMEM27) in selected cell line candidates.

Cell line	Cell Type	log2-transformed, median-centred Intensity	
		SLC6A19	TMEM27
Li-7	Hepatocellular carcinoma	4.60976	4.56135
HUH7	Hepatocellular carcinoma	2.84029	2.19699
GP2D	Colon Adenocarcinoma	3.84229	1.40495

Using RT-PCR (figure 2.3.5A), we detected B^0AT1 expression in HUH7, GP2d and LLC-PK1 cells, whereas the expression of collectrin was only seen in HUH7 and GP2d cells. Meanwhile, one band between 800bp and 1000bp was observed in LLC-PK1 cells, which was larger than the expected band for collectrin (700bp). This could be because the primers were designed for human collectrin, and may not be suitable for detecting collectrin expression in non-human cells. There are only 88.74% of the human TMEM27 (collectrin) sequence matching the sequence of its orthologue in dog, whereas the percentage of human sequence matching the pig sequence is even lower (81.98%) (Ensembl Genome Database). Next, I determined the expression of B^0AT1 and its auxiliary proteins collectrin and ACE2 by immunoblotting (figure 2.3.5B). Both B^0AT1 and collectrin were detected among the membrane proteins of our positive control, CHO-BC cells. None of these three proteins were found in the membrane of LLC-PK1 cells, which might be due to the lack of protein expression in the cell membrane or the species

reactivity of the antibodies. B^0AT1 and collectrin were not detected in the plasma membrane of HUH7 cells, either. However, robust ACE2 expression was found in this cell line. GP2d seemed to be the best candidate among the three cell lines, due to the abundance of B^0AT1 and ACE2 proteins as well as small amounts of collectrin at the surface of the membrane, which theoretically should give sufficient transport activity for measurement. Five cell line candidates along with CHO-BC cells were then tested in a functional assay using [^{14}C]isoleucine uptake (figure 2.3.5C). Surprisingly, only CHO-BC cells had obvious Na^+-dependent isoleucine uptake (at a rate of about 18nmol per mg of protein in 6min). Neither GP2d nor any other tested cell line (HUH7, LLC-PK1, MDCK and Li-7) had significant Na^+-dependent uptake of isoleucine. Therefore, we tried to increase the transport activity by enhancing the expression in these cell lines using transient transfection.

Firstly, because there was abundant ACE2 expression in the membrane of HUH7 cells (figure 2.3.5B), we tried to co-express B^0AT1 in this cell line. Since SLC6A19 was detected at mRNA level in HUH7 cells (figure 2.3.5A), I tried to co-transfect mouse HNF1α to enhance expression of endogenous B^0AT1. HNF1α was reported by our group as activating transcription factor of the Slc6a19 gene in villus enterocytes [184]. Moreover, HNF1α was also reported controlling the collectrin gene in kidney, which is the main organ expressing HNF1α [185]. Upon transfection with B^0AT1 only, its protein expression was significantly increased at the surface of the membrane. At the same time, ACE2 surface expression was also increased, compared to non-transfected WT cells, which was detected by immunoblotting (figure 2.3.6A). Transfection with HNF1α alone, however, did not promote any production of B^0AT1 protein in the membrane, and its co-transfection with B^0AT1 did not improve the surface expression of B^0AT1 or ACE2 (figure 2.3.6A), indicating that HNF1α was unable to induce B^0AT1 or ACE2 expression. Since B^0AT1 appeared at the cell surface after transfection, I tested whether this transfection also improved transport activity by measuring [^{14}C]isoleucine uptake in B^0AT1-transfected HUH7 cells. Despite the detection of protein in the membrane, Na^+-dependent isoleucine uptake was not significantly increased in transfected cells compared to WT cells (figure 2.3.6B). Since neither of B^0AT1, collectrin or ACE2 was seen in the membrane preparation of LLC-PK1 (figure 2.3.5B), but gene expression of B^0AT1 was detected in this cell line by RT-PCR (figure 2.3.5A), attempts were made to express functional human B^0AT1 by transfection with either B^0AT1 alone or together with collectrin in separate vectors. However, neither of the transfections increased Na^+-dependent isoleucine uptake, while the endogenous Na^+-independent and -dependent uptake level remained unchanged (figure 2.3.6C). Expression of B^0AT1 and collectrin in MDCK cells has been reported previously [80]. Transfecting B^0AT1

and collectrin simultaneously either through two separate vectors (pcDNA3.1/B^0AT1 and pcDNA3.1/collectrin) or combined in one vector (pIRES/B^0AT1/collectrin) did not obviously improve transport activity of B^0AT1 in this cell line (figure 2.3.6D). Although Lipofectamine™ 3000 was shown to have higher transfection efficiency than Lipofectamine™ 2000 in other cell lines such as HEK293 [186], it failed to improve transport activity after transfection (figure 2.3.6E). Finally, a hepatocellular carcinoma cell line, Li-7, was tried. According to Oncomine, both B^0AT1 and collectrin are naturally expressed in this cell line (table 2.3.1), however, little Na^+-dependent isoleucine uptake was observed (figure 2.3.5C). After introducing B^0AT1 and collectrin via two vectors solely or simultaneously, there was only a small increase in Na^+-dependent isoleucine uptake activity (figure 2.3.6F). Since none of the above attempts succeeded in providing a good cell model for this study, we began to generate our own B^0AT1 and collectrin stably-transfected cell line.

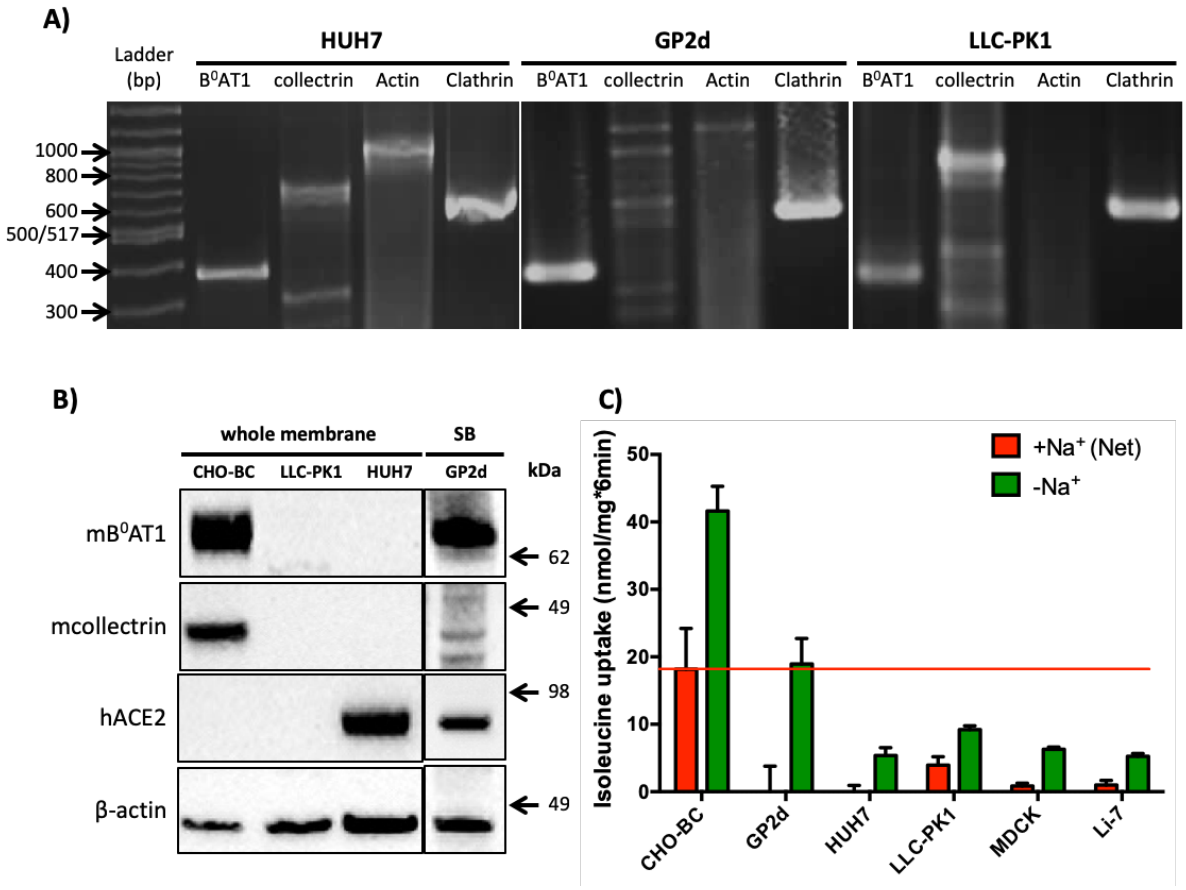

Figure 2.3.5: Expression of B^0AT1 and its auxiliary proteins in various cell lines. A) Gene expression of B^0AT1 and collectrin in HUH7, GP2d and LLC-PK1 cells was detected by RT-PCR, expected band sizes for B^0AT1 and collectrin are 378bp and 700bp, respectively. Actin and Clathrin were used as house-keeping genes (n=1, e=1). B) Protein expression of B^0AT1, collectrin and ACE2 in whole membrane preparations of CHO-BC, LLC-PK1 and HUH7 cells as well as at the cell surface (surface biotinylation) of GP2d cells. β-actin was used as a loading control (n=1, e=1). C) Uptake of [^{14}C]isoleucine into various candidate cell lines and CHO-BC cells. Cells were exposed to 100µM [^{14}C]isoleucine in Hank's $+Na^+$ or $-Na^+$ buffer for 6min. The net Na^+-dependent uptake activity (red columns) was calculated by subtracting uptake activity in the absence of Na^+ (green columns) from the total uptake. Data is shown as average ± std (n=3, e=1).

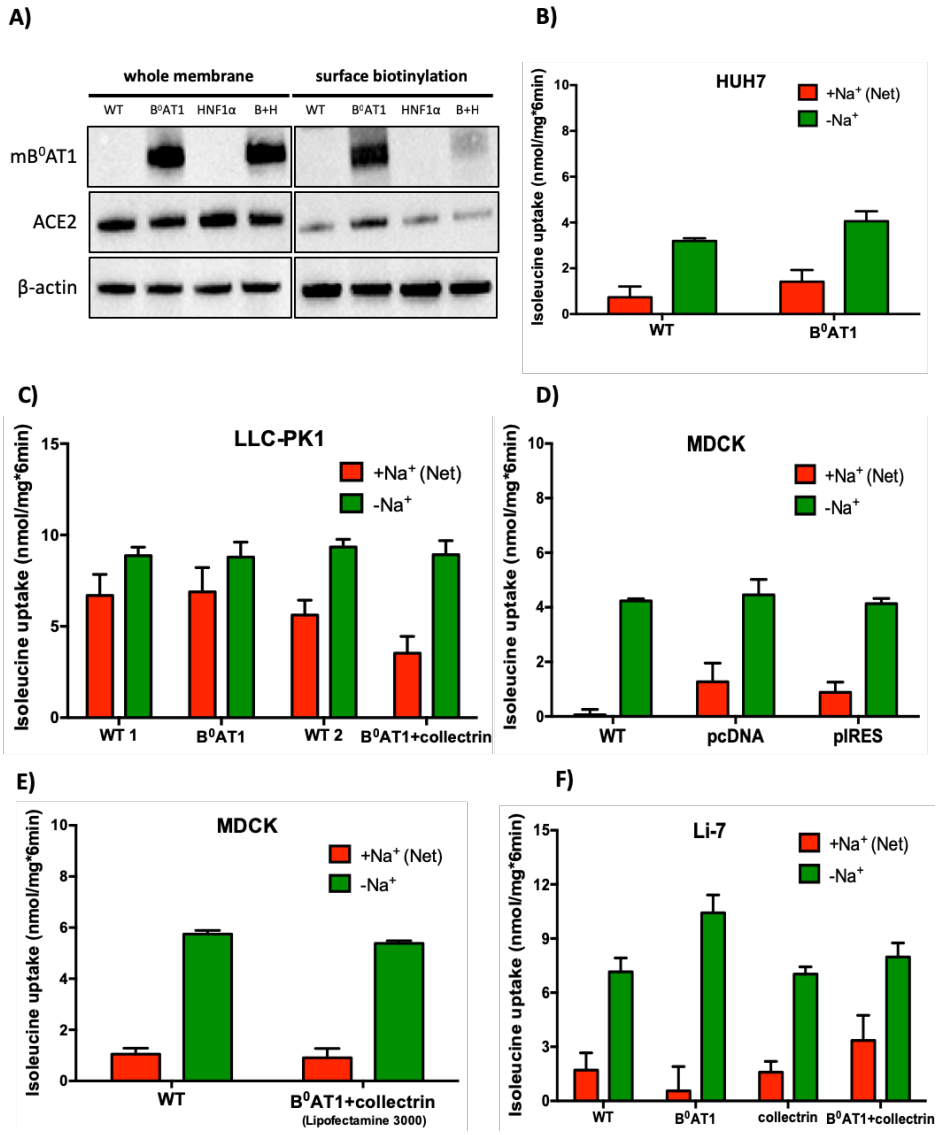

Figure 2.3.6: Transiently-transfected cell lines. A) HUH7 cells were transfected with either pcDNA3.1/hB^{0}AT1 or pCMV6/mHNF1α, or co-transfected with both, using Lipofectamine™ LTX. 48hr post transfection, the cells were harvested for whole membrane preparation (left panel) or surface biotinylation (right panel) to detect the expression of B^{0}AT1 and ACE2 by immunoblotting. β-actin was used as a loading control (n=1, e=1). B) Uptake of [^{14}C]isoleucine by WT and pcDNA3.1/hB^{0}AT1-transfected HUH7 cells. Cells were exposed to 100µM radiolabelled isoleucine in Hank's +Na$^+$ or -Na$^+$ buffer for 6min. The Na$^+$ (net) uptake activity (red columns) was calculated by subtracting the uptake activity in the absence of Na$^+$ (green columns) from the total uptake activity. Data is shown as average ± std (n=3, e=1). C) LLC-PK1 was either transfected with pcDNA3.1/hB^{0}AT1, or co-transfected with pcDNA3.1/hB^{0}AT1 and pcDNA3.1/hcollectrin (1.25µg of each plasmid DNA, 2.5µg in total), using Lipofectamine™ LTX, before measuring the uptake of [^{14}C]isoleucine (n=3, e=1). D) Isoleucine transport activity in MDCK cells transfected with pcDNA3.1/hB^{0}AT1+pcDNA3.1/hcollectrin (labelled as pcDNA in the figure), or with pIRES/hB^{0}AT1/hcollectrin (labelled as pIRES), using Lipofectamine™ LTX (n=3, e=1). (E) Uptake of [^{14}C]isoleucine in MDCK cells transfected with pcDNA3.1/hB^{0}AT1+pcDNA3.1/hcollectrin using Lipofectamine™ 3000 (n=3, e=1). F) Li-7 cells were transfected with pcDNA3.1/hB^{0}AT1, or pcDNA3.1/hcollectrin, or both, using Lipofectamine™ 3000, 48h before measuring the uptake of [^{14}C]isoleucine in the presence and absence of sodium ions (n=3, e=1).

2.3.4 Generation of hB^{0}AT1+hcollectrin stably transfected CHO cells using Flp-In^{TM} transfection system

The CHO-BC cell line showed that hB^{0}AT1 and collectrin can be expressed heterologously, but the use of the cell line was restricted due to contractual agreements with Sanofi-Aventis. As a result, we decided to recreate the cell line, which should also aid in the understanding of heterologous expression of this transporter complex.

The Flp-In^{TM} transfection system (Invitrogen) was used to generate our own stably-transfected cell line. The CHO Flp-In host cell line with a single integrated Flp Recombination Target (FRT) site was purchased from Invitrogen. The cloning strategy was to first integrate pcDNA5/FRT/hB^{0}AT1 via a Flp recombinase-mediated DNA recombination at the FRT site, then to cotransfect with hcollectrin. The two vectors, pcDNA5 and pcDNA3.1, held different antibiotic resistance genes, making cells resistant to Hygromycin B and Geneticin, respectively, once the transfection was successful. Therefore, an appropriate concentration of the antibiotics would be capable of killing untransfected cells without interfering with transfected ones. This concentration should be the minimum concentration killing all wild-type (WT) cells within 15 days. Firstly, the sensitivity of CHO host cell line to Hygromycin B was measured by IncuCyte technology. The growth curves of cells under different concentrations of Hygromycin B is shown as percentage of confluence at certain time points (figure 2.3.7A), and 400 µg/mL was determined as the concentration for subsequent selection of Hygromycin-resistant cells. The host cells were then transfected with pcDNA5/FRT/hB^{0}AT1 construct (#1 and #8) and plasmid pOG44 using Lipofectamine^{TM} 2000. Six colonies (4 from construct #1 and 2 from construct #8) were eventually propagated and tested for the expression of hB^{0}AT1. By RT-PCR, hB^{0}AT1 expression was clearly seen in all six clones as well as the positive control, CHO-BC cells, as illustrated by a band with the size of 378bp (figure 2.3.7B). However, B^{0}AT1 was not detected at protein level in cell homogenates (figure 2.3.7C), suggesting lack of translation or degradation of B^{0}AT1 in the absence of collectrin. Subsequently, one clone from construct #1 and one clone from construct #8 were used for collectrin transfection. Construct #1 and #8 were the two constructs selected after orientation check (figure 2.2.3E). Again, the sensitivity of B^{0}AT1-transfected cells to G418 (Geneticin) was measured with IncuCyte technology (figure 2.3.7D), and 800µg/mL was determined as the concentration for G418 selection. The procedures of hcollectrin transfection was the same as that of hB^{0}AT1, and ten G418-resistant colonies were isolated for further testing. This time, B^{0}AT1 protein was detected in membrane preparations of seven colonies although not at the same level as in CHO-BC cells (figure 2.3.7E). Notably, there was another strong band with higher molecular weight (around 100kDa)

detected in whole membrane samples of CHO-BC cells, which was only weakly expressed in the new clones (figure 2.3.7E). Colony #5 did not grow well and was discarded. Surprisingly, except for CHO-BC, I could not detect collectrin protein expression in any of the transfected colonies (figure 2.3.7E). To further investigate expression of B^0AT1, uptake of [^{14}C]isoleucine was measured in the new transfected cells. Net sodium dependent isoleucine uptake was lower in the new co-transfected colonies (3-21nmol/mg protein*6min) compared to CHO-BC cells (35±4nmol/mg protein*6min) (figure 2.3.7F, red bars). One possible explanation was the lack of collectrin protein expression at the membrane, suggesting that B^0AT1 protein was only partially trafficked to the plasma membrane, hence, having less transport activity than CHO-BC cells. Colony #6, #7 and #8 had relatively high levels of Na^+-dependent isoleucine uptake, and were picked for a repeat transfection with pcDNA3.1/hcollectrin. The re-transfected cells were passaged and propagated in medium containing Hygromycin B and G418 until functional tests were performed. There was an 43-45% increase in the Na^+-dependent isoleucine uptake in double-collectrin-transfected colonies #6 and #7 compared to single-collectrin transfected cells, and this increase was more than 2.6 folds in clone #8 (figure 2.3.8A), indicating that the repeated collectrin transfection did improve the transport activity. Similar to CHO-BC cells, a reduction in B^0AT1 activity after passaging was also seen in colony #6, #7 and #8, e.g. compare sodium-dependent isoleucine uptake in figure 2.3.7F (passage 2) and in figure 2.3.8A (passage 4). However, the improved Na^+-dependent isoleucine uptake (maximum 16nmol/mg*6min in colony #6) was still less than the activity observed in CHO-BC cells (30-40 nmol/mg*6min in figure 2.3.7F). Another potential reason for the lower transport activity could be due to the dilution of transfected cells by untransfected ones. To solve this problem, I isolated individual clones of double-collectrin-transfected cells by limiting dilution into a 96-well plate. B^0AT1 function was measured on these cloned cell lines by both membrane potential assay (figure 2.3.8B) and radioactive substrate uptake assay (figure 2.3.8C&D). Clone #8 H6 and clone #8 G3 were eventually selected as the best performing cell lines reaching 86% and 81%, respectively, of the depolarization peak induced by 1.5mM leucine in CHO-BC cells (figure 2.3.8B, highlighted by red rectangles). Na^+-dependent leucine uptake activity in subclones H6 and G3 reached 57% and 52%, respectively, of that observed in CHO-BC cells (figure 2.3.8D, highlighted by red rectangles). The endogenous Na^+-independent leucine uptake was similar to the level observed in CHO-BC cells (figure 2.3.8C, highlighted by red rectangles). The collectrin transfection was then repeated once again on these two selected clones. The Na^+-dependent leucine uptake activity reached 67% and 62% in clone #8 G3 and clone #8 H6, respectively, of that observed in CHO-BC cells. Notably, the Na^+-independent leucine uptake level increased in these two clones compared to CHO-BC (figure 2.3.8E). The triple-collectrin-

transfection brought B^0AT1 protein to the membrane although collectrin was still invisible in a total membrane preparation (figure 2.3.8F). However, large amounts of collectrin transcripts were observed in double- or triple- collectrin transfected clone #8 H6 cells, whereas collectrin mRNA was hardly detectable in triple-collectrin transfected clone #8 G3 cells, and even weaker in CHO-BC cells (figure 2.3.8G). The low mRNA level and high protein level of collectrin in CHO-BC cells and the opposite situation in triple-collectrin-transfected cells suggested that the translation efficiency of collectrin was likely to be higher in CHO-BC cells than in the newly generated cell lines. B^0AT1 mRNA was expressed evenly in all of the tested cells (figure 2.3.8G), again proving that B^0AT1 was successfully introduced into the genomic DNA. The loss of transgenes was also reported in MDCK cells overexpressing B^0AT1 and collectrin over several passages [187]. To see whether transient transfection could rescue B^0AT1 activity in later passages, triple-collectrin transfected clone #8 H6 cells after passage 7 were transiently re-transfected with pcDNA3.1/hcollectrin and tested or harvested just 48hr after transfection without passaging. The fresh transient transfection increased B^0AT1 activity to a similar level as in CHO-BC cells, according to the depolarization signal in the membrane potential assay (figure 2.3.9A) and the Na^+-dependent substrate transport activity in [^{14}C]leucine uptake assay (figure 2.3.9B). Protein expression of B^0AT1 and collectrin was clearly detected at the surface of the membrane (figure 2.3.9C&D), indicating that collectrin expression might be unstable or the protein is rapidly degraded. This may underlie the loss of B^0AT1 transport activity in stably transfected cells. It has been reported that lower incubation temperature can improve translation efficacy in CHO cells [188, 189]. Hence, we seeded the CHO-BC cells and triple-collectrin-transfected CHO-H6 cells in 96-well plates or 35mm dishes containing culture medium and incubated them at 37°C or 33°C in 5% CO2 incubators for two days before testing or harvesting. In support of this notion, low-temperature-incubation increased the leucine-induced depolarization peak in the membrane potential assay in both cell lines (figure 2.3.9E). However, it did not alter sodium-dependent [^{14}C]leucine uptake, which was slightly elevated in CHO-BC cells but decreased in CHO-H6 cells at lower temperature (figure 2.3.9F). The low-temperature incubation did not up-regulate the membrane expression of B^0AT1 and collectrin in both cell lines (figure 2.3.9G&H).

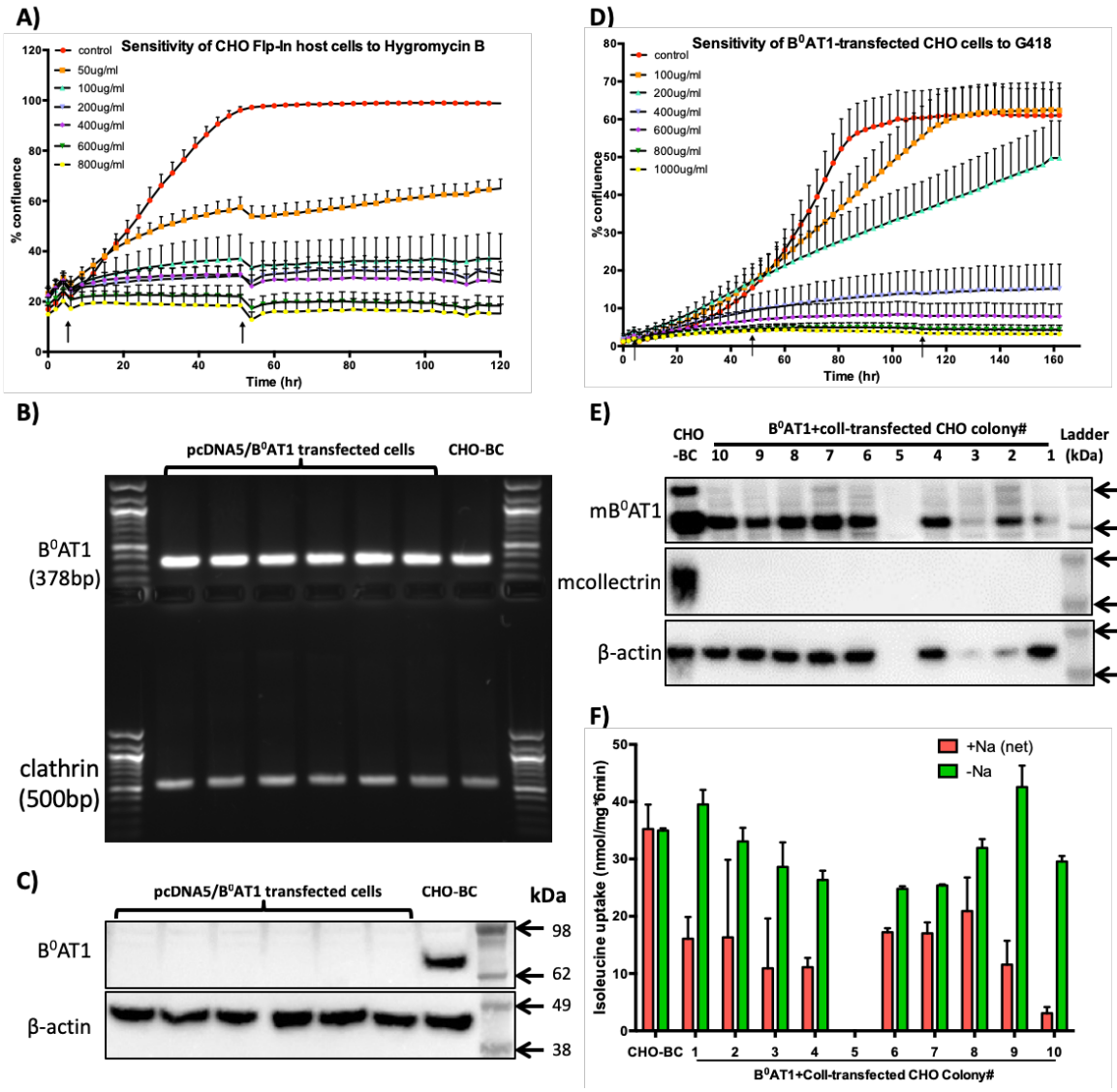

Figure 2.3.7: Generation of B^0AT1 and collectrin stably transfected CHO cells. A) Growth curves of CHO Flp-In host cells exposed to Hygromycin B. Cells were initially seeded in a 96-well plate at a density of 2000 cells/well. After attaching to the bottom of the plate, cells were challenged with different concentrations of Hygromycin B (0, 50, 100, 200, 400, 600, 800µg/mL, 12 wells/concentration). The growth curves were measured in an IncuCyte by monitoring the confluence of cells in each well every 3hr for up to 120hr. Arrows indicate time of medium change. The average of confluence in 12 wells ± std is shown as a growth curve. B) Gene expression level of B^0AT1 in pcDNA5/FRT/B^0AT1 transfected CHO cells. After transfection, six colonies of cells were split into 6cm dishes and maintained in selection medium. After reaching 80-90% confluence, RNA was extracted. CHO-BC cells were used as a positive control. Clathrin was used as a house-keeping gene. B^0AT1 mRNA was detected as a band of 378bp. C) Protein expression level of B^0AT1 in pcDNA/FRT/B^0AT1 transfected cells. Cells were homogenized with Ripa buffer (Sigma, #R0278), and approximately 90µg of protein was loaded for each sample. Left to right: transfected colony #1-6, CHO-BC, SeeBlue plus2 pre-stained protein marker (Invitrogen, LC5925). β-actin was used as a loading control. D) Growth curves of B^0AT1-transfected CHO cells exposed to G418. The cells were challenged with 0-1000µg/mL G418 for up to 160hr. E) Protein expression of B^0AT1 and collectrin after co-transfection. Membrane proteins were extracted from the cell lysate and about 10µg of protein was loaded for each sample. F) Uptake of 150µM [^{14}C]isoleucine by B^0AT1 and collectrin co-transfected cells was measured after 6min incubation.

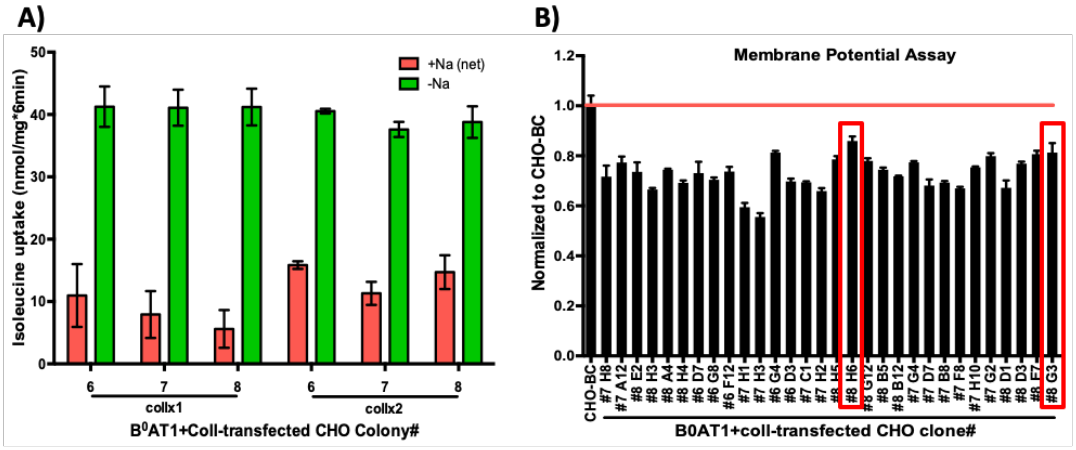
A)
B)
+Na (net)
-Na
Isoleucine uptake (nmol/mg*6min)
collx1
collx2
B0AT1+Coll-transfected CHO Colony#
Membrane Potential Assay
Normalized to CHO-BC
B0AT1+coll-transfected CHO clone#

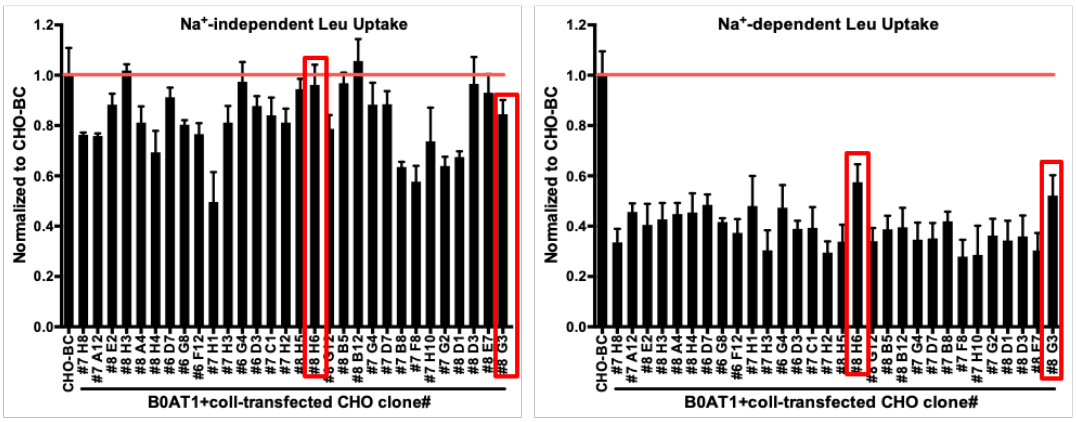
C)
D)
Na+-independent Leu Uptake
Na+-dependent Leu Uptake
Normalized to CHO-BC
B0AT1+coll-transfected CHO clone#

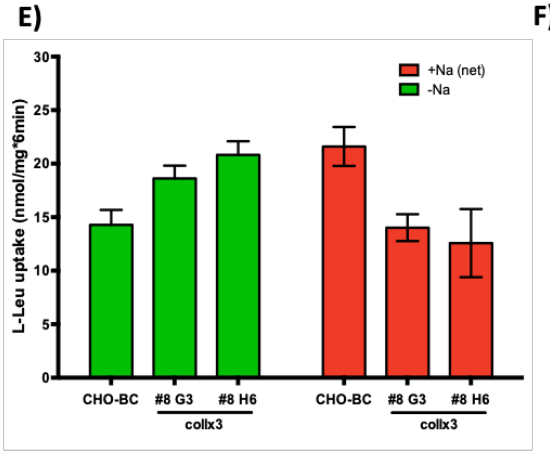
E)
+Na (net)
-Na
L-Leu uptake (nmol/mg*6min)
CHO-BC
#8 G3
#8 H6
collx3

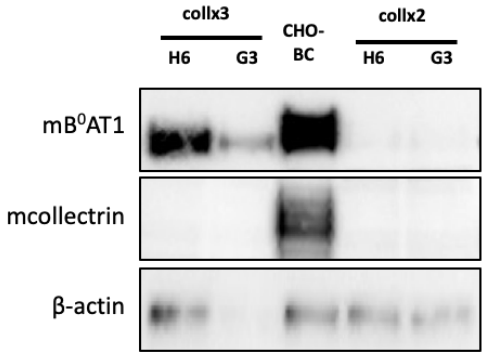
F)
collx3
CHO-BC
collx2
H6
G3
mB0AT1
mcollectrin
β-actin

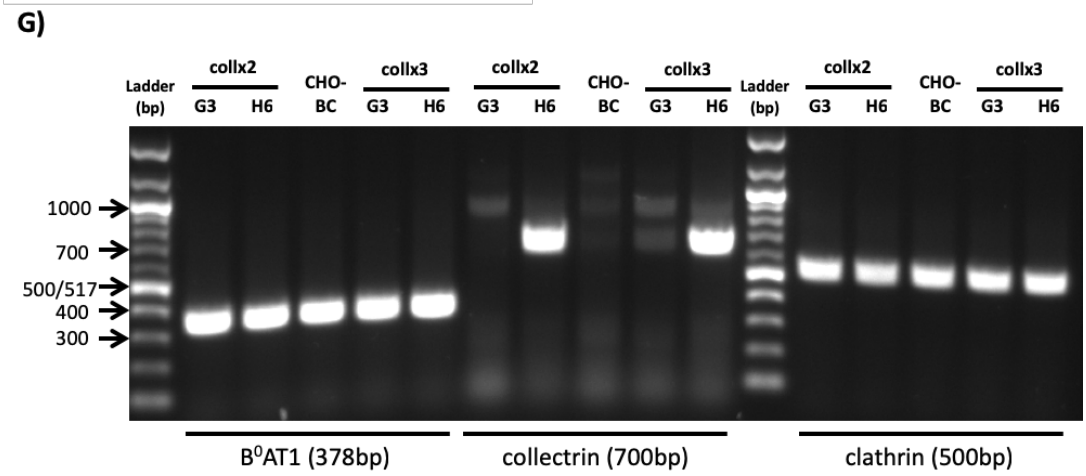
G)
Ladder (bp)
collx2
CHO-BC
collx3
G3
H6
1000
700
500/517
400
300
B0AT1 (378bp)
collectrin (700bp)
clathrin (500bp)

Figure 2.3.8 Optimisation of B^0AT1 and collectrin expression in stably transfected CHO cells. A) CHO B^0AT1+collectrin-transfected cell colony #6, #7 and #8 were re-transfected with pcDNA3.1/hcollectrin in the presence of Lipofectamine™ 2000. No antibiotics were added when Lipofectamine was present in the medium. 6hr after transfection, the transfection medium was replaced by CHO cell culture medium supplemented with 400µg/mL Hygromycin B and 800µg/mL G418. 48hr after transfection, the cells were split and transferred into a 25cm^2 flask for propagation until confluent enough to be seeded out for radiolabelled isoleucine uptake assay. The result is shown as mean of triplicates ± std in one experiment. B)-D) The double-collectrin-transfected CHO cells were seeded out in a 96-well plate by limiting dilution to propagate single clones. A total of 30 clones were eventually tested by membrane potential assay (B) as well as radioactive substrate uptake assay (C&D) in the presence and absence of Na^+. The results were normalized to the assay activity in CHO-BC cells to compare the data from three independent experiments. Clone #8 H6 and clone #8 G3 were eventually selected as the best performing cell lines, which are highlighted by red rectangles. E) Clone #8 G3 and H6 were transfected with pcDNA3.1/hcollectrin for the third time, and transport activity was measured by [^{14}C]leucine uptake assay. F) and G) B^0AT1 and collectrin expression at protein level in whole membrane preparation samples (F) and at mRNA level (G) in the double- and triple- collectrin transfected cells compared to CHO-BC cells.

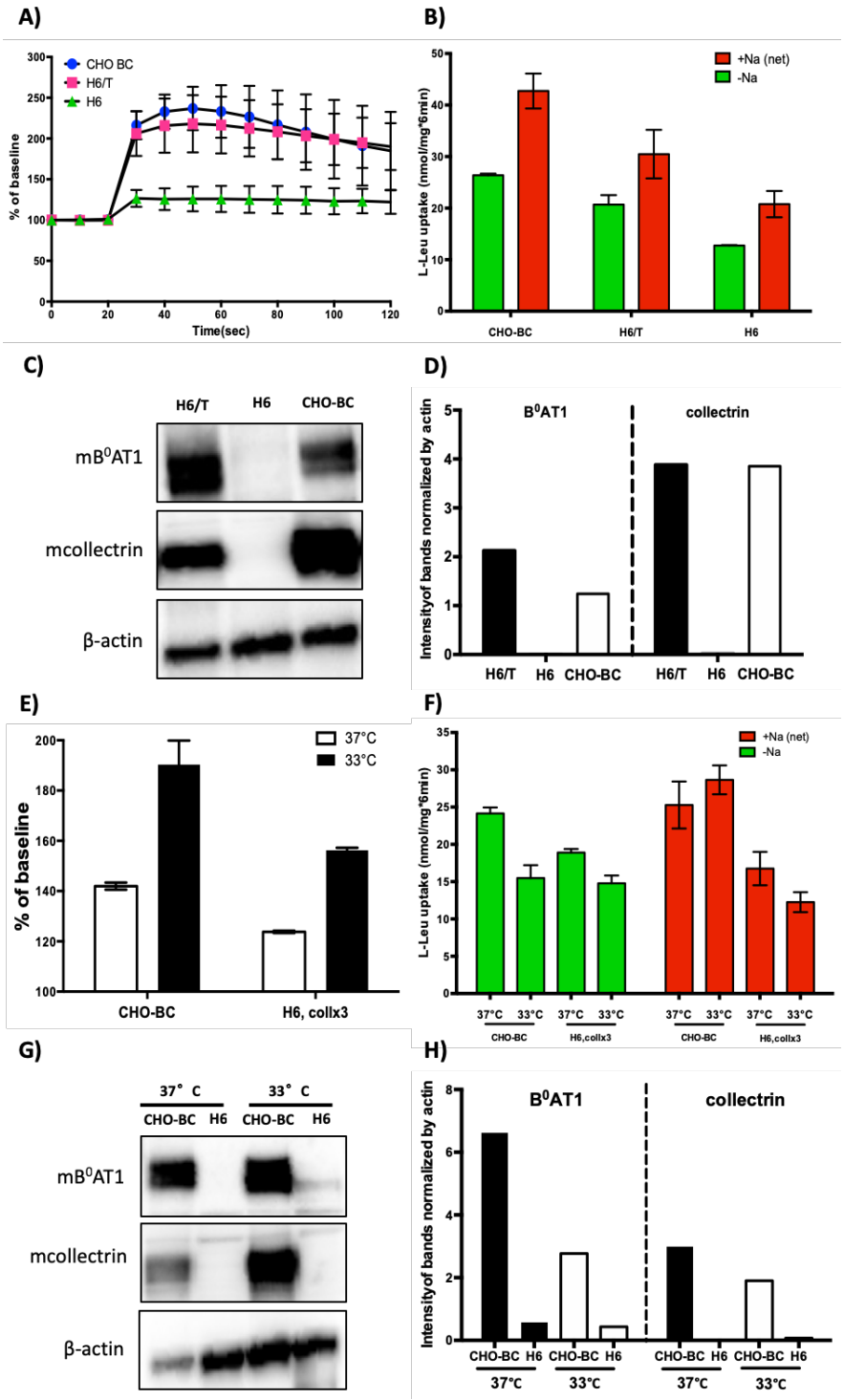

Figure 2.3.9: Characterisation of B^0AT1 and collectrin stably transfected single clones. Functional expression of B^0AT1 was evaluated by the following methods: A) membrane potential assay, B) [^{14}C]leucine uptake assay, and C) membrane protein expression using surface biotinylation samples. For all assays, cells were directly used after fresh transient transfection with pcDNA3.1/hcollectrin (H6/T) and compared to the cells at passage 7 without transient transfection (H6) and with CHO-BC cells. D) Intensity of bands in figure (C) normalized to the loading control β-actin. E) Membrane potential assay, F) [^{14}C]leucine uptake assay, and G) membrane protein expression measured on cells incubated at different temperatures for two days. H) Intensity of bands in figure (G) normalized to the loading control β-actin.

2.3.5 Validation of a sodium dye assay

The sodium dependence of the B^0AT1 transporter suggested that it might be possible to measure the uptake of AA substrate by a fluorescent sodium indicator, such as Asante NaTRIUM Green 2 (ANG-2). ANG-2 is loaded into the cells as an acetoxymethyl-ester. To calibrate the assay, I performed a sodium titration experiment (figure 2.3.10A&B). Two ionophores, Monensin (figure 2.3.10A) and Gramicidin (figure 2.3.10B), were used to equilibrate intra- and extracellular Na^+-concentration. The addition of these two ionophores to cells incubated in Na^+-free buffer generated small peaks but the signal returned to baseline immediately, indicating the depletion of intracellular sodium. Then the extracellular sodium concentration was increased to various levels, leading to the equilibration of intracellular and extracellular sodium ion concentration, resulting in corresponding increases in sodium indicator fluorescence. At the end of the experiment, 145mM KCl was added into the buffer. The sudden increase in extracellular potassium ion concentration caused an immediate outward flow of sodium ions in exchange for potassium ions, hence, decreasing the ANG-2 fluorescence sharply. This titration experiment showed a good response of the ANG-2 dye to changes of the Na^+-concentration in CHO-BC cells. The next step was to optimize the assay conditions in CHO-BC cells for the study of B^0AT1. According to the protocols (TEFLabs's protocol for ANG-2, Invitrogen's protocol for Pluronic F-127), several conditions could be optimized, including the concentration of working solution (no more than 1%, composition see table 2.3.2), the dye-loading buffer (serum-free medium or buffer), loading time (10-60min), and loading temperature (room temperature or 37°C). To minimize the background signal, we also tried using Hank's buffer devoid of sodium ions in the dye-loading phase and post-loading phase. After several baseline readings, 50µL of 30mM leucine in Hank's $+Na^+$ solution was added into 200µL post-loading buffer in each well to stimulate the signal by co-transporting Na^+ into the cells. In case of Hank's $-Na^+$ buffer as the post-loading buffer, the final concentration of sodium was 28mM (50µL of Hank's $+Na^+$ buffer containing 140mM Na^+ was added into 200µL Hank's $-Na^+$ buffer). Conditions tried during optimization are listed in table 2.3.2. In figure 2.3.10C, no signal indicating sodium influx was detected after the addition of amino acid substrate leucine under condition 1-3, suggesting no difference between Hank's buffer and DMEM as the dye-loading buffer, and between different dye-loading temperatures. However, cells looked healthier (less detached cells on the plate) when pre-loading for 10min (condition 3) compared to 30min (condition 2), while the fluorescence readings were not influenced by shortening the incubation time. Next, sodium depletion was tried during dye-loading (condition 4) as well as post-loading stages (condition 5), and only the latter one generated an obvious

leucine-induced signal. Further optimization was tried by varying the percentage of working solution. The dye and Pluronic F-127 were dissolved in dimethylsulfoxide (DMSO) in working solutions which are toxic to cells above 1% [190], hence, lower concentrations of working solution were tested. The leucine-stimulated signal was similar in cells pre-loaded with 0.5% working solution (condition 6) to cells pre-loaded with 0.2% working solution (condition 7). Since condition 6 (highlighted in table 2.3.2) had higher readings than condition 7, most likely due to the larger amount of dye loaded into the cells, it was selected as the preferred condition in the following validation. Surprisingly, when using different concentrations of leucine as the stimulus, lower concentrations (1, 3, 6mM) induced a higher fluorescent signal than the higher concentration (9mM), and even the addition of sodium ions (to the final concentration of 28mM) alone in the absence of leucine generated a large signal (figure 2.3.10D). Such sodium-induced signal was also seen in CHO parental cells (figure 2.3.10E). One explanation for the lack of B^0AT1-induced increases of cytosolic Na^+ may involve the immediate extrusion of cotransported Na^+ by the Na-K-ATPase. This would result in leucine-induced signals being weaker than expected. To reduce this compensation, we used Ouabain, a specific Na-K-ATPase inhibitor [191], or removed extracellular potassium [191], to render the Na-K-ATPase inactive and avoid the extrusion of Na^+ by the pump. The use of 1mM Ouabain in the dye loading stage did not increase the sodium-induced signal, furthermore, Ouabain diminished the leucine-induced signal (figure 2.3.10F), suggesting an inhibitory effect on B^0AT1. The depletion of potassium in the extracellular buffer also made no difference to the buffer containing K^+ (figure 2.3.10G). The washing step after dye-loading caused cells to detach from the plate. Instead of washing, it was reported that the extracellular ANG-2 dye after loading could be quenched by PillarBox Red Food Dye (Personal communication: Irina Vetter from the University of Queensland at Gage Conference 2017). This is the same principle as used in the FLIPR dye kit, in which fluorescent sensor is pre-combined with impermeable quenchers (either a blue quencher or a red quencher) to reduce the background fluorescence signal and to improve the signal-to-noise ratio without washing the cells after dye loading. Hence, we tried to use 1:50 diluted PillarBox Red for quenching. Figure 2.3.10H showed a small and lasting increase of the fluorescent signal before and after the addition of Hank's $+Na^+$ buffer with leucine compared to a lesser signal without leucine. Different from the curves in figure 2.3.10D, where the unloaded dye was removed, continued presence of the dye in the presence of PillarBox Red caused shifted upward drift of the fluorescent signal during baseline reading (100sec), and abolished the initial jump of fluorescence after the addition of leucine plus Na^+. Overall, the sodium assay could not be optimised to the point where it would be able to become an alternative assay to measure B^0AT1 activity.

Table 2.3.2: conditions tried during optimization of ANG-2 (AM) on CHO-BC cells.

Condition No.	**1**	**2**	**3**	**4**	**5**	**6**	**7**
Dye-loading buffer	Hank's $+Na^+$	DMEM	DMEM	Hank's - Na^+	Hank's - Na^+	Hank's - Na^+	Hank's $-Na^+$
% of working solution* in loading buffer	1%	1%	1%	1%	1%	0.5%	0.2%
Dye-loading temperature	RT	37°C	37°C	RT	RT	RT	RT
Dye-loading time	30min	30min	10min	10min	10min	10min	10min
Post-loading buffer	Hank's $+Na^+$	Hank's $+Na^+$	Hank's $+Na^+$	Hank's $+Na^+$	Hank's - Na^+	Hank's - Na^+	Hank's $-Na^+$
Na^+ Final conc. (mM)	140	140	140	140	28	28	28

*working solution contains 0.5mM ANG-2 Dye and 10% (w/v) Pluronic F-127 dissolved in DMSO.

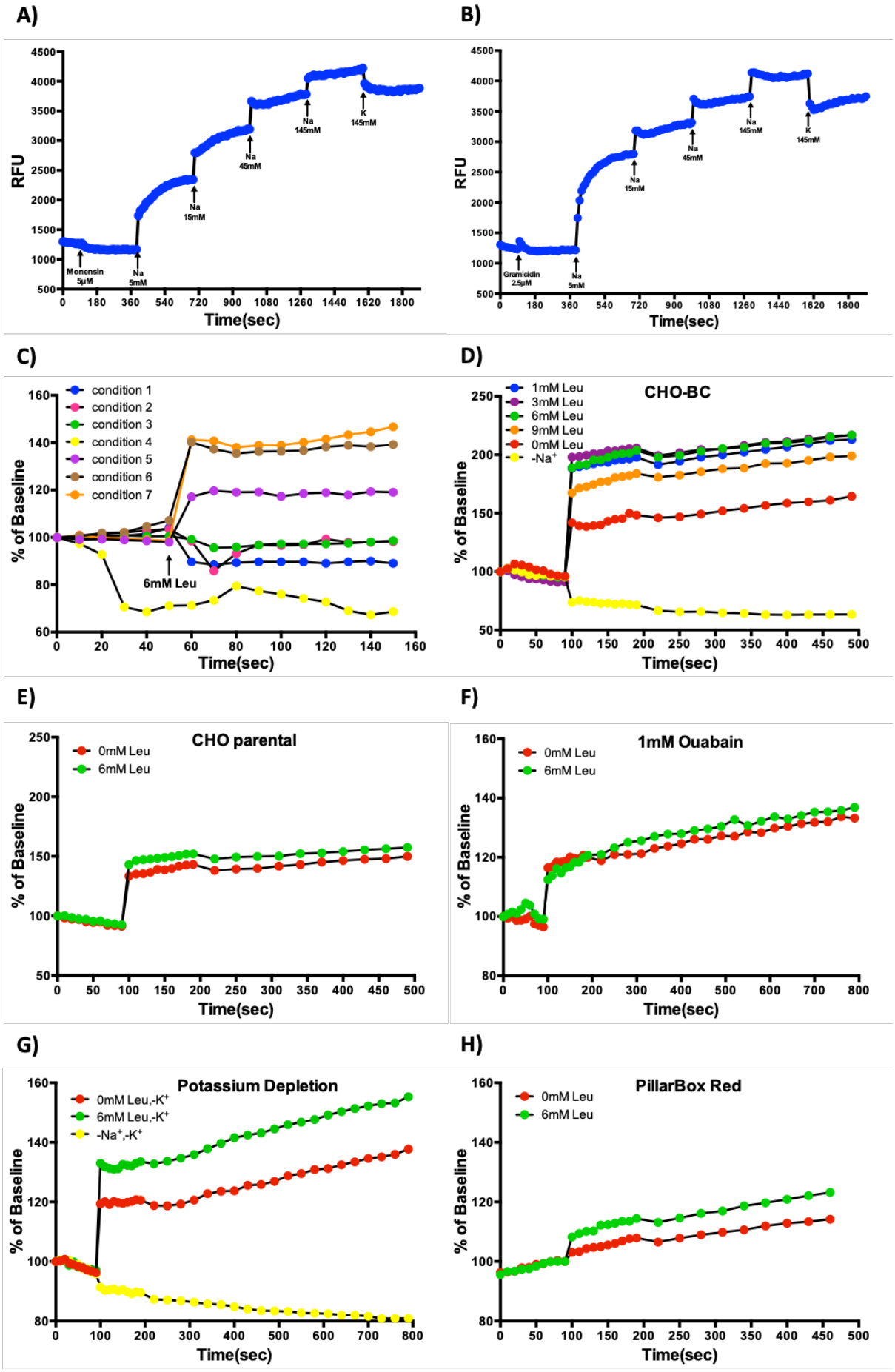
A)
RFU
Time(sec)
Monensin 5μM
Na 5mM
Na 15mM
Na 45mM
Na 145mM
K 145mM
B)
RFU
Time(sec)
Gramicidin 2.5μM
Na 5mM
Na 15mM
Na 45mM
Na 145mM
K 145mM
C)
% of Baseline
Time(sec)
condition 1
condition 2
condition 3
condition 4
condition 5
condition 6
condition 7
6mM Leu
D)
CHO-BC
% of Baseline
Time(sec)
1mM Leu
3mM Leu
6mM Leu
9mM Leu
0mM Leu
-Na+
E)
CHO parental
% of Baseline
Time(sec)
0mM Leu
6mM Leu
F)
1mM Ouabain
% of Baseline
Time(sec)
0mM Leu
6mM Leu
G)
Potassium Depletion
% of Baseline
Time(sec)
0mM Leu,-K+
6mM Leu,-K+
-Na+,-K+
H)
PillarBox Red
% of Baseline
Time(sec)
0mM Leu
6mM Leu

Figure 2.3.10: Validation of sodium dye assay in CHO-BC cells. The excitation wavelength was 488nm, and the emission wavelength was 540nm. A) & B) Calibration by sodium titration with different ionophores. After reaching a stable baseline signal, 5µM monensin (figure A) or 2.5µM Gramicidin A (figure B) was used to deplete cells of Na^+, followed by the addition of NaCl to various levels (5, 15, 45, 145mM), with 145mM KCl added in the end (n=3, e=1). C) Optimization of assay conditions in CHO-BC cells. Different dye loading buffer, temperature, time, concentration of dye, and post-loading buffer were tried as listed in table 2.3.2. After baseline readings, 6mM leucine in Hank's $+Na^+$ buffer was added to stimulate the fluorescent signal, as indicated by the arrow in the figure. Data points show the relative fluorescence in percentage of the first baseline reading (n=1, e=1). D) The ANG-2 fluorescent signal induced by different concentrations of leucine in the presence of Na^+. The CHO-BC cells were pre-loaded with Hank's $-Na^+$ buffer supplemented with 0.5% working solution at room temperature for 10min. The cells were washed twice with Hank's $-Na^+$ buffer and incubated in the same buffer after removing the dye solution. Hank's $+Na^+$ buffer containing different concentrations of leucine was added after recording the baseline, Hank's $-Na^+$ buffer was used as a negative control. Final concentrations of leucine are indicated in the figure (n=3, e=1). E) The CHO parental cells were pre-loaded with Hank's $-Na^+$ buffer with 0.5% working solution at RT for 10min, then washed twice with Hank's $-Na^+$ buffer and incubated in the same buffer after removing the dye solution. Hank's $+Na^+$ buffer with or without leucine was added after recording the baseline, final concentration of leucine was 6mM (n=3, e=1). F) The CHO-BC cells were pre-loaded with Hank's $-Na^+$ buffer and 0.5% working solution as well as 1mM Ouabain (from 100mM stock solution) at RT for 10min. After removing the pre-loading solution, the cells were incubated in Hank's $-Na^+$ buffer. After baseline readings, Hank's $+Na^+$ buffer with or without leucine was added (n=3, e=1). G) The CHO-BC cells were treated as in figure D, except that potassium was removed in the Hank's buffer used in this experiment (n=3, e=1). H) The CHO-BC cells were pre-loaded with Hank's $-Na^+$ buffer and 0.5% working solution at RT for 30min. After pre-loading, the excess unloaded dye was quenched by adding 1:50 PillarBox Red Food Dye into each well and incubating at RT for 15min. After incubation, the baseline readings were recorded without washing the cells, followed by the addition of Hank's $+Na^+$ buffer with or without leucine (n=3, e=1).

2.4 Discussion

For the high-throughput screening (HTS) and the secondary screening of B^0AT1 inhibitors, we first needed a cell line expressing functional B^0AT1 at the surface of the membrane. Our collaborator, Sanofi Aventis Pharmaceutical Company, had generated single clones of a CHO stable cell line by co-expressing hB^0AT1 and hcollectrin with the aid of the Flp-In™ transfection system. Its applications for the expression of cytosolic or membrane proteins were reported in various host cell lines [133-138]. CHO-K1 was chosen as a host cell line in this study because its endogenous uptake of isoleucine was purely Na^+-independent (figure 2.3.1D) and electroneutral (figure 2.3.1E), allowing us to introduce the Na^+-dependent electrogenic transport of amino acids by B^0AT1 without any interference from the endogenous transporters. Based on the competition uptake experiment (figure 2.3.4C), the endogenous transport of isoleucine in CHO-K1 cells was most likely occurring via the hamster isoform of system L amino acid transporters [148]. The basic characteristics of B^0AT1 (sodium-dependent, electrogenic and substrate preference) was confirmed in CHO-BC cells. These characteristics of B^0AT1 were identical to those reported previously using electrophysiological recordings on Xenopus oocytes [84, 96]. The Km values of leucine and isoleucine determined by both membrane potential assay (figure 2.3.4E&F) and radioactive substrate uptake assay (figure 2.3.4G&H) were also consistent with the published data [73, 84, 182]. Although the Km values for these two substrates were very close, isoleucine seemed to be a more specific substrate for B^0AT1, indicated by the lack of a background signal in CHO parental cells in the FLIPR assay (figure 2.3.1E). Leucine, on the other hand, generated a small depolarization peak in parental cells (figure 2.3.1F), suggesting that leucine can be transported by other electrogenic transporters endogenously expressed in CHO cells, e.g. system A [192]. Hence, isoleucine was selected as the substrate used in the uptake assay for the secondary screening. One major problem of CHO-BC cells was the loss of activity of the heterologously expressed proteins after several cell culture passages (figure 2.3.2). The passaging, however, did not influence the endogenous sodium-independent transport activity. Torrente et al. reported a similar reduction of transgene expression at passage 10 when overexpressing B^0AT1 and collectrin in MDCK cells, arguing that high extracellular amino acid concentration in cell culture medium down-regulated the constitutive expression of the transporter [187]. In another study, the limitation of essential amino acids (EAAs) such as methionine and cysteine was reported to reactivate the transgene expression in mammalian cells by down-regulation of histone deacetylase 4 (HDAC4) [193]. However, I have not tried restriction of EAAs in culture medium as a strategy to solve this problem. When using stably transfected CHO cells, Bjork et al. noticed a loss of

homogeneity in expression of the α_{2A}-adrenergic receptor after passage 13 and an attenuation of function after passage 20 [194]. The author noted the dissociation of receptor expression from antibiotic resistance, possibly caused by an inappropriate amount of antibiotics used in the maintenance of transfected clones, however, the specific mechanisms remained unclarified. Osmotic loading was proposed to increase after inducing the expression of GLT-1, a sodium-dependent glutamate transporter, in CHO cells, indicated by the increased cell size [195]. However, addition of extracellular sucrose to CHO-BC cells did not improve the transport activity or cell growth (figure 2.3.3A&B). Hence, we only used CHO-BC cells with less than 10 passages for functional tests.

ACE2 and collectrin are auxiliary proteins of B^0AT1 expression in intestine and kidney, respectively [79]. They are important not only for the trafficking of B^0AT1 to cell surface, but also for the catalytic function of the transporter. However, the peptidase domain of ACE2 was proved to be irrelevant to the surface expression and catalytic function of B^0AT1 [40]. Furthermore, collectrin was smaller in size compared to ACE2 due to the lack of its catalytic domain. Hence, we chose to co-express collectrin with B^0AT1 to generate the cell model for the study of this transporter. The co-expression of collectrin was proved to be essential to the surface expression of B^0AT1, based on our observation that B^0AT1 was absent in whole membrane proteins of pcDNA5/FRT/B^0AT1-transfected cells (figure 2.3.7C). This was in agreement with previous studies [79-81, 96]. As expected, the co-expression of collectrin was critical for the function of the transporter, as indicated by (i) higher sodium-dependent substrate uptake in CHO-BC cells; (ii) higher protein levels of B^0AT1 and collectrin; (iii) further increase of transport activity and protein expression of B^0AT1 and collectrin after transient transfection with collectrin. Notably, repeated collectrin transfection increased transcript levels but did not result in higher protein expression, suggesting limitations of the translation of collectrin or its degradation (figure 2.3.8E). Post-transcriptional modifications and protein degradation were reported as reasons for discrepancies between mRNA and protein levels [196]. In our experiments, B^0AT1+collectrin transiently transfected CHO cells (0.6mg/mL G418 in culture medium) were more resistant to selection antibiotic G418 compared to CHO-BC cells (0.275mg/mL G418 in culture medium), thus, the high concentration of antibiotic in the culture medium could be toxic to protein synthesis. It is noteworthy that a higher-molecular-weight (HMW) band of about 98kDa was consistently detected in the blots of B^0AT1 when analyzing membrane proteins of CHO-BC cells (figure 2.3.1A, 2.3.7E). This may represent a SDS resistant heterodimer formed between B^0AT1 (64kDa) and collectrin (43kDa). However, such a HMW band was not detectable in the collectrin blot, thus, it might also represent a homodimer

of B^0AT1, although the molecular weight seemed to be lower than expected. Interestingly, this HMW band was undetectable in transiently transfected cells (figure 2.3.6A), or much less obvious in other B^0AT1+collectrin-transfected CHO clones (figure 2.3.1C, 2.3.7E) with lower transport activity. Its presence possibly correlates with transport activity measured by functional tests. Therefore, formation of higher-order complexes may play an important role in the function of the transporter. Heteromeric design is commonly observed in amino acid transporters. The most well-studied examples are the heavy subunits 4F2hc and rBAT, which associate by a disulfide bridge with the light subunits of system L/y+L amino acid transporters (LAT1, LAT2, y^+LAT1 and y^+LAT2) and system $b^{0,+}$ amino acid transporters, respectively [197-199]. The functions of these two heavy chains are slightly different. Both 4F2hc and rBAT are necessary for trafficking the light chain to the surface of the plasma membrane, but 4F2hc alone is expressed on the cell surface even without the coexpression of a light chain, whereas rBAT does not reach the plasma membrane alone [200]. Moreover, 4F2hc only plays a role in the trafficking of the light chain to the membrane [201], but rBAT itself takes part in the transport activity [198]. Due to the heteromeric design, mutations in either rBAT or $b^{0,+}AT$ will cause lack of reabsorption of cystine and cationic amino acids in the kidney and thus lead to cystinuria [106]. Similarly, a profound aminoaciduria was also seen in collectrin-deficient mice, accompanied by decreased B^0AT1 protein expression at the renal cortical plasma membrane [81]. Unlike 4F2hc, collectrin was only measurable when co-expressing with B^0AT1 at the membrane of our cell lines. It was absent in membrane fractions of LLC-PK1 and HUH7 cells when B^0AT1 was not expressed (figure 2.3.5B). Furthermore, collectrin was shown to be essential for transport activity in a previous study of our lab [40]. Thus, the interaction of collectrin and B^0AT1 was more similar to that of rBAT and $b^{0,+}AT$. Homodi- and multimerization is frequently observed in ion channels and transporters. Two examples are the potassium ion transporter TrkH in bacteria [202] and the SCN1B sodium channel in mammalian cells for the enhancement of cell-cell adhesion [203]. Dimerization of TrkH and SCN1B proteins occur via the transmembrane domain and extracellular domain, respectively. It is noteworthy that the neurotransmitter and sodium symporters in the SLC6 family often require oligomerization rather than heteromerization for endoplasmic reticulum (ER) exit to the plasma membrane [204]. The SDS-resistance is seen as an indicator of the hydrophobicity and stability of a protein complex at the plasma membrane [205]. Occasionally, protein-protein interactions, both in the form of a homodimer or heterodimer, can even be determined by mass spectrometry [206].

To generate a cell model without IP restrictions for future studies of B^0AT1, we tried both transient and stable transfections in different cell lines. The former method involves temporal expression of the gene of interest without its integration into the genome of the host. The introduced DNA will be degraded after several cell divisions. The latter method involves insertion of the foreign DNA into the host genome, and consequently sustained expression of the transgene is observed [131]. Although stable transfection is widely used in pharmacological studies and gene therapies, the integration event has much lower efficiency than transient transfection [207] and requires isolation of single clones. It becomes even more complex when multiple genes are required to be expressed. As a result, I searched the Oncomine microarray database for cell lines that naturally express either SLC6A19 or collectrin or both, and found several candidates including HUH7, GP2d and Li-7. Surprisingly, no sodium-dependent isoleucine uptake was seen in GP2d cells (figure 2.3.5C) even though B^0AT1 and ACE2 were detected at the protein level on the cell surface (figure 2.3.5B). Similarly, transient expression of B^0AT1 in HUH7 cells in which endogenous ACE2 was detectable (figure 2.3.6A), failed to show sodium-dependent isoleucine uptake (figure 2.3.6B). This could be due to the failure of heterodimerization between B^0AT1 and ACE2, leading to the instability of B^0AT1 at the cell surface. It was previously reported that Janus-activated kinase-2 (JAK2) [88] and protein kinase B (PKB/Akt) [87] could enhance the surface expression of B^0AT1 in the presence of ACE2 or collectrin and thus promote the transport of neutral amino acids. Therefore, addition of agonists of these pathways may be used to increase activity of B^0AT1 during functional assays.

Because transient expression of B^0AT1 and collectrin was unsuccessful, stable transfection was applied. The host cell line purchased from Invitrogen has only one FRT site, so the two genes of interest, B^0AT1 and collectrin, had to be separately introduced into the genome [58, 186, 188, 189, 208-211]. Stable simultaneous overexpression of multiple genes creates a number of problems, such as uneven expression and difficulties to select double transfected genes. Various methods have been reported for the integration stage as well as the selection stage. For example, a plasmid based multigene expression system called MultiLabel was reported to allow the assembly of independent expression vectors by a Cre/LoxP reaction into a single plasmid with multiple expression cassettes, yielding highly efficient co-transfection of multiple genes [212]. A Flp recombinase mediated cassette exchange (RMCE) technique was reported for the co-expression of protein complex subunits in two independent exchange loci in CHO Lec3.2.8.1 cells. The binary master cell line showed stable expression levels of a toll-like receptor and its chaperone after transfection. The author pointed out the possibility of generating multi RMCE

expression system on the basis of this protocol [213]. To improve the efficiency of cell selection after transfection, fluorescence activated cell sorting (FACS) technology was applied, and the successfully transfected cells could be sorted by different fluorescence-tagged plasmids, e.g. GFP-tagged (green) [210] or mCherry-tagged (red) [211]. It was also reported that a two-colored fluorescence marking system was used when introducing two proteins into HEK293-T cells. After antibiotic selection, the double-labelled transfected cells were further sorted by flow cytometry to ensure the success of co-expression [214].

Combination of two HTS assays can reduce the number of false-positive and false-negative hits. For instance, combination of the FLIPR membrane potential assay and the ANG-2 sodium indicator assay showed that both assays yield a large amount of unique hits in the HTS [177]. Unfortunately, the sodium indicator assay did not seem to provide a satisfactory transport-dependent signal on our cell model. Inhibition of Na^+-K^+-ATPase by Ouabain (figure 2.3.10G) or by depletion of extracellular K^+ (figure 2.3.10G) failed to reduce the background signal, indicating the existence of other factors mediating sodium influx in this cell line. Very few studies reported using ANG-2 as a sodium indicator mainly to probe neuronal circuits [174, 215]. Although there is a concentration difference between extracellular (120-150mM) and intracellular (5-15mM) sodium ion concentration, the difference is not as high as that of Ca^{2+}. As a result, it is more challenging to monitor sodium ions crossing plasma membrane, and there are less commercially available dyes as compared to Ca^{2+} indicators. In addition to the ANG-2 sodium dye used in this study, two more dyes, namely SBFI (sodium-binding benzofuran isophthalate) and CoroNa^{TM} Green, were tested and compared in prostate cancer cell lines. In this study, SBFI showed the slowest cell permeability even with the help of the dispersion agent Pluronic F127, whereas CoroNa exhibited the lowest sensitivity [172]. In a review paper, the authors pointed out that the relatively lower assay sensitivity and poorer signal-to-background ratio of the above three sodium indicators as compared to membrane potential assay dyes are the main disadvantages of them to be used in HTS [216].

Chapter 3: High-throughput Screening and Optimization of Inhibitors

3.1 Introduction

We used computational screening (also called virtual screening) as an initial tool to discover compounds that would inhibit B^0AT1. It makes use of virtual chemical compound libraries. The Zinc library, for instance, is a database containing 727,842 commercially available compounds for structure-based virtual screening [217]. Apart from the Zinc library, several smaller chemogenomic libraries from different providers are also commonly used in virtual screening. For example, the Sigma library of pharmacologically active compounds is comprised of 1280 commercially available compounds particularly targeting G protein-coupled receptors (GPCRs); the Prestwick Chemical Library only covers approved drugs with safety and bioavailability data; and the library provided by National Centre for Advancing Translational Sciences is particularly used for anticancer agent screening [218]. Homology modelling and docking are two key components for virtual screening when the structure of the real target is not available. A homology model refers to the molecular model of a target protein generated from the 3D structure of a homologous protein, whereas docking is the method to predict the orientation and binding sites of molecules when interacting with the target protein. Although much more economical compared to experimental HTS, the disadvantages of virtual screening are significantly greater hit rates including many false-positive and false-negative predictions. Major problems of virtual screening include the complexity of receptor structures and dynamic changes in receptor shapes when binding to their ligands, and difficulties in the calculation of ligand-receptor binding energies [219]. In different studies, the hit rates of virtual screening could be 100- to 1000- fold higher than experimental screenings [220, 221], however, the hits from experimental and computational approaches often show little overlap [220], indicating that they could be used complementarily.

The availability of the high-resolution structure of the leucine transporter from *Aquifex aeolicus* ($LeuT_{Aa}$) has provided us with a suitable homology model for the virtual screening. LeuT is composed of 12 transmembrane helices, with helices 1-5 and 6-10 showing two-fold inverse symmetry. This 5+5 inverted repeat fold is called LeuT fold, which is also seen in B^0AT1 as well as neurotransmitter transporters [222]. The structure of LeuT revealed one substrate binding pocket and two sodium ion binding sites, with sodium site 1 being in coordination with the carboxyl-group of the substrate leucine [223]. The reliability of the model is illustrated by its use to analyse transporter mutations found in the SLC6A19 in inherited disorders [109]. B^0AT1 (SLC6A19) is functionally closer to LeuT than the related neurotransmitter transporters

in the SLC6 family for two reasons. Firstly, leucine is a shared substrate of both LeuT and B^0AT1. Secondly, both LeuT and B^0AT1 are Na^+-dependent but Cl^--independent. One significant discrepancy is the presence of two Na^+-binding sites in LeuT, whereas only one functional binding site is observed in B^0AT1 [224]. Another notable difference is that tryptophan is a competitive inhibitor of LeuT [225] but a substrate, although weak, of B^0AT1 [84]. More recently, the dopamine transporter from Drosophila melanogaster (dDAT) has been crystallized and could be regarded as a more accurate homology model of B^0AT1 due to its higher sequence identity (33%) with B^0AT1 than LeuT (18%) [226]. A high-resolution structure of the B^0AT1 transporter has not been determined.

Apart from the computational screening, experimental high-throughput screening (HTS) is another way to identify ligands for particular targets. HTS is a method used in drug discovery, which involves a large quantity of chemical, biochemical or pharmacological tests conducted in a relatively short period of time to identify molecular structures that selectively bind to and modulate the activity of a biological target. More complex screening methods can stimulate and measure a desired phenotype in a cell or organism population. Cell-based screening is one of the most frequently used approaches to identify compounds modulating a specific biological target, especially after the development of microfluidic devices using the perfusion flow mode, the droplet mode and the microarray mode [227]. HTS of small molecule compound libraries using cell lines overexpressing the transporters of interest has been widely used to identify lead compounds for the treatment of certain diseases [228, 229]. There are mainly four types of HTS assays for compound screening, namely ligand-binding assays, flux-based assays, fluorescence-based assays and automated electrophysiological assays [216]. Ligand-binding assays are used to measure the affinity of a labelled ligand to the target binding site without measuring functional changes of the receptor such as inhibition or activation. One example is the scintillation proximity assay (SPA), in which the receptor is immobilized on a bead and the ligand is labelled with a radioactive isotope [230]. It is often used in HTS because it can readily be adapted to multiwell formats [231]. Flux assays are radioactive assays that can measure transport function. An inhibitor reduces the accumulation of labelled substrate inside the cell or vesicle [232]. Flux assays can be conducted in a multi-well format with high sensitivity and high quality of data, but the safety considerations of radioactive disposal have restrained its application in HTS [233, 234]. Fluorescence-based assays are the most frequently used assays for HTS making use of voltage sensitive dyes (e.g. $DiBAC_4(3)$ dye and FLIPR membrane potential assay kit) or ion-specific fluorescent probes (e.g. Fluo-4 calcium sensitive dye and ANG-2 sodium indicator), both of which have a wide range of applications in HTS for

transporter/ion channel inhibitors [235, 236]. Automated electrophysiological assays provide a high information content but are more costly and provide medium throughput [216].

Although HTS is a relatively time- and cost- effective way to identify potential drug candidates, it has limitations at the same time. Fluorescence-based assays can be interfered by fluorescence from the test compounds. Orange or red fluorophores can be used in some cases as the interfering light emissions from test compounds are more likely to occur at shorter wavelengths [237]. Moreover, non-specific inhibition caused by the aggregation of test compounds could lead to false-positive hits, which is a problem affecting 1.7-1.9% of total compounds in libraries [237-239]. Increasing the hit threshold might be able to reduce the false-positive rate, but at the same time increases the false-negative rate. Hence, the optimization of hit threshold compound concentration is a critical task during pilot screening [240].

After HTS, dose-response curves are generated for each identified lead compound. Then selected compounds are further tested with regard to their action on the target by secondary assays such as a second messenger assays or tissue-specific bioassays. This is used to identify lead compounds with a potency of 100nM-5μM, followed by the optimization of these leading compounds [241]. Subsequently, in vitro and in vivo assays are frequently employed to accumulate information on absorption, distribution, metabolism and excretion (ADME), as well as physicochemical and pharmacokinetic (PK) values. For channels and transporters, *Xenopus laevis* oocytes, which are immature egg cells from the South African clawed frog, are commonly used as a tool for secondary screening. The advantages of oocytes include easy handling and low background. They are used for the overexpression of membrane proteins by cRNA injections of various molecular targets [242]. For example, automated oocyte electrophysiological assays have been developed for drug screening of ion channels [243]. In addition, *Xenopus* oocytes are used in combination with radiotracer uptake assay to study transporters, channels and receptors [244]. Tissue-based assays are also used for secondary screening. For instance, mouse small intestine was used to measure glucose transport [245]. At a later stage, leading compounds are often tested in disease-specific animal models [246] to collect important in-vivo data such as efficacy and toxicity before clinical trials in humans. In-vivo studies are critical to identify compounds with high sensitivity and specificity to the target [247, 248].

3.2 Material and Methods

3.2.1 Computational screening

The large-scale virtual screening of B^0AT1 inhibitors was done by Nishank Shah in his honour's project. Since a high-resolution structure of B^0AT1 was not available, high-resolution structures of two related proteins were used, namely LeuT and dDAT (the dopamine transporter from Drosophila melanogaster), to generate homology models of B^0AT1. The virtual screening started with 14,434 compounds of the ZINC database (Version 12 [217]), which were selected by the following criteria: (1) the compounds are listed in the National Cancer Institute (NCI) diversity set; (2) compounds known to bind to or inhibit other SLC6 family members and their structural analogues; (3) the published B^0AT1 inhibitor nimesulide [249], and its analogues. All docking runs were conducted using AutoDock 4.2 compiled on the AVOCA IBM Blue Gene/Q supercomputer cluster [250] maintained by the Victorian Life Sciences Computation Initiative (VLSCI), and eventually 40 highest scoring compounds from various clusters were ordered from the Developmental Therapeutics Program of the NCI for further experimental tests. The second round of computational screening was based on a set of 158 structural analogues of two best B^0AT1 inhibitors (NSC63912 and 186059) from the above compounds in *in vitro* experiments, resulting in another 38 compound candidates requested from NCI [251].

3.2.2 RT-PCR to analyse expression of various transporters in cell lines

Sequence of primers are listed in the appendix.

The set-up of PCR reactions and PCR programs was the same as for hB^0AT1 and hcollectrin in Chapter 1. For visualisation, the PCR products were mixed (5:1) with 6x sample loading buffer (Invitrogen) and analysed on 1% (w/v) agarose gels containing SYBR™ Safe DNA Gel Stain. 1x TAE (Invitrogen, #S33111) was used as a running buffer. PCR products were detected under UV light. The expected band sizes of the analysed transporters were 407bp for hLAT1 (PROLIGO), 432bp for hLAT2 (PROLIGO), 481bp for 4F2hc (Sigma), 394bp for $hATB^{0,+}$, (PROLIGO) and 351bp for hASCT2 (PROLIGO).

3.2.3 Animals

The animal studies were performed in accordance with the National Health and Medical Research Council's (NHMRC) Australian Code for the Care and Use of Animals for Scientific Purposes and the ACT Animal Welfare Act 1992, and were approved by the Animal

Experimentation ethics committee of the Australian National University (A2014/20 for the use of X. laevis and A2013/39 for the use of mice, updated version A2016/41).

Male and female C57BL/6J mice (Animal services, the Australian National University) were sacrificed for intestinal substrate uptake assay at an age of 4-6 months, and C57BL/6NCrl female mice were used in the pharmacological study at an age of 6-8 months. Mice were held in individually ventilated cages (<5 mice per cage) under specified pathogen-free conditions with a 12hr light/12hr dark cycle and were checked daily for general health. Cervical dislocation or euthanasia with CO_2 flow were used to sacrifice animals before taking out organs or at the end of the experiment.

X.laevis were housed in tanks (<20 animals per tank) with tank water filtered in a closed system. Frogs were anesthetized by submersion in water containing MS-222 until loss of reflexes. The surgical procedures and preparation and injections of oocytes has been described previously [252] and was conducted by Angelika Broer and Stephen Fairweather.

3.2.4 Radio-labelled substrate uptake assay on injected oocytes

After being maintained in OR2+ buffer (82.6mM NaCl; 2.55mM KCl; 1.27mM Na_2HPO4; 2.1mM $MgCl_2$; 5mM HEPES) overnight, healthy oocytes were selected for injection. Into each oocyte, 10ng hB^0AT1 cRNA construct and/or 2ng hcollectrin cRNA construct was injected. The uptake assays were performed 4-5 days after the cRNA injection. Before the assay, the non-injected and injected oocytes were observed under microscope and 10-12 healthy ones were transferred into tubes for each treatment. The oocytes were pre-washed three times with 4mL ND96 buffer (96.2mM NaCl; 2mM KCl; 2.1mM $MgCl_2$; 5mM HEPES) (room temperature), then incubated in buffers containing ^{14}C-labelled substrate (leucine or isoleucine) for 15 min, in the presence of 300μM inhibitors as indicated in the figures. At the end of the treatment, the radioactive buffer was removed immediately and the oocytes were washed four times with 4mL ice-cold ND96 buffer. Each oocyte was transferred into one scintillation vial containing 200μL of 10% SDS. The lysis of oocytes was completed in 2-3hr. After that, 2.5-3mL of scintillation fluid was added into each vial and the radioactivity was measured by a scintillation counter. The activity of non-injected oocytes was subtracted before data analysis.

3.2.5 Radio-labelled substrate uptake assay on inverted sections of mouse small intestine

Before the assay, the following buffers were freshly prepared.

Buffer 1: 0.9% (w/v) NaCl + 1mM glutamine + Protease Inhibitor Cocktail Tablet (1 tablet per 50mL, Roche, #11873580001) in ddH_2O, pre-cooled on ice;

Buffer 2: 90% Hank's -Na^+ buffer + 10% Hank's +Na^+ buffer + 1mM glutamine + Protease Inhibitor Cocktail Tablet, one 50mL tube pre-cooled on ice, one 50mL tube pre-warmed in 37°C water bath;

Buffer 3: Hank's -Na^+ buffer + 1mM glutamine + Protease Inhibitor Cocktail Tablet, pre-warmed in 37°C water bath;

Buffer 4: 90% Hank's -Na^+ buffer + 10% Hank's +Na^+ buffer + Protease Inhibitor Cocktail Tablet, two tubes pre-warmed in 37°C water bath;

Buffer 5: Hank's -Na^+ buffer + Protease Inhibitor Cocktail Tablet, two tubes pre-warmed in 37°C water bath;

For the uptake assay C57BL/6J mice at an age of 4-6 months were sacrificed and the complete small intestine was taken out immediately afterwards. The small intestine was immersed in ice-cold buffer 1 and the intestinal lumen was rinsed with the same buffer using a syringe with a blunt-end needle. Then the small intestine was fitted to the outside of a metal rod before being inverted from one end to another to expose villi and microvilli. It was then pulled off the rod and immediately transferred to a glass plate containing ice-cold buffer 2 and cut into 1cm pieces. The small pieces were slid onto plastic enzyme spatulas and immersed in pre-warmed buffer 2 or buffer 3 for measuring sodium-dependent or -independent uptake, respectively. The pieces in buffer 2 were successively washed in two tubes of buffer 4 (to remove glutamine), while pieces in buffer 3 were washed in buffer 5. After washing, the intestinal pieces were pre-incubated in tubes containing 2mL treatment buffer (buffer 4 for Na^+-dependent uptake and buffer 5 for Na^+-independent uptake, together with 300µM of the indicated inhibitors) at 37°C for 15min, then transferred to uptake buffer (Hank's +Na^+ buffer for Na^+-dependent uptake and Hank's -Na^+ buffer for Na^+-independent uptake, supplemented with 150µM [^{14}C]leucine and 300µM inhibitor) at 37°C for 30sec. Then each intestinal piece was briefly immersed in three tubes of ice-cold stopping buffer (Hank's +Na^+ buffer, 4mL/tube) to terminate the uptake. Every intestinal piece was transferred to one scintillation tube containing 400µL 10% SDS. After 2-3hr when the lysis was completed, the radioactivity was quantified by scintillation counting in the presence of scintillation fluid (2.5-3mL/tube).

3.2.6 Mouse feeding and 24hr urine/faecal sample collection for pharmacological studies

For the pharmacological *in vivo* study, fourteen C57BL/6NCrl female mice at an age of 6-8 months were ordered from the Australian Phenomics Facility (APF) and held in separate cages (one mouse per cage) in the animal holding room (Room 3.049, Building 134, the Australian National University). The administration of drugs and intraperitoneal glucose tolerance test (IPGTT) were all conducted in the laminar flow hood. Littermates were randomly assigned to treatment group and control group, so that the age and genetic background between two groups were matched. According to a previous study on food and water intake in 28 mouse strains, the daily food intake for C57BL/6 strain is approximately 4-5 grams per mouse [253]. Benztropine was reported to be used at a maximal dosage of 250mg/kg diet on mice in a study of energy expenditure [254]. Accordingly, 1.25mg benztropine in 5g of chow was given to each mouse every day. To administer the drug, benztropine mesylate powder (≥98% (HPLC)) was purchased from Sigma (#SML0847) and dissolved in ddH_2O at a concentration of 1.25mg per 250μL water. Since each mouse in the treatment group was provided with 5g chow, the pellets were soaked in 250μL water containing 1.25mg benztropine. The fortified pellets were given for 14 days. Each mouse in the control group was provided with same amount of chow soaked in 250μL water. The prepared chow pellets were stored at 4°C and pre-warmed to 37°C before providing them to mice. The consumption of chow pellet was recorded to calculate the daily drug dose.

For each mouse, 24hr urine and faecal samples were collected before and after the administration of benztropine (d0 for baseline, d7 and d14 after drug administration on day 1). The mice were trained inhabiting metabolic cages for at least three days (2-3hr per day) before the first sample collection to minimize their stress in the new environment. Sample collection started at 5pm and ended at 5pm the following day, with sufficient drinking water provided. After overnight starvation (no more than 16hr) in metabolic cages, the mice were offered 5g chow pellet containing 1.25mg benztropine for 2hr in their original cages in the morning, before returning the mice to metabolic cages for further sample collection. The remainder of the chow pellet was weighed and the consumed amount of drug was calculated as the dose for 24hr. The urine and faecal samples were collected in separate containers standing in dry ice. After collection, the aliquots of urine and faecal samples were stored at -80°C until GC-MS analysis.

3.2.7 Intraperitoneal glucose tolerance test (IPGTT)

Intraperitoneal glucose tolerance test (IPGTT) was performed on mice before and after the treatment with benztropine. The body weight of each mouse was recorded before the test. D-

glucose test solution was prepared by dissolving 2g of D-glucose in 0.9% (w/v) NaCl in water. After overnight starvation (~16hr), the fasting blood glucose concentration was measured by an ACCU-CHEK Performa glucometer (Roche). Blood from the tail vein was used and a drop of blood was applied to the glucometer strip after getting rid of the first drop. Then each mouse was injected intraperitoneally with pre-prepared glucose solution (2g glucose per kg body weight), and the blood glucose concentration was measured at 15, 30, 60, 90, 120min after the injection.

3.2.8 Sample preparation for GC/MS analysis

Metabolites in urine and faecal samples were analysed by GC/MS. After thawing, the samples were spun down at 13,000rpm and 4°C for 5min. The osmolarity of the supernatant of urine samples was measured and adjusted to 500 mOsm/kg by ddH_2O. Urea in the sample was hydrolysed by urease into carbon dioxide and ammonia (Sigma, #U1500-20kU, 1.28mg [50 units] dissolved in 8µL ddH2O for 20µL urine sample). The hydrolysis was performed by incubation at 37°C for 60min with mixing at 15-minute intervals. The samples were cooled on ice immediately after urease treatment and centrifuged at full speed (16,000 x g) for 1min in a benchtop centrifuge. Then 90 µL of supernatant was mixed with 720µL methanol, 180µL H_2O and 10µL of internal standard Ribitol (2mg/mL in methanol) in a new microcentrifuge tube. After incubation on ice for 20min, the mixture was centrifuged at 13,000rpm and 4°C for 15min, and 60µL of the supernatant was transferred to a glass vial and dried in a vacuum centrifuge overnight. The rest of the supernatant was stored at -80°C. Two vials containing amino acid standard solution and two vials containing quality controls (QCs, a mixture of aliquots from each sample) were also dried in the vacuum centrifuge.

Faecal samples were lyophilized for 2 days until completely dry. Then the faecal samples were ground into powder with ball bearings using a Tissue Lyser II (Qiagen). Approximately 20mg of each faecal sample was added into a new microcentrifuge tube, and extracted with methanol/H_2O (8:2) in the presence of 20µL of internal standard Ribitol in methanol (2mg/mL). The volume of methanol/H_2O was adjusted to 1mL per 20mg faecal sample. Then the mixture was continuously vortexed for 10min, followed by centrifugation at 13,000rpm and 4°C for 5min. The supernatant was transferred to a new tube and centrifuged again to completely remove any debris. Finally, 30µL supernatant was transferred to a glass vial and dried in a speed vac overnight together with vials containing AA standards and QCs (a mixture of aliquots from each sample). The rest of the supernatant was stored at -80°C.

After drying, the samples were ready for derivatisation and analysis by gas chromatography-mass spectrometry (GC-MS).

3.2.9 Statistical Analysis

Data are shown as mean ± S.D, and the Na^+ -dependent net uptake was the difference between the uptake level in -Na^+ buffer and the total uptake level in +Na^+ buffer. The fluorescent signals measured in the FLIPR assay were normalized to baseline readings (before the addition of substrates set at 100%). IC_{50} curves were generated by non-linear regression log[inhibitor] vs. response, and IC_{50} values were calculated using the equation $y = y_{max}\left(1 - \frac{[x]}{[x]-IC_{50}}\right)$. Eadie-Hofstee transformation of transport data was used to determine the mode of inhibition. T-test was used to compare two groups, whereas One-way ANOVA was used to compare multiple groups.

3.3 Results

3.3.1 Inhibition of B^0AT1 by substrate analogues

Firstly, 24 analogues of amino acid substrates were purchased from Sigma and their inhibitory effects on B^0AT1 transport was tested using CHO-BC cells. Compound No. 1-17 were analogues of L-cysteine, No. 18-20 were analogues of L-methionine, and No. 21-24 were analogues of L-serine. These compounds were first screened using the membrane potential assay at an inhibitor concentration of 300μM and a substrate concentration of 1.5mM (figure 3.3.1A). Generally, analogues of L-cysteine showed stronger inhibition of B^0AT1 activity compared to L-methionine and L-serine analogues. Four compounds caused an apparent membrane hyperpolarization rather than depolarization in the presence of 1.5mM leucine (the fluorescence signals became lower than baseline after the addition of leucine) and could not be analysed. Apart from the compounds with poor inhibition at 300μM (height of the bar was close to or above the red line in figure 3.3.1A), the rest of the analogues were further tested in dose-response experiments. IC_{50} values were determined by both membrane potential assay and radioactive substrate uptake assay, and the four best inhibitors with the lowest IC_{50} values are listed in Table 3.3.1 and highlighted in figure 3.3.1A by purple frames. The dose-response curves of S-Benzyl-L-Cysteine are shown in figure 3.3.1C as an example, inhibiting leucine uptake with an IC_{50} of 14±2μM according to the FLIPR assay, but a much higher IC_{50} of 398±29μM was determined using a [^{14}C]isoleucine uptake assay (Table 3.3.1, figure 3.3.1C). S-Benzyl-L-Cysteine was a more potent inhibitor of endogenous Na^+-independent amino acid transport with an IC_{50} of 33±3μM (figure 3.3.1C). Next, the possibility of these analogues to be B^0AT1 substrates was measured using the membrane potential assay in the absence of a physiological substrate (figure 3.3.1B). Three of the four selected compounds in table 3.3.1 appeared to be substrates of B^0AT1, inducing even higher depolarization peaks than the same concentration (300μM) of leucine, except S-(4-Tolyl)-L-Cysteine.

Table 3.3.1: IC_{50} values of AA substrate analogues as B^0AT1 inhibitors.

No.	Compound	Structure	IC_{50}(FLIPR)	IC_{50}(Uptake)
1	L-Cysteine S-sulfate	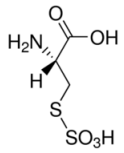		
2	S-Carboxymethyl-L-cysteine	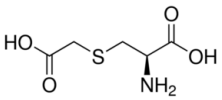		
3	L-Cysteine(Z)-OH	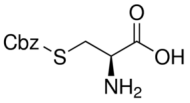		
4	S-Benzyl-L-Cysteine	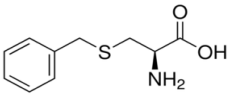	14±2µM	398±29µM
5	S-(4-Tolyl)-L-Cysteine	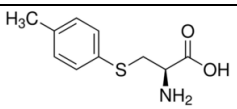	23±14µM	205±46µM
6	(+)-S-Trityl-L-cysteine	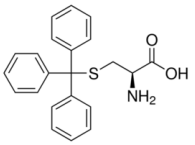		
7	S-Acetamidomethyl-L-cysteine HCl	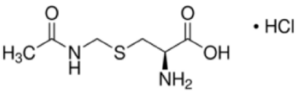		
8	S-tert-Butylmercapto-L-cysteine	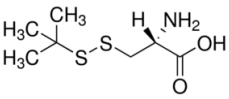		
9	S-Phenyl-L-cysteine	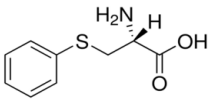	49±23µM	
10	S-Allyl-L-cysteine	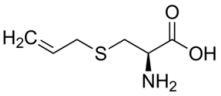		
11	S-Benzyl-L-cysteine sulphone	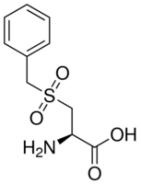		
12	H-Cys(4-methoxytrityl)-OH	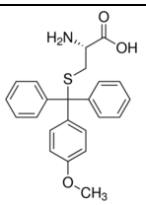		

No.	Compound	Structure	IC_{50}(FLIPR)	IC_{50}(Uptake)
13	H-Cys(carbamoyl)-OH	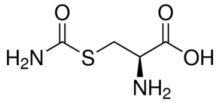		
14	H-Cys(Fm)-OH	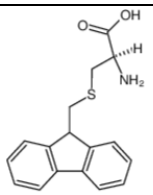		
15	H-Cys(Dpm)-OH	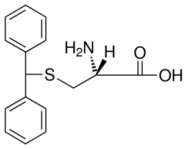		
16	H-Cys(Bzl)-OH	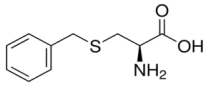		
17	S-Cys(aminoethyl)-OH HCl	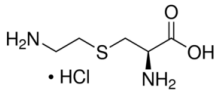		
18	L-methionine sulfoximine	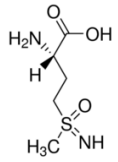		
19	L-methionine sulfone	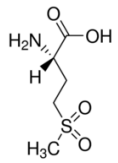		
20	L-methionine sulfoxide	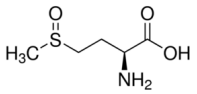		
21	O-Benzyl-L-serine	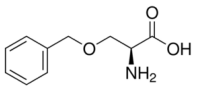	14±5μM	810±176μM
22	O-Phospho-L-serine	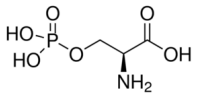		
23	O-Acetyl-L-serine HCl	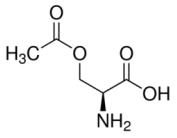		
24	O-tert-Butyl-L-serine	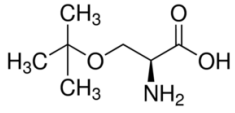		

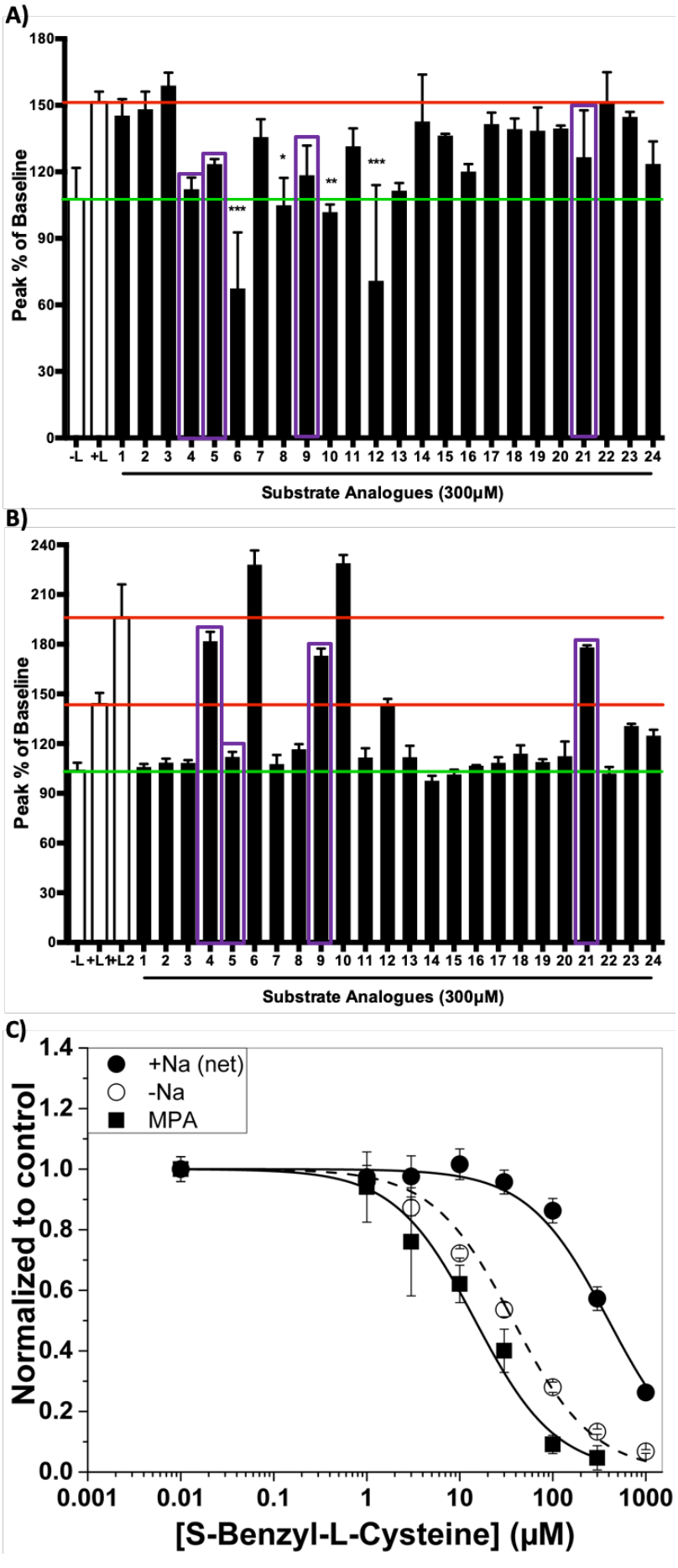
A)
Peak % of Baseline
180
150
120
90
60
30
0
-L +L 1 2 3 4 5 6 7 8 9 10 11 12 13 14 15 16 17 18 19 20 21 22 23 24
Substrate Analogues (300µM)
B)
Peak % of Baseline
240
210
180
150
120
90
60
30
0
-L +L1 +L2 1 2 3 4 5 6 7 8 9 10 11 12 13 14 15 16 17 18 19 20 21 22 23 24
Substrate Analogues (300µM)
C)
+Na (net)
-Na
MPA
Normalized to control
1.4
1.2
1.0
0.8
0.6
0.4
0.2
0.0
0.001
0.01
0.1
1
10
100
1000
[S-Benzyl-L-Cysteine] (µM)

Figure 3.3.1: Screening of amino acid analogues. A) Inhibition of B^0AT1 transport by substrate analogues. CHO-BC cells were pre-loaded with blue dye in Hank's $+Na^+$ buffer containing 300µM substrate analogues at RT for 30min. After baseline reading, 50µL of leucine solution was automatically injected into each well to a final concentration of 1.5mM to induce a depolarization peak (red line indicated positive control), while 50µL of Hank's $+Na^+$ buffer was injected as a negative control (green line). The bar graph shows the peak hyperpolarization or depolarization as percent of baseline as average ± std (n=3, e=1). *, $p<0.05$; **, $p<0.01$; ***, $p<0.001$, as compared to +leucine control. Inhibitors chosen for radioactive uptake experiments are shown in purple boxes. B) Response of CHO-BC cells to inhibitors in the absence of amino acid substrate. CHO-BC cells were pre-loaded with the blue dye in Hank's $+Na^+$ buffer at RT for 30min. After baseline reading, 50µL of substrate analogues was manually injected into each well to a final concentration of 300µM, with leucine (300µM for L1 and 1.5mM for L2) serving as positive controls (two red lines), while 50µL of Hank's $+Na^+$ buffer was injected as a negative control (green line) (n=3, e=1). C) IC_{50} values of S-Benzyl-L-Cysteine determined by membrane potential assay (MPA, squares) and [^{14}C]isoleucine uptake assay (circles). The [^{14}C]isoleucine uptake assay was performed in the presence and absence of Na^+ to determine the effect on B^0AT1 (filled circles) and on the CHO-BC cell endogenous transporters (open circles). Various concentrations of S-Benzyl-L-Cysteine (1, 3, 10, 30, 100, 300 and 1000µM) were either incubated with blue dye for 30min in the MPA, or with the 150 µM [^{14}C]isoleucine for 6min in the uptake assay. The results were normalized to positive controls, which was 1.5mM leucine stimulation in the MPA and uptake of 150 µM [^{14}C]isoleucine in the absence of S-Benzyl-L-Cysteine (n=3, e=5).

3.3.2 Screening of NCI compounds

A total number of forty compounds were selected from virtual screening and requested from NCI. The membrane potential assay was used as the initial screening tool for these compounds and 11 of them showed significant inhibition of B^0AT1 transport function at a concentration of 300μM (figure 3.3.2A). Three of the 11 compounds caused an apparent membrane hyperpolarization instead of depolarization after the addition of 1.5mM leucine. Compound No. 5 and 19 were excluded from figure 3.3.2A because of their high toxicity to the cells, indicated by the detachment of cells at the end of the incubation. After further testing compound NSC63912 (No. 11) and NSC186059 (No. 25) (highlighted with orange boxes in figure 3.3.2A) were identified as the strongest inhibitors in this batch based on their IC_{50} values (figure 3.3.2B&D). The IC_{50} values of NSC63912 (benztropine) were 44±9μM and 71±8μM by FLIPR assay and uptake assay, respectively (figure 3.3.2B). The IC_{50} values of NSC186059 were 61±25μM and 92±22μM by FLIPR assay and uptake assay, respectively (figure 3.3.2D). In the membrane potential assay (figure 3.3.2F), 300μM NSC63912 (benztropine) resulted in a depolarization peak similar to that observed after addition of 300μM leucine, whereas same concentration of NSC186059 did not alter the membrane potential. A second round of computational screening was based on a similarity search starting with NSC63912 and NSC186059 (figure 3.3.2C&E), resulting in another 38 compound candidates which were requested from NCI.

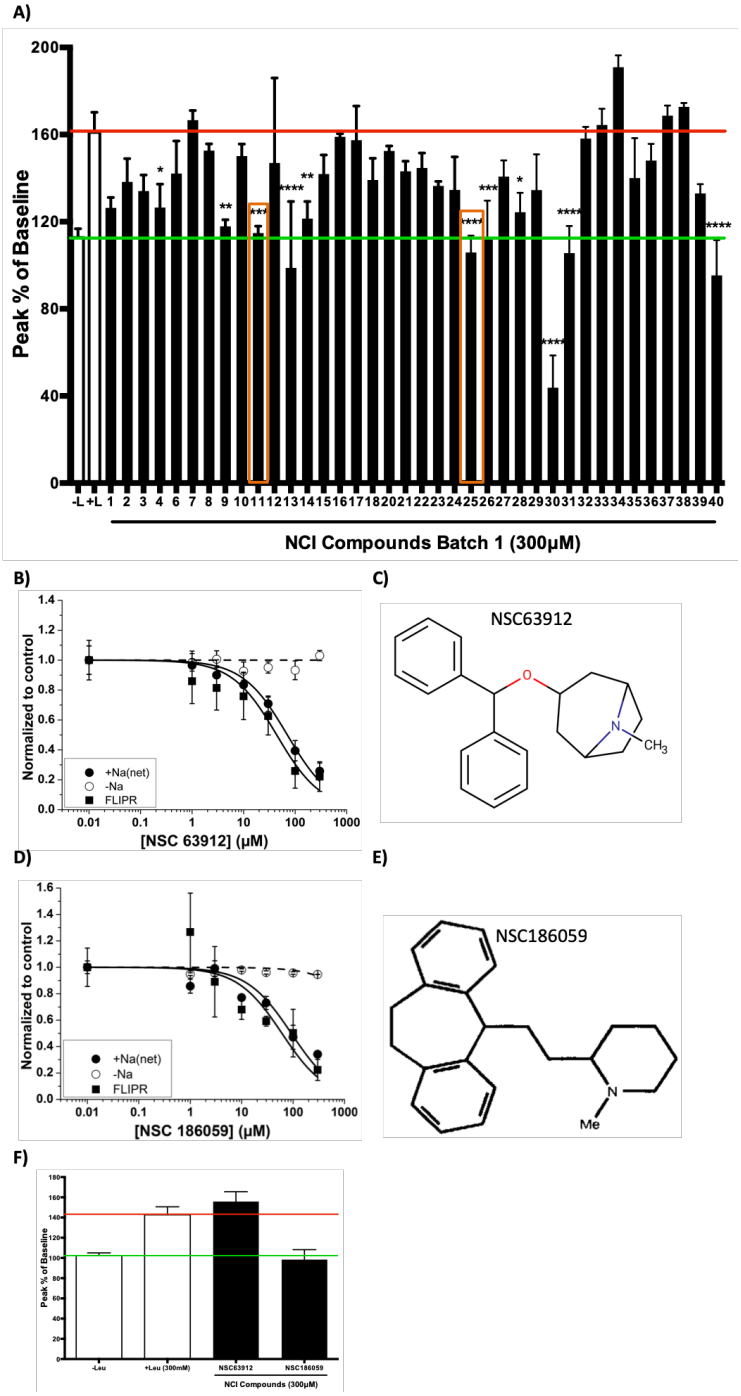

Figure 3.3.2: Screening of NCI compounds Batch 1. A) Inhibitory effects of 40 NCI compounds on B^0AT1 transport measured by membrane potential assay. *, $p<0.05$; **, $p<0.01$; ***, $p<0.001$; ****, $p<0.0001$, as compared to +leucine control (n=3, e=1). B) and D) IC_{50} values of NSC63912 (compound 11) (n=3, e=5) and NSC186059 (compound 25) (n=3, e=1) determined by membrane potential assay (FLIPR, filled squares) or by [^{14}C]isoleucine uptake assay (circles). The [^{14}C]isoleucine uptake assay was performed in the presence and absence of Na^+ to determine the effect on B^0AT1 (filled circles) and on the CHO-BC cell endogenous transporters (open circles). C) and E) Chemical structures of NSC63912 and NSC186059. F) Test whether inhibitors are B^0AT1 substrates by membrane potential assay. After baseline reading, 50μL of compounds was manually injected into each well to the final concentration of 300μM, with 300μM leucine as a positive controls (red line), while 50μL of Hank's $+Na^+$ buffer was injected as a negative control (green line) (n=3, e=1).

3.3.3 Screening of NCI compounds Batch 2

Among the 38 compounds of the second batch, 21 caused significant inhibition of B^0AT1 transport function at a concentration of 300μM (figure 3.3.3A). The positive rate of this batch (55%) was 2-fold higher than that in the first batch (27.5%). Among these 21 compounds, two caused membrane hyperpolarization after the addition of 1.5mM leucine (No. 68 and No. 76). No compound was excluded due to toxicity as judged by cell adherence. Further functional tests confirmed that compound NSC22789 (No. 44) and NSC39706 (No. 51) (highlighted with orange boxes in figure 3.3.3A) were the most potent B^0AT1 inhibitors in this batch. The IC_{50} values of NSC22789 were 90±21μM and 78±16μM by FLIPR assay and uptake assay, respectively (figure 3.3.3B). The IC_{50} values of NSC39706 were 13±3μM and 70±21μM by FLIPR assay and uptake assay, respectively (figure 3.3.3D). The [^{14}C]isoleucine uptake assay was performed in the presence and absence of Na^+ to determine the effect on B^0AT1 (filled circles) and on the CHO-BC cell endogenous transporters (open circles). In the membrane potential assay (figure 3.3.3F), 300μM NSC39706 caused a depolarization peak similar to that observed after addition of 300μM leucine, whereas the same concentration of NSC22789 raised the membrane potential to a lesser extent. The chemical structures of these two B^0AT1 inhibitors are shown in figure 3.3.3C&E.

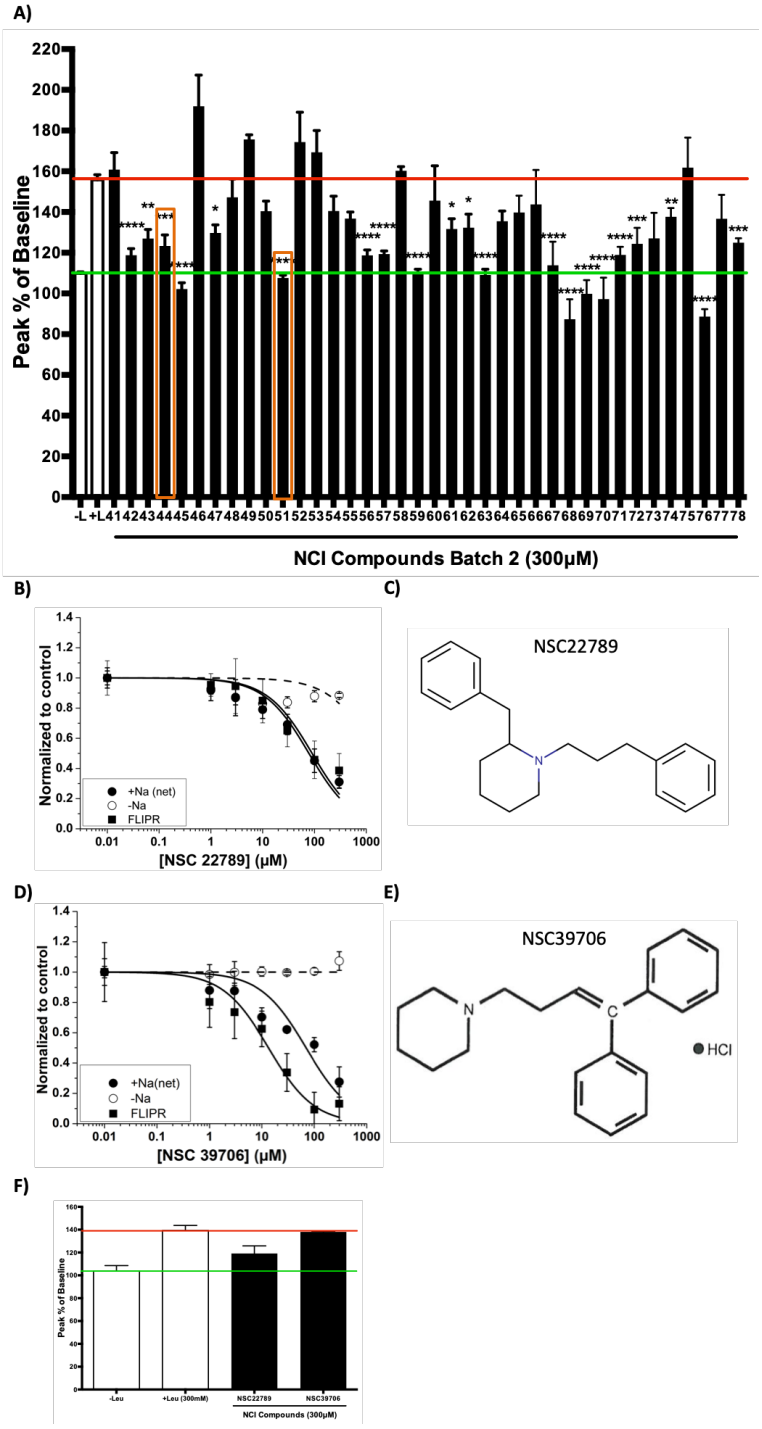

Figure 3.3.3: Screening on NCI compounds Batch 2. A) Inhibitory effects of 38 NCI compounds on B^0AT1 transport measured by membrane potential assay. *, p<0.05; **, p<0.01; ***, p<0.001; ****, p<0.0001, as compared to +leucine control (n=3, e=1). B) and D) IC_{50} values of NSC22789 (compound 44) (n=3, e=5) and NSC39706 (compound 51) (n=3, e=1) determined by membrane potential assay (FLIPR, filled squares) and uptake of [^{14}C]isoleucine (filled circles). Inhibition of the endogenous transporter is shown for comparison (open circles). C) and E) Chemical structures of NSC22789 and NSC39706. F) NSC22789 and NSC39706 were tested as putative substrates (300µM) of B^0AT1 using the membrane potential assay. Leucine (300µM) was used as a positive control and Hank's buffer as a negative control. NSC39706 elicited a similar depolarization signal as leucine, while NSC22789 was weaker (n=3, e=1).

3.3.4 Other transporter Inhibitors

Nimesulide was previously reported as a B^0AT1 inhibitor [249], hence, we tested this compound in our cell model. Surprisingly, nimesulide only inhibited B^0AT1 after a 4hr-preincubation, with an IC_{50} of 178±40μM (figure 3.3.4A). Loratadine is a published inhibitor of B^0AT2 [255] and its structure is closely related to benztropine. However, it did not inhibit the transport of leucine via B^0AT1 at 300μM (figure 3.3.4B). Another compound ALX1393, reported as an inhibitor of the glycine transporter 2 (GlyT2) [256], inhibited the endogenous Na^+-independent isoleucine uptake rather than Na^+-dependent uptake in CHO-BC cells (figure 3.3.4C). Thus, none of these inhibitors was superior to the inhibitors selected from computational screening.

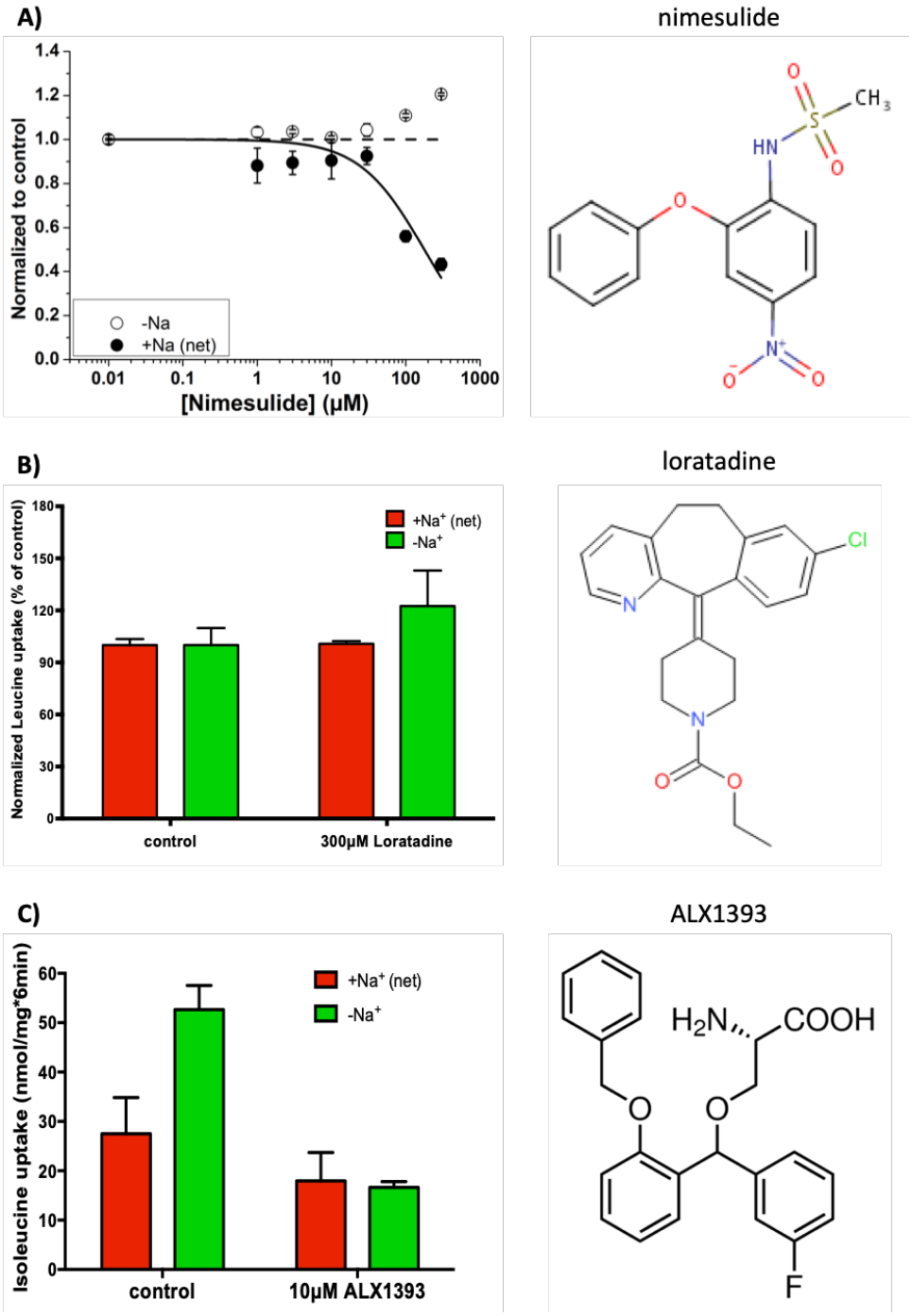

Figure 3.3.4: Testing known inhibitors of B^0AT1 and related transporters. The [^{14}C]isoleucine uptake assay was performed in the presence and absence of Na^+ to determine the effect on B^0AT1 (filled circles or red bars) and on the CHO-BC cell endogenous transporters (open circles and green bars). A) Dose-response curve (left) of nimesulide measured by radioactive substrate uptake assay after 4hr pre-incubation with the indicated concentration of the compound (n=3, e=1) and chemical structure of nimesulide (right). B) The inhibition of B^0AT1 by 300µM loratadine (Sigma, L9664) was tested by measuring the uptake of 100µM [^{14}C]leucine over 6min in the presence of the inhibitor without pre-incubation (n=3, e=1) (left). Chemical structure of loratadine is shown on the right. C) The inhibition of B^0AT1 by 10µM compound ALX1393 (Sigma, A5475) was tested by measuring the uptake of 150µM [^{14}C]isoleucine over 6min, in the presence of the inhibitor without pre-incubation (n=3, e=1). Chemical structure of ALX1393 is shown on the right.

3.3.5 Mechanism of inhibition

To characterise the selected B^0AT1 inhibitors further, I investigated the mechanism of inhibition. Under physiological condition, the substrate and sodium ion bind to their binding sites on the transporter before being transported into the cells. In the presence of a competitive inhibitor, however, one or both binding sites will be occupied by the inhibitor, preventing binding of the substrate to the transporter. Because the inhibitor binds reversibly to the transporter, the inhibitor can be displaced by adding more substrate. Hence, regardless of the concentration of a competitive inhibitor, a sufficiently high substrate concentration will always displace the inhibitor from the active binding site, allowing the transport to reach its Vmax albeit at a higher substrate concentration, i.e. an increased K_m is observed in the presence of a competitive inhibitor. In the Eadie-Hofstee transformation of transporter kinetics, the V_{max} is the intercept of the regression line with the y-axis, while the slope is the - K_m. For competitive inhibitors, different slopes are observed, while all regression lines converge on the ordinate. This pattern is shown by the substrate analogue S-Benzyl-L-cysteine and NCI inhibitors NSC63912 (benztropine) and NSC39706 (figure 3.3.5A, B, E). The membrane potential assay showed that these three compounds were substrates of B^0AT1, with similar or even higher preference compared to leucine (figure 3.3.1B, 3.3.2F, 3.3.3F), indicating their binding at the substrate binding site.

On the contrary, a non-competitive inhibitor binds to a site distinct from the substrate binding site of the transporter. It can form a complex with the transporter or the transporter-substrate complex to inhibit the transport activity. The inhibitor does not prevent binding of the substrate to the transporter, therefore, the increase of the substrate concentration cannot displace the inhibitor from the transporter. As a result, a constant K_m and decreased V_{max} is observed in the presence of increased non-competitive inhibitor. This pattern is shown by NCI compounds NSC186059 (figure 3.3.5C) and NSC22789 (figure 3.3.5D). The membrane potential assay showed no inhibitor-induced depolarization in NSC186059-treated cells (figure 3.3.2F), and only a small depolarization peak in NSC22789-treated cells (figure 3.3.3F). This is consistent with both compounds inhibiting B^0AT1 in a non-competitive manner.

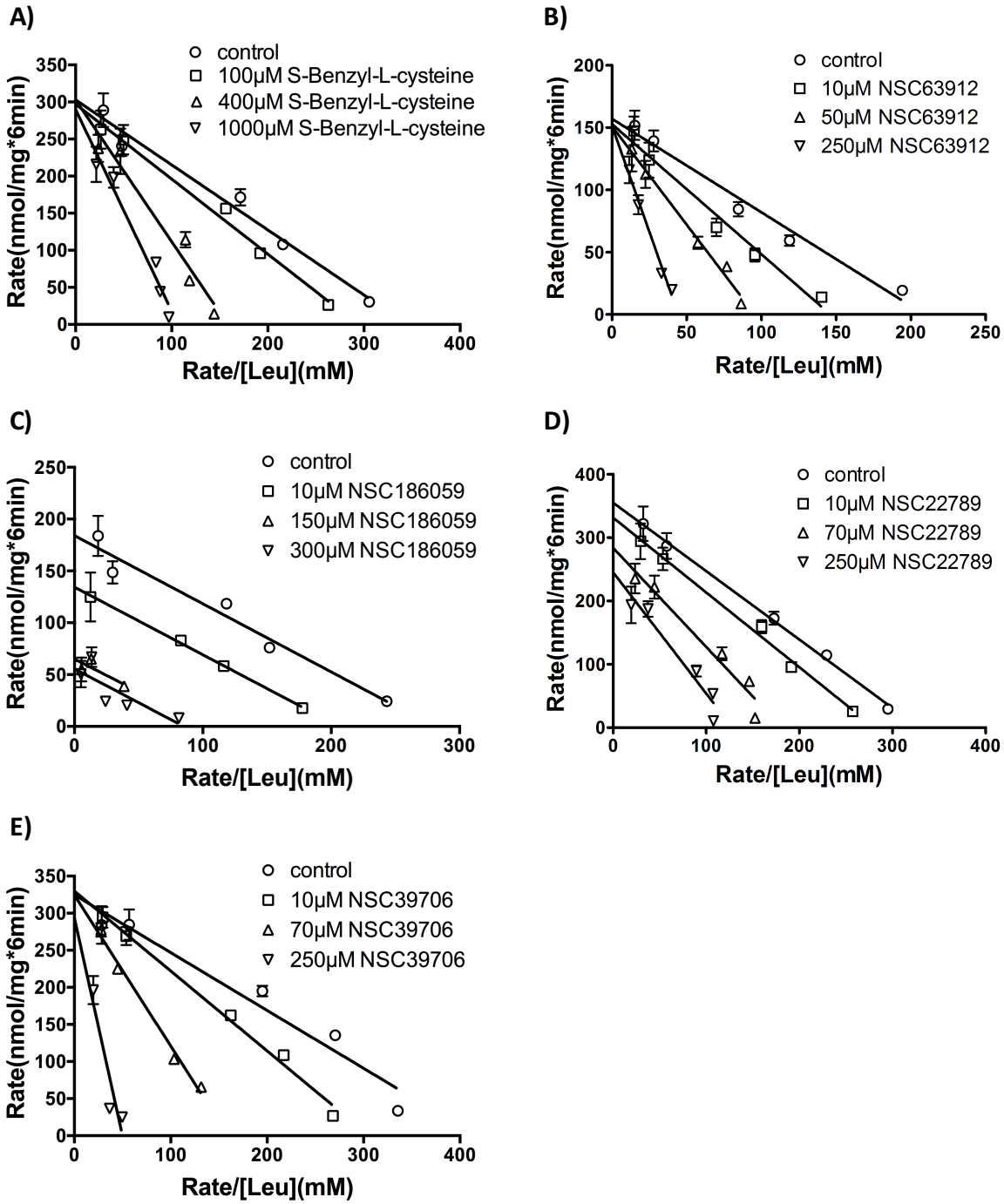

Figure 3.3.5: Mechanism of inhibition. Eadie-Hofstee transformation of the data was used to analyze the mode of inhibition. CHO-BC cells were exposed to Hank's buffer containing different concentrations of inhibitors as indicated in the figures as well as different concentrations of amino acid substrate (0.1, 0.5, 1, 5, 10mM [^{14}C]leucine) for 6min before harvesting and counting of radioactivity. A) S-Benzyl-L-cysteine was determined to be a competitive inhibitor based on a constant V_{max} but altered K_m with changing compound concentration. B) NSC63912 (benztropine) was also determined to be a competitive inhibitor. C) NSC186059 was determined to be a non-competitive inhibitor indicated by a constant K_m but altered V_{max} with changing compound concentration. D) NSC22789 was determined to be a non-competitive inhibitor, as well. E) NSC39706 was determined to be a competitive inhibitor.

3.3.6 B^0AT1 inhibitors tested in other systems

After the *in vitro* characterisation in CHO-BC cells, the selected inhibitors of B^0AT1 were further tested in other systems. *Xenopus* oocytes are widely used for the characterisation of transporters including hB^0AT1 and hcollectrin [40, 73]. As shown in figure 3.3.6A, expressing hB^0AT1 was not sufficient to facilitate sodium-dependent uptake of isoleucine. Expression of hcollectrin alone in oocytes induced a small transport activity, while co-expressing hB^0AT1 as well as hcollectrin induced an obvious intake of isoleucine in the presence of Na^+. After the validation of this expression system, the inhibitory effects on B^0AT1 by selected inhibitors were tested by incubating oocytes expressing hB^0AT1 and hcollectrin in the presence of 300µM inhibitors and 100µM [^{14}C]isoleucine for 15min. Almost no inhibition of Na^+-dependent isoleucine uptake was observed in the presence of NSC63912 (benztropine) and NSC186059, whereas a slight reduction of isoleucine uptake was caused by the substrate analogue, S-(4-Tolyl)-L-cysteine (figure 3.3.6B). When inhibitors were injected into the oocytes (figure 3.3.6C), or pre-incubated with oocytes for 30min (figure 3.3.6D), a more obvious decrease of Na^+-dependent isoleucine or leucine uptake was observed by both NSC63912 (benztropine) and NSC22789, the latter showing stronger inhibition. To study the action of selected inhibitors in an *in vitro* system that is closer to the *in vivo* situation, we used sections of inverted mouse small intestine. In this preparation, similar amounts of leucine were taken by sodium-dependent transport (B^0AT1) as well as sodium-independent transport of unknown origin. The two inhibitors NSC63912 (benztropine) and NSC22789 blocked the sodium-dependent uptake significantly without interfering with the sodium-independent uptake (figure 3.3.6E).

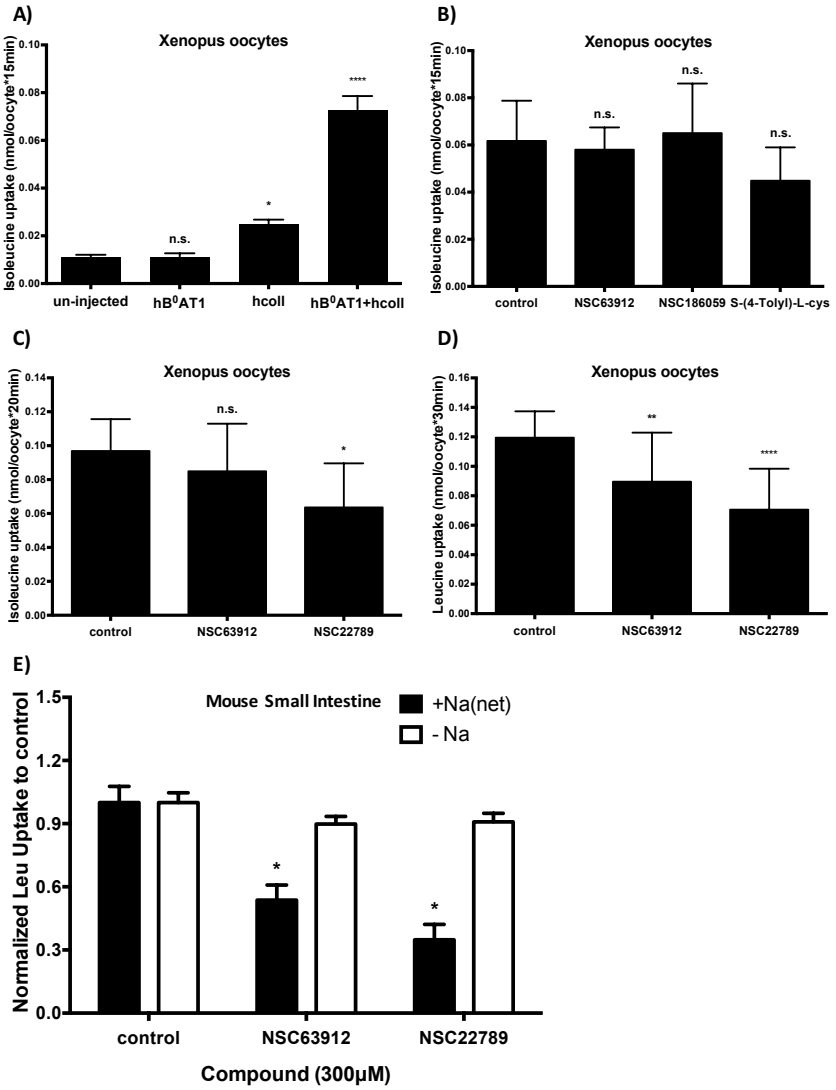

Figure 3.3.6: Efficacy of B^0AT1 inhibitors in different systems. A) Xenopus oocytes were injected with cRNA encoding hB^0AT1, hcollectrin or combinations thereof. Four days post injection, [^{14}C]isoleucine (100µM) uptake was measured over a period of 15min. Ten oocytes were selected from each group and un-injected oocytes were used as negative controls. *, $p<0.05$; ****, $p<0.0001$; n.s. no significance, as compared to un-injected oocytes. B) Four days after injection, [^{14}C]isoleucine uptake was measured over a period of 15min in the presence of 300µM inhibitors. Data is presented as the uptake level in hB^0AT1+hcollectrin cRNA injected oocytes minus the uptake level in uninjected oocytes. C) Three days after injection with cRNA encoding hB^0AT1 and hcollectrin, Xenopus oocytes were injected with 40nL of 3mM compound NSC63912 and NSC22789 dissolved in 100mM KCl. Uptake of [^{14}C]isoleucine (100µM) was measured over a period of 20min 47min post inhibitor injection. D) Four days after injection, the oocytes were pre-incubated in buffer containing 300µM inhibitors for 30min before the measurement of [^{14}C]isoleucine uptake over 30min in the presence of 300µM inhibitors. Data is shown as the uptake activity of hB^0AT1+hcollectrin cRNA injected oocytes after subtracting the uptake activity of uninjected oocytes. This experiment was performed by Stephen Fairweather. *, $p<0.05$; **, $p<0.01$; ****, $p<0.0001$; n.s. no significance, as compared to control (hB^0AT1 and hcollectrin co-injected oocytes with substrate incubated only). E) Inhibition by compound NSC63912 and NSC22789 (300µM) of Na^+ -dependent leucine uptake in inverted sections of mouse small Intestine (n=4, e=5). *, $p<0.05$; as compared to control (inverted mouse small intestine with substrate incubated only).

3.3.7 Specificity of B^0AT1 inhibitors

The endogenous sodium-independent transport of the amino acid substrate in CHO-BC cells served as initial test of the selectivity of B^0AT1 inhibitors. In addition, I tested the specificity of compound NSC63912 and NSC22789 by measuring their ability to inhibit amino acid transport via related transporters expressed in various cell lines. ASCT2 is an amino acid exchanger for neutral amino acids with partially overlapping substrate specificity. The activity of ASCT2 was measured as Na^+-dependent L-glutamine (100μM) uptake level in 143B cells, a cancer cell line highly expressing ASCT2 [58]. The Na^+-independent L-glutamine uptake level was negligible in this cell line [58], therefore, I only measured L-glutamine uptake in sodium containing buffer to represent its Na^+-dependent transport by ASCT2 without subtraction of the Na^+-independent uptake activity (figure 3.3.7A). Even closer in substrate specificity to B^0AT1 are the system L amino acid exchangers LAT1 and LAT2. RT-PCR (figure 3.3.7B) showed gene expression of both LATs as well as the heavy chain of the transporter, 4F2hc, in MCF-7 breast cancer cells. System $ATB^{0,+}$ and ASCT2 were also detected in this cell line. The activity of these transporters in this cell line could be discriminated by a competition uptake assay (figure 3.3.7C). To this end, the uptake of 100μM leucine was challenged by 10mM amino acids (arginine, threonine and leucine) or the amino acid analogue 2-aminobicyclo[2.2.1]heptane-2-carboxylic acid (BCH), an inhibitor of LAT1 and LAT2. The Na^+-independent leucine uptake level in MCF-7 cells was more than two-fold higher than Na^+-dependent uptake of leucine, the latter most likely mediated by ASCT2 and $ATB^{0,+}$. The Na^+-independent leucine uptake was completely blocked by leucine itself, as well as by BCH. It was largely inhibited by Thr (a substrate more preferred by LAT2), but not by Arg, which is not transported by system L. The Na^+-dependent leucine uptake was also inhibited by leucine and BCH (substrates of $ATB^{0,+}$), Thr (substrate of both ASCT2 and $ATB^{0,+)}$ and slightly inhibited by Arg (substrate of $ATB^{0,+}$). To discriminate between LAT1 and LAT2, α-methyl-L-Tyrosine (specific inhibitor of LAT1 [257]) was employed. In figure 3.3.7D, the combined Na^+-independent L-leucine uptake by LAT1 and LAT2 was inhibited by BCH (inhibitor of both LAT1 and LAT2), whereas α-methyl-L-Tyrosine was used to visualize the contribution by LAT1. Both NSC63912 and NSC22789 partially inhibited ASCT2 and system L in these two cell lines, but NSC22789 showed higher selectivity as demonstrated by lesser inhibition of system L and ASCT2 (figure 3.3.7A&D). The substrate analogue S-Benzyl-L-Cysteine, by contrast, showed poor selectivity, as demonstrated by strong inhibition of system L in MCF-7 cells (figure 3.3.7D).

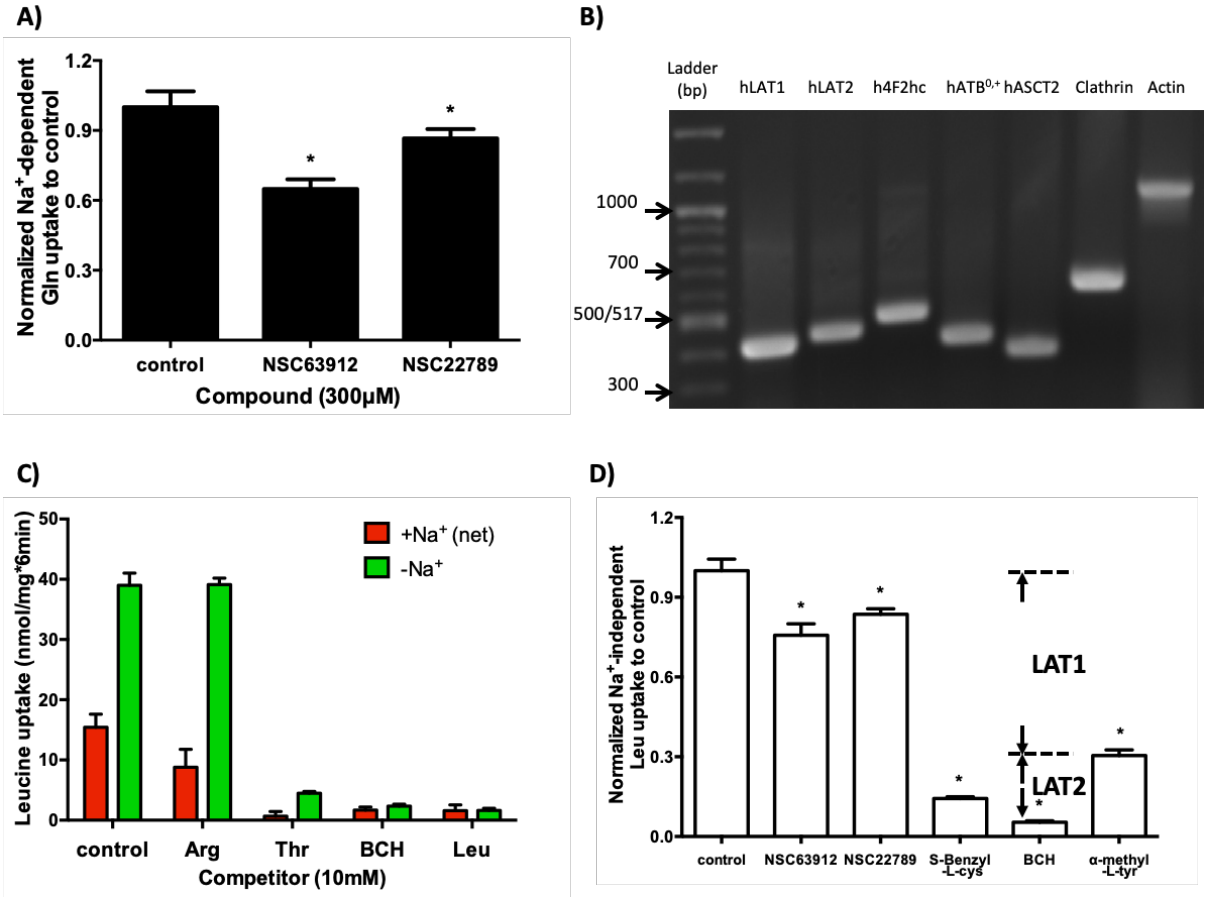

Figure 3.3.7: Specificity of B^0AT1 Inhibitors. A) The uptake of [^{14}C]glutamine (100µM) was measured in Na^+-containing transport buffer over a period of 6min in the presence of 300µM inhibitors as an indicator of ASCT2 activity (n=3, e=5). B) Gene expression of amino acid transporters in MCF-7 cells detected by RT-PCR. The expected bands are: LAT1 (407bp), LAT2 (432bp), 4F2hc (481bp), ATB0,+ (394bp), ASCT2 (351bp). Clathrin and Actin were used as house-keeping genes (n=1, e=1). C) MCF-7 cells were incubated in Hank's +/-Na^+ buffer containing 100µM [^{14}C]leucine as well as 10mM competitors (arginine, threonine, BCH, leucine) for 6min before measuring the accumulation of radioactivity. The result is shown as average leucine uptake ± std, and the Na^+ (net) uptake (red columns) was calculated by subtracting -Na^+ uptake (green columns) from the total leucine uptake (n=3, e=1). D) The sodium-independent uptake of [^{14}C]leucine (100µM) was measured over a period of 6min in the presence of 300µM B^0AT1 inhibitors, 10mM BCH (LAT1 and LAT2 inhibitor), or 1mM α-methyl-L-Tyrosine (LAT1 specific inhibitor) in Na^+ depleted Hank's buffer. Data was normalized to the uptake level of control cells, which were only treated with leucine (n=3, e=5). *, $p<0.05$, as compared to control.

3.3.8 In-vivo test of benztropine in C57BL/6NCrl female mice

The B^0AT1 inhibitor benztropine is commercially available and was previously used in mice to study its influence on energy expenditure [254]. Hence, we tested this compound in 6-8-month-old C57BL/6NCrl female mice to see whether inhibition of B^0AT1 *in vivo* contributed to the effect on energy expenditure. We have previously described that mice lacking Slc6a19 have improved glucose tolerance [42] and therefore decided to measure the effect of benztropine on blood glucose levels. Five pairs of littermates and two pairs of mice matched by date of birth (DOB) were separately and randomly distributed to treated- and untreated-groups in this pharmacological study, and the drug was given to the mice orally by mixing with chow. Inhibition of B^0AT1 is readily detectable by increases of the amino acid levels in 24hr urine and faecal samples (Kiran Javed personal communication). Hence, urine and faecal samples were collected before (d0) and after (d7 and d14) the administration of the drug and processed for metabolomic analysis by GC-MS to observe whether benztropine inhibited B^0AT1 *in vivo*. In addition, we performed intraperitoneal glucose tolerance tests (IPGTT) on d0 and d14 to measure the effect of benztropine on glucose homeostasis. Overall, benztropine-treated mice had improved glucose tolerance on d14 compared to d0 ($p<0.005$), but the untreated group did not (figure 3.3.8A&B). When comparing the IPGTT data on d14 between these two groups, the benztropine-treated mice had a significantly better glucose tolerance than the untreated mice (figure 3.3.8C). The average body weight was slightly decreased 14 days after drug administration in the treated group, without reaching statistical significance, while there was no change in body weight in the untreated group throughout the whole experiment (figure 3.3.8D).

With regard to amino acid levels in urine (figure 3.3.9) and faecal (figure 3.3.10) samples, we did not observe increases of any amino acids in samples from the drug-treated group compared to untreated mice, nor in post-treated samples compared to pre-treated samples. However, we did see increases of some amino acid related metabolites in urine samples from the benztropine-treated group, which are not substrates of B^0AT1. These included N-Acetyl Glycine, Adipic acid, 2-Hydroxyadipic acid, and N-Acetyl Glutamic acid (figure 3.3.11).

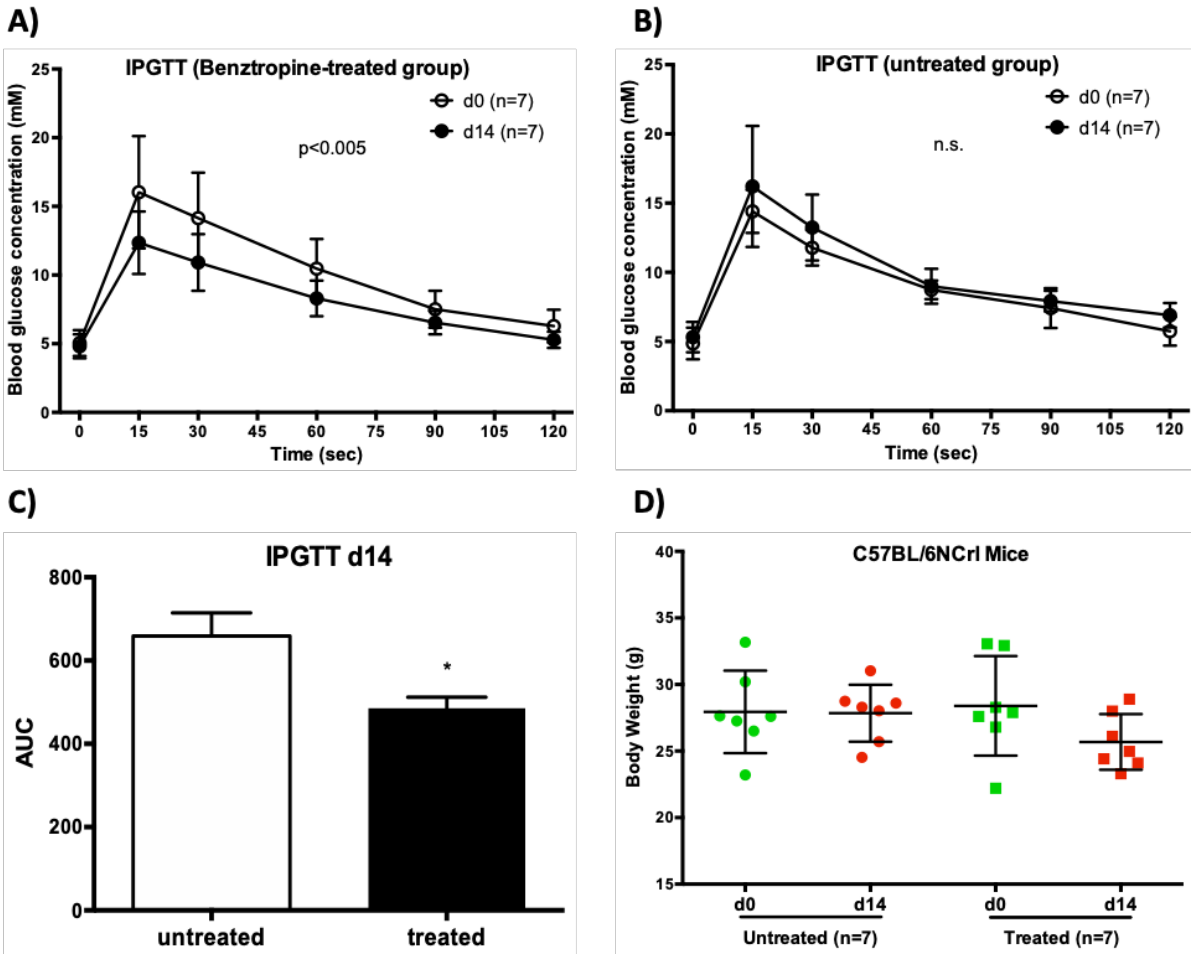

Figure 3.3.8: Glucose tolerance and body weight of benztropine-treated mice compared to untreated mice. A) IPGTT before treatment (d0) and 14 days after oral administration of benztropine (1.25mg per 5g chow per day) (d14) in the treated group. B) IPGTT on d0 and 14 days after eating normal chow soaked with the same amount of water in untreated group. Area Under Curve (AUC) was compared for statistical significance between d0 and d14 in A) and B). C) Average AUC at d14 was compared between benztropine-treated group and untreated group. *, $p<0.05$. D) Average body weight (g) of mice in the two groups on d0 (green) and d14 (red). n=7

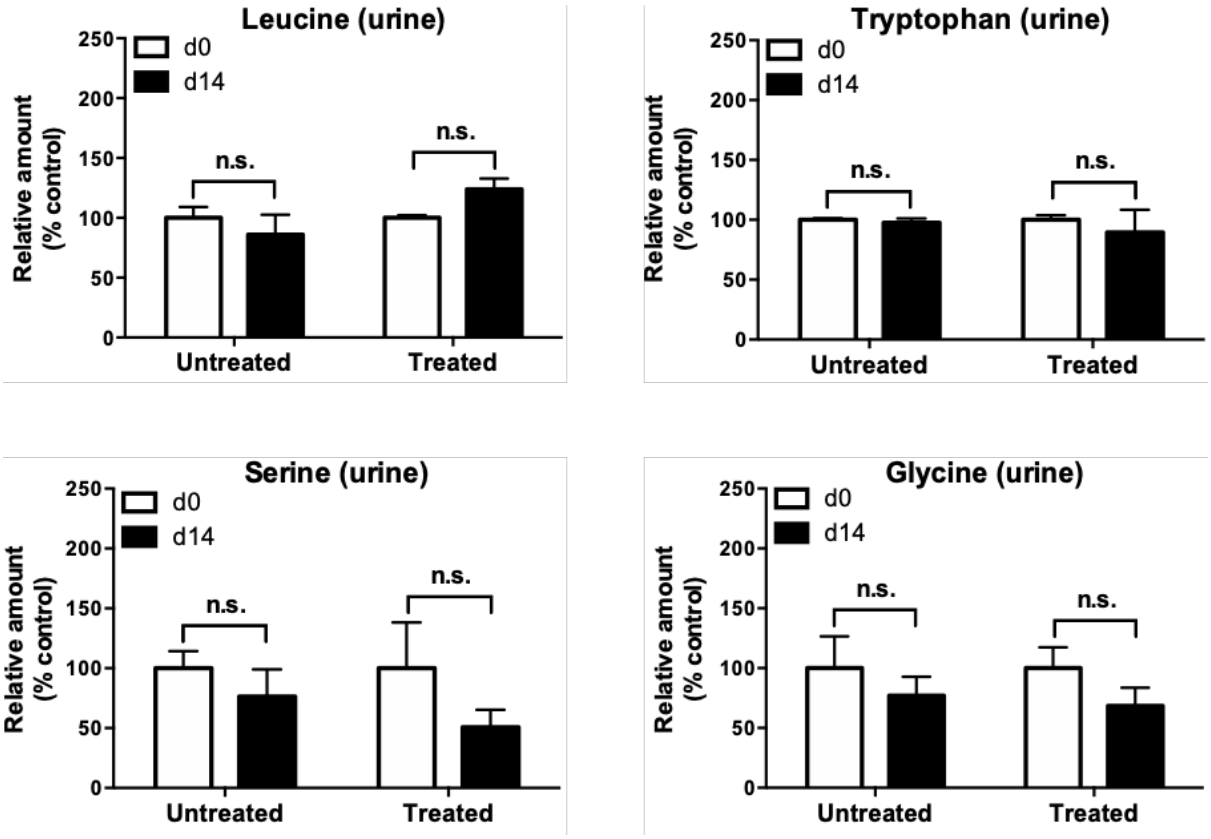

Figure 3.3.9: Comparison of amino acid levels between 24hr urine samples of benztropine-treated mice and untreated control mice. The samples were collected on day 0 (baseline) and day 14 after treatment and analyzed by GC-MS. The d14 data of each group was normalized to the d0 data of the same group, and the latter one was regarded as 100., T-test was used for analysis of differences between groups (n=7).

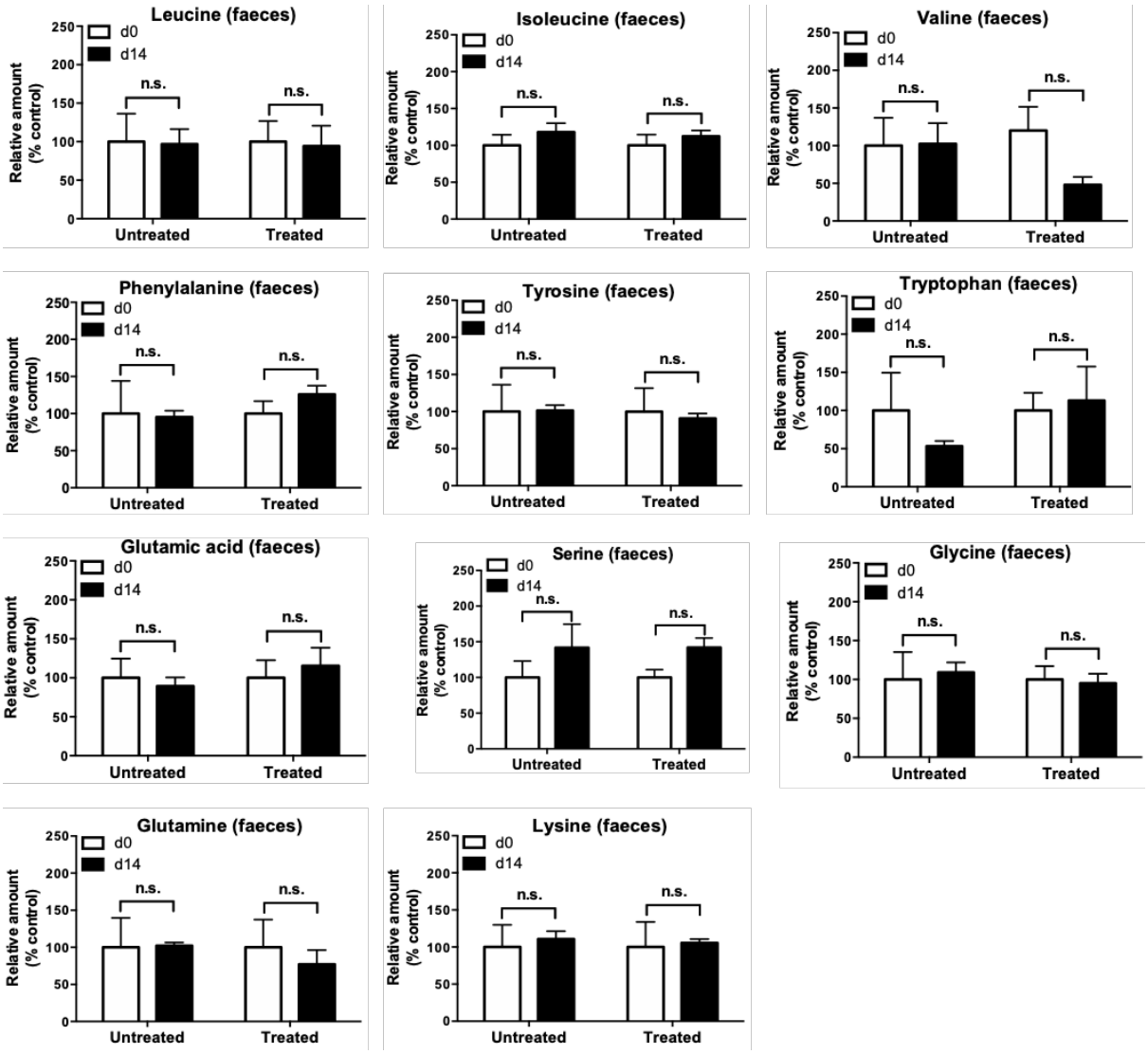

Figure 3.3.10: Comparison of amino acid levels between 24hr faecal samples of benztropine-treated mice and untreated control mice. The samples were collected on day 0 (baseline) and day 14 after treatment and analyzed by GC-MS. The d14 data of each group was normalized to the d0 data of the same group, and the latter one was regarded as 100%. T-test was used to analyze differences between groups (n=7).

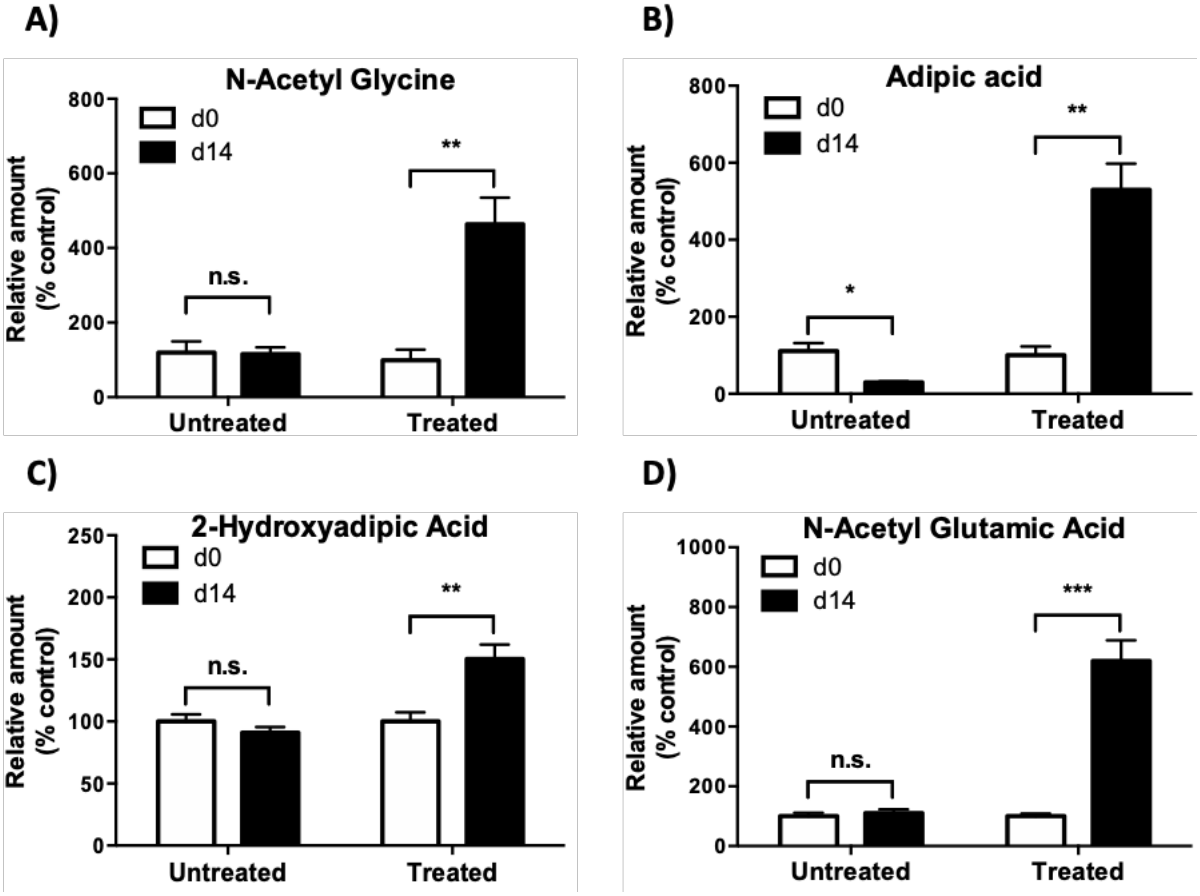

Figure 3.3.11: Comparison of amino acid related metabolites between 24hr urine samples of benztropine-treated mice and untreated control mice. A) N-Acetyl glycine; B) Adipic acid; C) 2-Hydroxyadipic acid; D) N-Acetyl glutamic acid. The samples were collected on day 0 (baseline) and day 14 after treatment and analyzed by GC-MS. The d14 data of each group was normalized to the d0 data of the same group, and the latter one was regarded as 100%. T-test was used to analyze differences between groups (n=7). *, $p<0.05$; **, $p<0.01$; ***, $p<0.001$.

3.3.9 Structure-activity relationships of NSC63912 and NSC22789 related compounds

As shown above, NSC63912 (benztropine) and NSC22789 were identified as the two best B^0AT1 inhibitors. However, their IC_{50} values of 70-80μM suggested that they were not potent enough as drug candidates, which was confirmed in the *in vivo* experiments. The pharmacophore of B^0AT1 inhibitors was comprised of two aromatic rings and the presence of a nitrogen-containing ring at a distance from the aromatic rings. In order to improve these tool compounds, our collaborators Praveen Kumar Tiwari and Indrapal Singh Aidhen (Indian Institute of Technology Madras) generated a series of systematically modified compounds to explore structure-activity relationships of inhibitors related to NSC63912 and NSC22789. It was concluded that converting the piperidine ring to a morpholine ring (labelled 3 in figure 3.3.12) improved IC_{50} (a1<a2, b1<b2, c1<c2, d1<d2, e1<e2), whereas attaching a methyl-, methoxy- group or fluorine on the benzene ring (labelled 2 in figure 3.3.12) did not (by comparing a, b, c series). Next, I investigated whether these modified compounds were B^0AT1 substrates as measured using the membrane potential assay (figure 3.3.13). Generally, the morpholine-based compounds (a1, b1, c1, d1, e1) were substrates of B^0AT1 while the piperidine-based compounds (a2, b2, c2, d2, e2) were not, and compounds without side chain or with smaller side chains were more likely binding to B^0AT1 compared to those with larger side chains (the likelihood was decreased from top to bottom in figure 3.3.12). Overall, the change of compound activity was relatively minor.

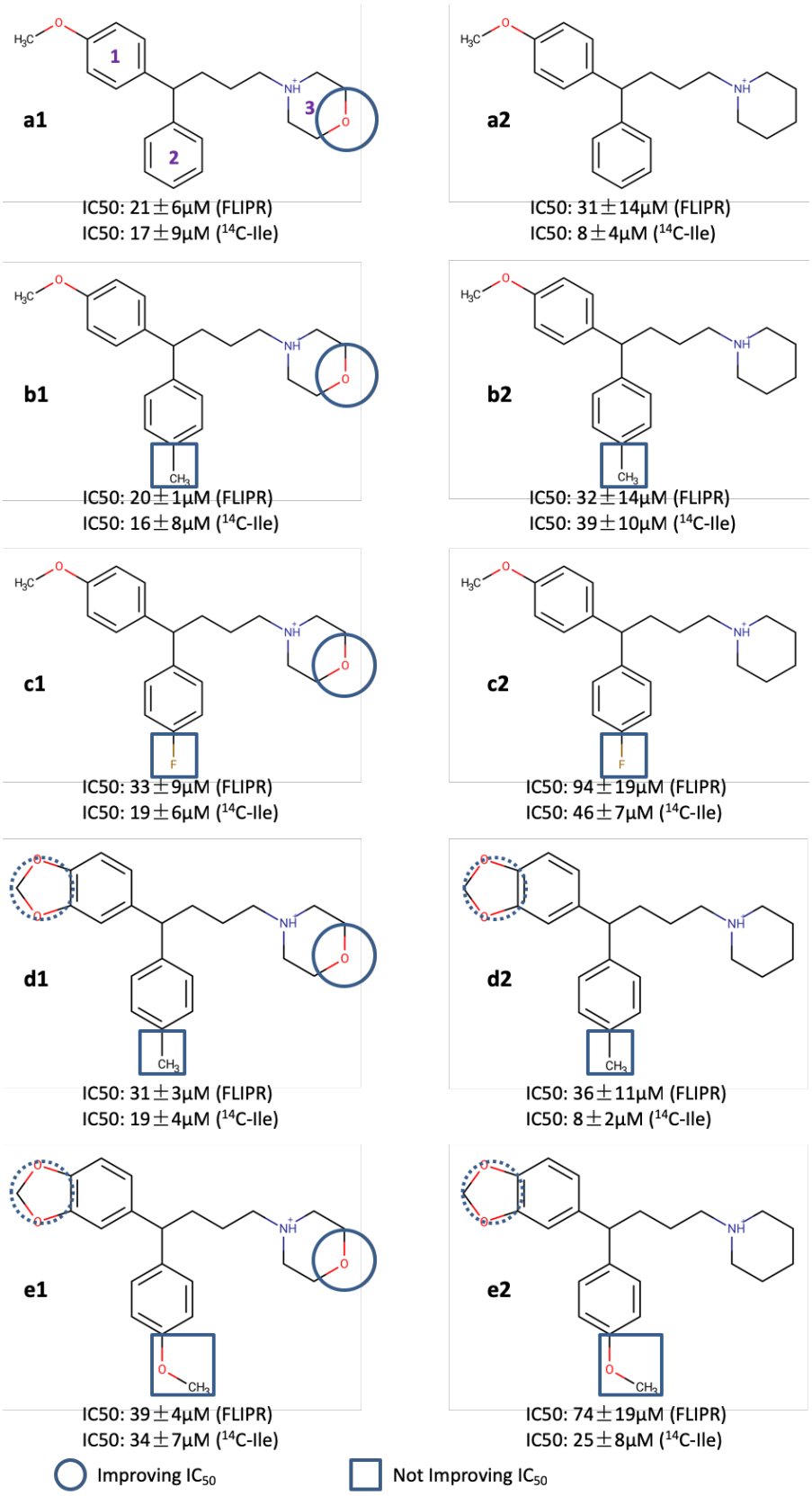

Figure 3.3.12: Structure-activity relationships of B^0AT1 inhibitors. IC_{50} values were measured by both FLIPR assay and [^{14}C]isoleucine uptake assay. Encircled structural elements improve the IC_{50} while structures highlighted by a square reduced affinity. Structure-activity relationships are discussed in the main text.

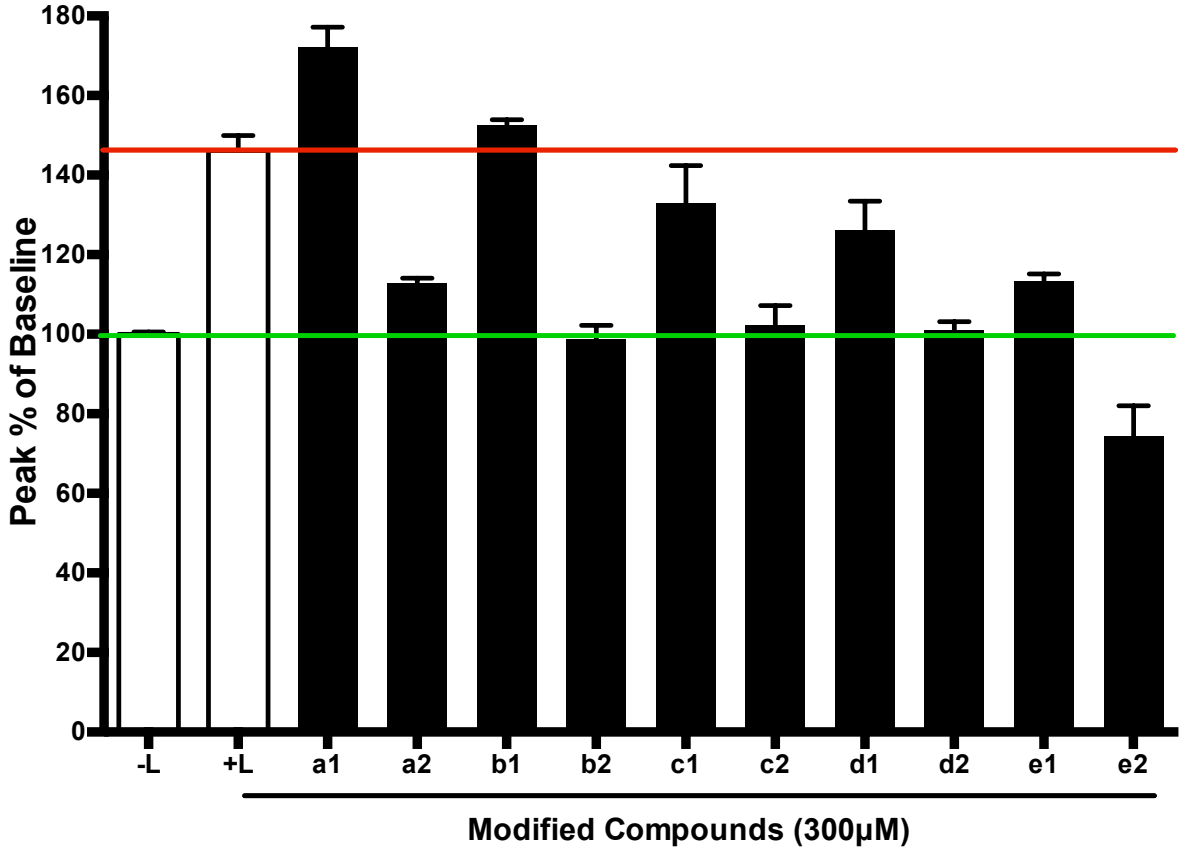

Figure 3.3.13: Testing inhibitors of B^0AT1 as putative substrates. CHO-BC cells were pre-loaded with the blue dye in Hank's $+Na^+$ buffer at room temperature for 30min. After baseline reading, 50µL of different B^0AT1 inhibitors (labelled as shown in figure 3.3.12) were manually injected into each well at a final concentration of 300µM, with leucine (300µM) serving as a positive control (red line), while 50µL of Hank's $+Na^+$ buffer was injected as a negative control (green line) (n=3, e=1).

3.3.10 High-throughput screening at the Australian Drug Discovery Centre

The high-throughput screening was conducted in the Australian Drug Discovery Centre using a liquid handling robot (Hamilton). The membrane potential assay was adapted to a 384-well format and used to screen a subset of the WECC diversity library, which is composed of 160,000 selected small molecules from a number of different chemical compound vendors. Staff of the Australian Cancer Research Foundation (ACRF) Drug Discovery Centre randomly selected 20,000 compounds from this library in a way to ensure there was the largest spread of different sub libraries to maximally enlarge the structural variety. Each compound was tested in duplicate at a final concentration of 10μM. Based on the strongest inhibition of leucine-induced depolarization, six compounds were selected for further characterization. Two novel inhibitors (WECC-0020422 and -0105368) were identified and showed higher potency compared to benztropine and NSC22789, with IC_{50} values of 1±0.4μM and 6±2μM, respectively. The IC_{50} curves were determined by radioactive uptake assay (chemical structures withheld for IP reasons) and are shown in figure 3.3.14.

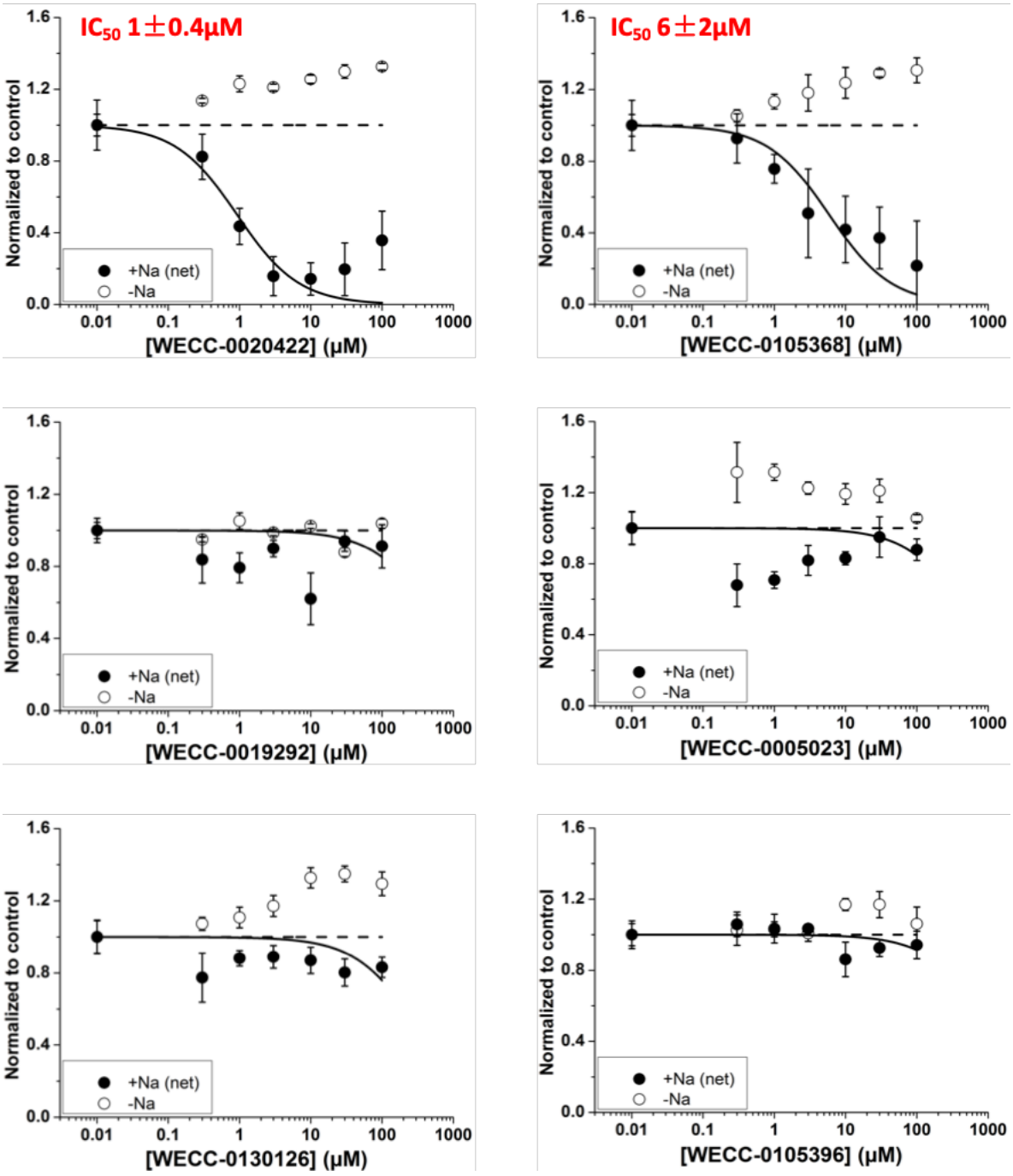

Figure 3.3.14: Chemical compounds selected from high-throughput screening. The IC_{50} values were determined by [^{14}C]leucine uptake assay. The radioactivity was measured from lysates of cells treated for 6min with Hank's +/-Na^+ buffer containing 100µM substrate and different concentrations (0.3, 1, 3, 10, 30, 100µM) of compounds. The +Na^+ (net) uptake (solid circle) was calculated by subtracting -Na^+ uptake (hollow circle) from the total uptake, and the results were normalized to controls and shown as average of triplicates ± std (n=3, e=1).

3.4 Discussion

The high capacity and simple procedure of the FLIPR membrane potential assay renders it suitable for measurement in a 96-well format and was later adapted to 384-well format. As a result, it was used for the primary experimental screening for B^0AT1 inhibitors using CHO-BC cells. Voltage sensitive dyes have been widely employed in the screening of ion channel inhibitors [151, 258, 259] and transporter inhibitors [235, 260]. Amino acid analogues are frequently used as inhibitors of amino acid transporters. For example, the non-metabolized analogue of L-leucine, 2-aminobicyclo[2.2.1]heptane-2-carboxylic acid (BCH), is used as an inhibitor of system L transporters (LAT), but has to be applied at a concentration of 10mM to inhibit this transport activity completely [261]. At this concentration, BCH was also found to suppress B^0AT1 [73]. The non-metabolized neutral amino acid analogue and system A substrate, N-Methylaminoisobutyric acid (MeAIB), has been used for many years as a competitive inhibitor of system A transporters [262]. The amino acid analogues can not only be transportable substrates and competitive inhibitors for amino acid transporters, but also be non-transportable noncompetitive blockers, e.g. α-methyltryptophan was identified as a blocker for SLC6A14 ($ATB^{0,+}$) [263]. Due to the structural similarity to the original amino acids, these analogues are often substrates of the transporters as well. Accordingly, they often exert inhibitory effects by competitively and reversibly binding to the target transporters. Moreover, they are usually unsuitable for clinical development of drug candidates due to limited specificity with regard to the transporter target and low affinity. To systematically identify novel B^0AT1 inhibitors, we selected 24 commercially available substrate analogues (analogues of L-cysteine, L-methionine and L-serine) and tested them in two screening systems (FLIPR and radioactive uptake assays). Among them, S-benzyl-L-cysteine was identified as the most potent B^0AT1 inhibitor with an IC_{50} of 398±29μM based on the radioactive uptake assay (figure 3.3.1C). As a substrate analogue, S-benzyl-L-cysteine was also accepted as a substrate of the transporter (compound No.4 in figure 3.3.1B). Accordingly, it acted as a competitive inhibitor of the transport (figure 3.3.5A). However, S-Benzyl-L-Cysteine was a more potent inhibitor of the endogenous system L transporter, inhibiting this transporter with an IC_{50} value of 33±3μM in CHO-BC cells and also strongly inhibiting system L in MCF-7 cells. Thus, using amino acid analogues did not seem to be a promising strategy to identify specific B^0AT1 inhibitors, which was also reported in the inhibitor screening of other transport systems [264]. We also noticed an obvious discrepancy of IC_{50} values determined by our two assays. The IC_{50} values were overall lower in the FLIPR membrane potential assay compared to the radioactive substrate uptake assay, which was also demonstrated in previous studies [265]. Because cells cannot be

washed after incubation with the dye and the amount of available inhibitor is usually small, the inhibitors have to be incubated with the FLIPR blue dye for 30min on the cells before the assay, whereas the cells were only exposed to the inhibitors for 6min during the radioactive uptake assay and in the immediate presence of substrate. The prolonged exposure time in the FLIPR assay could cause some non-specific effects on the fluorescent signals, for example, by activating or inhibiting endogenous ion channels, which would change the membrane potential. The compounds could also quench the dye inside the membrane. The longer exposure may also facilitate diffusion of the inhibitors across the phospholipid bilayer, allowing them to bind to the transporter on the cytosolic face. Together these effects may explain the lower IC_{50} values generated in this assay. Such bias once again emphasizes the importance of using assays other than the FLIPR assay for compound screening studies especially when determining the characteristics of the inhibitors.

Since substrate analogues were not suitable as drug candidates, we performed virtual screening of compound libraries including a variety of compounds inhibiting other SLC6 family members and their analogues. Moreover, we also analyzed nimesulide, a previously published B^0AT1 inhibitor [249]. Virtual screening uses computational techniques to screen small-molecule compound libraries to identify structures that are most likely to bind to a drug target. With the development of computational techniques and the elucidation of high-resolution structures of protein receptors, it is increasingly used in the early stage of drug discovery studies [266, 267]. Based on the data of the docking study, we eventually selected the 40 highest-scoring chemical compounds from a 14,434 compound subset of the ZINC database for the first round of screening. While more economical than experimental screening, computational screening has a number of shortcomings, such as exclusion of protein flexibility, incomplete accounting of water molecules in binding and incomplete accounting of specialized interactions [266]. To overcome these obstacles, molecular dynamics (MD) simulation technique was developed to observe the dynamic processes of molecules with high resolution in space and time, improving the molecular docking in which proteins are considered rigid and the accuracy of predicted docking poses was low [268]. However, MD is computationally demanding and can only be used for selected compounds. To exclude false positives derived from computational screening, it is frequently used in a combination with a high-throughput *in vitro* cell-based assay. When testing the 40 compounds selected from virtual screening at a concentration of 300µM by FLIPR membrane potential assay, only 11 of them inhibited the leucine stimulated signal (figure 3.3.2A). The second round of virtual screening was based on a similarity search starting with two selected inhibitors from batch 1, namely NSC63912 and NSC186059. This process

yielded another 40 compounds, which were selected from 158 structurally-similar compounds and subsequently tested *in vitro*. This time, the fraction of molecules that were active inhibitors was obviously higher compared to that of the 1st batch (21 out of 40 compounds significantly inhibited leucine-induced depolarization) (figure 3.3.3A). Our best two compounds so far, NSC63912 (benztropine) and NSC22789 (2-benzyl-1-(3-phenylpropyl)piperidine), were characterized as competitive and non-competitive inhibitors, respectively (figure 3.3.5 B&D), with IC_{50} values of 44-90μM (FLIPR assay) and 71-78μM (uptake assay) (figure 3.3.2B and 3.3.3B), which is significantly above the recommended range for drug candidates (IC_{50} within lower micromolar to nanomolar range [269, 270]). Competitive inhibitors are competing with the substrates for the binding site, so the inhibitory effect will fade away when more substrates are present, for instance after food intake. On the contrary, non-competitive inhibitors block the transport of the substrate without binding to the active binding site, hence, the inhibitory effect will not be influenced by increased concentration of extracellular substrate. For drug development, non-competitive inhibitors are preferred, because the competition by end products of protein digestion will not occur.

We also noticed that in the presence of some substrate analogues or NCI compounds, hyperpolarization signals were seen instead of depolarization peaks after the addition of transport substrate leucine (figure 3.3.1A, 3.3.2A, 3.3.3A). The cause of this hyperpolarization is unknown at this stage, but is typically caused by activation of K^+ efflux or Cl^- influx, however, there is no endogenous voltage gated potassium channels expressed in CHO cells [271].

To improve the potency of initial lead structures, similarity searches [272], and modifications of their chemical structures [273] are commonly performed. The modifications can include the removal, addition or replacement of the side chains or rings to increase the hydrophobicity or hydrophilicity of the compound [274]. Pharmacophore modelling could be used to increase the number of compounds that can be screened by molecular docking. This technique uses the geometric and chemical characteristics of ligands or receptors to identify common functional groups and geometric arrangements. Large number of compounds can be quickly screened computationally for the presence and geometrical arrangements of the identified molecular features. This method was previously used to identify novel inhibitors for neurotransmitter transporters from SLC6 family [275]. Pharmacophore screening can be performed by ligand-based or structure-based methods [276]. The ligand-based method uses common structural features of a series of known ligands to identify the essential parts for the interaction between ligands and the targeted receptor. It allows certain modifications to the pharmacophore to study structure-activity relationships of a series of related inhibitors (figure 3.3.10). Structure-based

methods, by contrast, involve a comprehensive analysis of the 3D structure of a targeted receptor, or a ligand-receptor complex, to set up a pharmacophore based on the analyzed features of the active binding site and its spatial relationships [276].

Xenopus laevis oocytes are commonly used as an ex-vivo system to study the activity and function of the transporters [73, 277]. Surprisingly, the inhibitory effect of the two selected compounds (NSC63912 and NSC22789) was much weaker when the transporter was expressed in this system. At 300μM NSC63912 and NSC22789 only caused a 10-30% reduction of leucine uptake either after injecting compounds directly into the oocyte (figure 3.3.6C) or after pre-incubating the oocytes with compounds for 30min (figure 3.3.6D). Without these manipulations, no inhibition of leucine uptake was observed (figure 3.3.6B). Weaker inhibition in the oocyte expression system compared to mammalian cell models was seen in other studies, such as targeting amino acid transporter LAT3 for anti-prostate cancer therapies. In this case, the IC_{50} value determined in mammalian cell lines was almost 20-fold lower than that measured in oocytes [278]. Moreover, compounds inhibiting a renal organic cation transporter were found to have a much lower Ki value in stably expressed MDCK cells compared to the transporter transiently expressed in oocytes [279]. A potential explanation for this could be that the vitellin layer surrounding oocytes forms a natural barrier for hydrophobic compounds [280], or that inhibitors block the transporters from the inside of the oocytes, where the inhibitors are captured by the abundant egg-yolk [281].

Apart from affinity, the selectivity of novel inhibitors is another important factor when choosing a suitable lead compound. High potency but poor selectivity may cause toxicity and side effects in the clinic, hence, the selectivity of compounds is usually monitored in the very early stages of drug development [282]. In this study, we used two cell lines to test the selectivity of B^0AT1 inhibitors: 143B cells, a cell line highly expressing ASCT2, and MCF7 cells, which highly express LAT1 and LAT2 together with their heavy chain 4F2hc, as well as $ATB^{0,+}$. $ATB^{0,+}$ (SLC6A14) is upregulated in a variety of cancer tissues to provide all essential amino acids for cell growth [283, 284]. It is difficult to differentiate the uptake of leucine by LAT1 and LAT2, because the amino acid analogue BCH inhibits both isoforms, while the more recently developed inhibitor α-methyl-L-tyrosine proved to be more selective for LAT1 over LAT2 [257]. Hence, the difference between the inhibition caused by this compound and by BCH was regarded as the activity of LAT2 (figure 3.3.7D). B^0AT1 inhibitors NSC63912 (benztropine) and NSC22789 showed moderate inhibition of sodium-dependent glutamine uptake in 143B cells (figure 3.3.7A) and of sodium-independent leucine uptake in MCF-7 cells (figure 3.3.7D). However, benztropine was previously identified as a potent inhibitor of the

dopamine transporter (SLC6A3) with an IC_{50} of around 0.2μM, as well as the human proline transporter hPROT (SLC6A7) with an IC_{50} of 0.75μM [285]. Both transporters are in the same family as B^0AT1. Thus, more potent and selective inhibitors of B^0AT1 are required to be further developed as drug candidates.

In humans, mutations inactivating B^0AT1 cause a largely benign clinical condition named Hartnup disorder. It mainly manifests with aminoaciduria and occasionally a pellagra-like skin rash [77]. In rodents, the SLC6A19 knockout (KO) mice demonstrated significant improvement of glycaemic control and prevention of obesity and insulin resistance, without showing any congenital defects or severe conditions [42, 105]. The metabolic phenotype of these KO mice was generated by a series of physiological changes, such as increased glucose removal particularly by heart, decreased adipose tissue mass, browning of white adipose tissue, increased ketone bodies production, decreased hepatic glucose output and liver triglycerides levels. These physiological changes were most likely caused by elevated release of GLP-1, GIP and FGF21 [105]. Therefore, there are sufficient reasons for us to suggest that B^0AT1 can be inhibited in adult humans without severe side-effects. It will be of great interest to analyse the metabolic phenotype of Hartnup disorder patients, to find out whether it is similar to that of Slc6a19 deficient mice, which would provide a much stronger link between B^0AT1 inhibitors and their presumed antidiabetic effect. However, due to the limited number of diagnosed cases in Australia and around the world, it is problematic to collect sufficient patient samples for statistical analysis. One of the identified inhibitors, benztropine, was previously tested at the maximal daily dose of 250mg/kg diet in mice to observe its effect on energy expenditure, showing no long-term effect on energy balance or body composition in both obese and lean animals [254]. Moreover, benztropine was also used in the past as a drug to treat Parkinson's disease [286] and proved to be effective in the treatment of secondary progressive multiple sclerosis as well [287]. When we treated wild-type C57BL6/NCrl mice with benztropine for 2 weeks, an improved glucose tolerance was seen after intraperitoneal injection of glucose in treated mice compared to untreated mice (figure 3.3.8C, $p<0.05$), and the benztropine-treated group demonstrated a better glucose tolerance after 2 weeks' treatment as compared to baseline (figure 3.3.8A, $p<0.005$), whereas the untreated group did not (figure 3.3.8B). However, the amino acid levels in urine and faecal samples were not increased (figure 3.3.9&3.3.10), and only the levels of amino acid related metabolites were elevated in benztropine-treated urine samples (figure 3.3.11), whereas loss of neutral amino acid in urine was observed in the SLC6A19 KO mice [105], suggesting that the influence of benztropine on glucose metabolism was through mechanisms other than inhibition of B^0AT1. For example, urinary excretion of

acetylglycine was increased post BCAA dietary restriction in Zucher-fatty rats due to the restoration of skeleton muscle glycine levels, which reduce the acyl CoA burden from insulin resistance by conjugation with the acyl groups to gain membrane permeability [288]. Adipic aciduria was previously reported as a secondary outcome to food, specifically gelatins [289]. More importantly, to evaluate the efficacy of B^0AT1 inhibitors in vivo, reliable biomarkers in varied samples (urine, faecal or plasma) are required to detect successful inhibition of the transporter [290].

Conclusion

Docking studies using homology models were used as a preliminary screening method to identify potential inhibitors from a set of approximately 15,000 compounds. The computational screening performed in combination with suitable validated transport function assays eventually allowed us to identify novel inhibitors for B^0AT1. Affinity and selectivity was evaluated in various *in vitro*, *in vivo* and *ex vivo* systems. However, compounds with improved potency (IC_{50} within lower micromolar to nanomolar range) and improved selectivity for B^0AT1 are required for future lead development and for testing in rodents or even humans. The leading compounds identified in this study can be the base of future compounds with higher affinities for this transporter by using the structure-activity approach. Pharmacological inhibition of B^0AT1 by small molecules should be capable of replicating the advantageous metabolic phenotype of Slc6a19 deficient mice, including better glycaemic control and improved lipid profile [105]. As compared to dietary protein restriction, the inhibition of amino acid absorption in small intestine and reabsorption in kidney by the application of B^0AT1 blockers should be more well-tolerated by diabetic patients. This study has provided useful tools for drug discovery studies, from the generation of cell models, the validation of screening assays, to the characterization and modification of inhibitors.

References

1. Deshpande, A.D., M. Harris-Hayes, and M. Schootman, *Epidemiology of diabetes and diabetes-related complications.* Phys Ther, 2008. **88**(11): p. 1254-64.
2. Prentki, M. and C.J. Nolan, *Islet beta cell failure in type 2 diabetes.* J Clin Invest, 2006. **116**(7): p. 1802-12.
3. Giesbertz, P. and H. Daniel, *Branched-chain amino acids as biomarkers in diabetes.* Current Opinion in Clinical Nutrition and Metabolic Care, 2016. **19**(1): p. 48-54.
4. Tai, E.S., et al., *Insulin resistance is associated with a metabolic profile of altered protein metabolism in Chinese and Asian-Indian men.* Diabetologia, 2010. **53**(4): p. 757-67.
5. Wang, T.J., et al., *Metabolite profiles and the risk of developing diabetes.* Nat Med, 2011. **17**(4): p. 448-53.
6. Tremblay, F. and A. Marette, *Amino acid and insulin signaling via the mTOR/p70 S6 kinase pathway. A negative feedback mechanism leading to insulin resistance in skeletal muscle cells.* J Biol Chem, 2001. **276**(41): p. 38052-60.
7. Harrington, L.S., et al., *The TSC1-2 tumor suppressor controls insulin-PI3K signaling via regulation of IRS proteins.* J Cell Biol, 2004. **166**(2): p. 213-23.
8. Tremblay, F., et al., *Identification of IRS-1 Ser-1101 as a target of S6K1 in nutrient- and obesity-induced insulin resistance.* Proc Natl Acad Sci U S A, 2007. **104**(35): p. 14056-61.
9. Um, S.H., et al., *Absence of S6K1 protects against age- and diet-induced obesity while enhancing insulin sensitivity.* Nature, 2004. **431**(7005): p. 200-5.
10. Ozes, O.N., et al., *A phosphatidylinositol 3-kinase/Akt/mTOR pathway mediates and PTEN antagonizes tumor necrosis factor inhibition of insulin signaling through insulin receptor substrate-1.* Proc Natl Acad Sci U S A, 2001. **98**(8): p. 4640-5.
11. Tremblay, F., et al., *Overactivation of S6 kinase 1 as a cause of human insulin resistance during increased amino acid availability.* Diabetes, 2005. **54**(9): p. 2674-84.
12. Broer, S. and A. Broer, *Amino acid homeostasis and signalling in mammalian cells and organisms.* Biochem J, 2017. **474**(12): p. 1935-1963.
13. Bar-Peled, L. and D.M. Sabatini, *Regulation of mTORC1 by amino acids.* Trends Cell Biol, 2014. **24**(7): p. 400-6.
14. Soultoukis, G.A. and L. Partridge, *Dietary Protein, Metabolism, and Aging.* Annu Rev Biochem, 2016. **85**: p. 5-34.
15. Yoon, M.S., *The Emerging Role of Branched-Chain Amino Acids in Insulin Resistance and Metabolism.* Nutrients, 2016. **8**(7).
16. D'Antona, G., et al., *Branched-chain amino acid supplementation promotes survival and supports cardiac and skeletal muscle mitochondrial biogenesis in middle-aged mice.* Cell Metab, 2010. **12**(4): p. 362-72.
17. Lynch, C.J. and S.H. Adams, *Branched-chain amino acids in metabolic signalling and insulin resistance.* Nat Rev Endocrinol, 2014. **10**(12): p. 723-36.
18. Mirzaei, H., J.A. Suarez, and V.D. Longo, *Protein and amino acid restriction, aging and disease: from yeast to humans.* Trends Endocrinol Metab, 2014. **25**(11): p. 558-66.
19. Rizza, W., N. Veronese, and L. Fontana, *What are the roles of calorie restriction and diet quality in promoting healthy longevity?* Ageing Res Rev, 2014. **13**: p. 38-45.
20. Nezu, U., et al., *Effect of low-protein diet on kidney function in diabetic nephropathy: meta-analysis of randomised controlled trials.* BMJ Open, 2013. **3**(5).
21. Solon-Biet, S.M., et al., *The ratio of macronutrients, not caloric intake, dictates cardiometabolic health, aging, and longevity in ad libitum-fed mice.* Cell Metab, 2014. **19**(3): p. 418-30.
22. Tremblay, F., et al., *Role of dietary proteins and amino acids in the pathogenesis of insulin resistance.* Annu Rev Nutr, 2007. **27**: p. 293-310.
23. Wang, J., X. Yang, and J. Zhang, *Bridges between mitochondrial oxidative stress, ER stress and mTOR signaling in pancreatic beta cells.* Cell Signal, 2016. **28**(8): p. 1099-104.

24. Gulati, P., et al., *Amino acids activate mTOR complex 1 via Ca2+/CaM signaling to hVps34.* Cell Metab, 2008. **7**(5): p. 456-65.
25. Nobukuni, T., S.C. Kozma, and G. Thomas, *hvps34, an ancient player, enters a growing game: mTOR Complex1/S6K1 signaling.* Curr Opin Cell Biol, 2007. **19**(2): p. 135-41.
26. Yan, L., et al., *PP2A T61 epsilon is an inhibitor of MAP4K3 in nutrient signaling to mTOR.* Mol Cell, 2010. **37**(5): p. 633-42.
27. Sancak, Y., et al., *The Rag GTPases bind raptor and mediate amino acid signaling to mTORC1.* Science, 2008. **320**(5882): p. 1496-501.
28. Xu, L., et al., *Phospholipase D mediates nutrient input to mammalian target of rapamycin complex 1 (mTORC1).* J Biol Chem, 2011. **286**(29): p. 25477-86.
29. Kim, S., et al., *Amino acid signaling to mTOR mediated by inositol polyphosphate multikinase.* Cell Metab, 2011. **13**(2): p. 215-21.
30. Goodman, B.E., *Insights into digestion and absorption of major nutrients in humans.* Adv Physiol Educ, 2010. **34**(2): p. 44-53.
31. Mackenzie, B., et al., *Mechanisms of the human intestinal H+-coupled oligopeptide transporter hPEPT1.* J Biol Chem, 1996. **271**(10): p. 5430-7.
32. Verrey, F., et al., *Kidney amino acid transport.* Pflugers Arch, 2009. **458**(1): p. 53-60.
33. Jorgensen, K.E., U. Kragh-Hansen, and M.I. Sheikh, *Transport of leucine, isoleucine and valine by luminal membrane vesicles from rabbit proximal tubule.* J Physiol, 1990. **422**: p. 41-54.
34. Smith, D.E., B. Clemencon, and M.A. Hediger, *Proton-coupled oligopeptide transporter family SLC15: physiological, pharmacological and pathological implications.* Mol Aspects Med, 2013. **34**(2-3): p. 323-36.
35. Kanai, Y., et al., *The neuronal and epithelial human high affinity glutamate transporter. Insights into structure and mechanism of transport.* J Biol Chem, 1994. **269**(32): p. 20599-606.
36. Palacin, M., G. Borsani, and G. Sebastio, *The molecular bases of cystinuria and lysinuric protein intolerance.* Curr Opin Genet Dev, 2001. **11**(3): p. 328-35.
37. Boll, M., et al., *Functional characterization of two novel mammalian electrogenic proton-dependent amino acid cotransporters.* J Biol Chem, 2002. **277**(25): p. 22966-73.
38. Broer, A., et al., *Sodium translocation by the iminoglycinuria associated imino transporter (SLC6A20).* Mol Membr Biol, 2009. **26**(5): p. 333-46.
39. Quan, H., et al., *Hypertension and impaired glycine handling in mice lacking the orphan transporter XT2.* Mol Cell Biol, 2004. **24**(10): p. 4166-73.
40. Fairweather, S.J., et al., *Molecular basis for the interaction of the mammalian amino acid transporters B0AT1 and B0AT3 with their ancillary protein collectrin.* J Biol Chem, 2015. **290**(40): p. 24308-25.
41. Hagglund, M.G., et al., *B(0)AT2 (SLC6A15) is localized to neurons and astrocytes, and is involved in mediating the effect of leucine in the brain.* PLoS One, 2013. **8**(3): p. e58651.
42. Broer, A., et al., *Impaired nutrient signaling and body weight control in a Na+ neutral amino acid cotransporter (Slc6a19)-deficient mouse.* J Biol Chem, 2011. **286**(30): p. 26638-51.
43. Broer, S., J.A. Cavanaugh, and J.E. Rasko, *Neutral amino acid transport in epithelial cells and its malfunction in Hartnup disorder.* Biochem Soc Trans, 2005. **33**(Pt 1): p. 233-6.
44. Broer, S., *Amino acid transport across mammalian intestinal and renal epithelia.* Physiol Rev, 2008. **88**(1): p. 249-86.
45. Kanai, Y., et al., *Expression cloning and characterization of a transporter for large neutral amino acids activated by the heavy chain of 4F2 antigen (CD98).* J Biol Chem, 1998. **273**(37): p. 23629-32.
46. Le Cam, A. and P. Freychet, *Neutral amino acid transport. Characterization of the A and L systems in isolated rat hepatocytes.* J Biol Chem, 1977. **252**(1): p. 148-56.
47. Segawa, H., et al., *Identification and functional characterization of a Na+-independent neutral amino acid transporter with broad substrate selectivity.* J Biol Chem, 1999. **274**(28): p. 19745-51.

48. Babu, E., et al., *Identification of a novel system L amino acid transporter structurally distinct from heterodimeric amino acid transporters.* J Biol Chem, 2003. **278**(44): p. 43838-45.
49. Oda, K., et al., *L-type amino acid transporter 1 inhibitors inhibit tumor cell growth.* Cancer Sci, 2010. **101**(1): p. 173-9.
50. Imai, H., et al., *Inhibition of L-type amino acid transporter 1 has antitumor activity in non-small cell lung cancer.* Anticancer Res, 2010. **30**(12): p. 4819-28.
51. Janpipatkul, K., et al., *Downregulation of LAT1 expression suppresses cholangiocarcinoma cell invasion and migration.* Cell Signal, 2014. **26**(8): p. 1668-79.
52. Yothaisong, S., et al., *Inhibition of l-type amino acid transporter 1 activity as a new therapeutic target for cholangiocarcinoma treatment.* Tumour Biol, 2017. **39**(3): p. 1010428317694545.
53. Hayashi, K., et al., *LAT1 acts as a crucial transporter of amino acids in human thymic carcinoma cells.* J Pharmacol Sci, 2016. **132**(3): p. 201-204.
54. Guan, J., et al., *The xc- cystine/glutamate antiporter as a potential therapeutic target for small-cell lung cancer: use of sulfasalazine.* Cancer Chemother Pharmacol, 2009. **64**(3): p. 463-72.
55. Jin, L., G.N. Alesi, and S. Kang, *Glutaminolysis as a target for cancer therapy.* Oncogene, 2016. **35**(28): p. 3619-25.
56. van Geldermalsen, M., et al., *ASCT2/SLC1A5 controls glutamine uptake and tumour growth in triple-negative basal-like breast cancer.* Oncogene, 2016. **35**(24): p. 3201-8.
57. Schulte, M.L., et al., *2-Amino-4-bis(aryloxybenzyl)aminobutanoic acids: A novel scaffold for inhibition of ASCT2-mediated glutamine transport.* Bioorg Med Chem Lett, 2016. **26**(3): p. 1044-1047.
58. Broer, A., F. Rahimi, and S. Broer, *Deletion of Amino Acid Transporter ASCT2 (SLC1A5) Reveals an Essential Role for Transporters SNAT1 (SLC38A1) and SNAT2 (SLC38A2) to Sustain Glutaminolysis in Cancer Cells.* J Biol Chem, 2016. **291**(25): p. 13194-205.
59. Bridges, R.J. and C.S. Esslinger, *The excitatory amino acid transporters: pharmacological insights on substrate and inhibitor specificity of the EAAT subtypes.* Pharmacol Ther, 2005. **107**(3): p. 271-85.
60. Choi, D.W., *Glutamate receptors and the induction of excitotoxic neuronal death.* Prog Brain Res, 1994. **100**: p. 47-51.
61. Mattson, M.P., *Excitotoxic and excitoprotective mechanisms: abundant targets for the prevention and treatment of neurodegenerative disorders.* Neuromolecular Med, 2003. **3**(2): p. 65-94.
62. Billups, B., et al., *Physiological and pathological operation of glutamate transporters.* Prog Brain Res, 1998. **116**: p. 45-57.
63. Takahashi, K., J.B. Foster, and C.L. Lin, *Glutamate transporter EAAT2: regulation, function, and potential as a therapeutic target for neurological and psychiatric disease.* Cell Mol Life Sci, 2015. **72**(18): p. 3489-506.
64. Fontana, A.C., *Current approaches to enhance glutamate transporter function and expression.* J Neurochem, 2015. **134**(6): p. 982-1007.
65. Drgonova, J., et al., *Deletion of v7-3 (SLC6A15) transporter allows assessment of its roles in synaptosomal proline uptake, leucine uptake and behaviors.* Brain Res, 2007. **1183**: p. 10-20.
66. Kohli, M.A., et al., *The neuronal transporter gene SLC6A15 confers risk to major depression.* Neuron, 2011. **70**(2): p. 252-65.
67. Santarelli, S., et al., *SLC6A15, a novel stress vulnerability candidate, modulates anxiety and depressive-like behavior: involvement of the glutamatergic system.* Stress, 2016. **19**(1): p. 83-90.
68. Harvey, R.J. and B.K. Yee, *Glycine transporters as novel therapeutic targets in schizophrenia, alcohol dependence and pain.* Nat Rev Drug Discov, 2013. **12**(11): p. 866-85.
69. Goff, D.C., *Bitopertin: the good news and bad news.* JAMA Psychiatry, 2014. **71**(6): p. 621-2.
70. Vandenberg, R.J., et al., *Glycine transport inhibitors for the treatment of pain.* Trends Pharmacol Sci, 2014. **35**(8): p. 423-30.

71. Takahashi, K., et al., *Inhibition of ASCT2 is essential in all-trans retinoic acid-induced reduction of adipogenesis in 3T3-L1 cells.* FEBS Open Bio, 2015. **5**: p. 571-8.
72. Broer, S., *The SLC6 orphans are forming a family of amino acid transporters.* Neurochem Int, 2006. **48**(6-7): p. 559-67.
73. Broer, A., et al., *Molecular cloning of mouse amino acid transport system B0, a neutral amino acid transporter related to Hartnup disorder.* J Biol Chem, 2004. **279**(23): p. 24467-76.
74. Romeo, E., et al., *Luminal kidney and intestine SLC6 amino acid transporters of B0AT-cluster and their tissue distribution in Mus musculus.* Am J Physiol Renal Physiol, 2006. **290**(2): p. F376-83.
75. Fukui, K., et al., *The HNF-1 target collectrin controls insulin exocytosis by SNARE complex formation.* Cell Metab, 2005. **2**(6): p. 373-84.
76. Akpinar, P., et al., *Tmem27: a cleaved and shed plasma membrane protein that stimulates pancreatic beta cell proliferation.* Cell Metab, 2005. **2**(6): p. 385-97.
77. Seow, H.F., et al., *Hartnup disorder is caused by mutations in the gene encoding the neutral amino acid transporter SLC6A19.* Nat Genet, 2004. **36**(9): p. 1003-7.
78. Kleta, R., et al., *Mutations in SLC6A19, encoding B0AT1, cause Hartnup disorder.* Nat Genet, 2004. **36**(9): p. 999-1002.
79. Kowalczuk, S., et al., *A protein complex in the brush-border membrane explains a Hartnup disorder allele.* FASEB J, 2008. **22**(8): p. 2880-7.
80. Danilczyk, U., et al., *Essential role for collectrin in renal amino acid transport.* Nature, 2006. **444**(7122): p. 1088-91.
81. Malakauskas, S.M., et al., *Aminoaciduria and altered renal expression of luminal amino acid transporters in mice lacking novel gene collectrin.* Am J Physiol Renal Physiol, 2007. **292**(2): p. F533-44.
82. Vanslambrouck, J.M., et al., *Renal imino acid and glycine transport system ontogeny and involvement in developmental iminoglycinuria.* Biochem J, 2010. **428**(3): p. 397-407.
83. Fairweather, S.J., et al., *Intestinal peptidases form functional complexes with the neutral amino acid transporter B(0)AT1.* Biochem J, 2012. **446**(1): p. 135-48.
84. Bohmer, C., et al., *Characterization of mouse amino acid transporter B0AT1 (slc6a19).* Biochem J, 2005. **389**(Pt 3): p. 745-51.
85. Anderson, C.M., et al., *H+/amino acid transporter 1 (PAT1) is the imino acid carrier: An intestinal nutrient/drug transporter in human and rat.* Gastroenterology, 2004. **127**(5): p. 1410-22.
86. Bohmer, C., et al., *The serum and glucocorticoid inducible kinases SGK1-3 stimulate the neutral amino acid transporter SLC6A19.* Cell Physiol Biochem, 2010. **25**(6): p. 723-32.
87. Bogatikov, E., et al., *Up-regulation of amino acid transporter SLC6A19 activity and surface protein abundance by PKB/Akt and PIKfyve.* Cell Physiol Biochem, 2012. **30**(6): p. 1538-46.
88. Bhavsar, S.K., et al., *Stimulation of the amino acid transporter SLC6A19 by JAK2.* Biochem Biophys Res Commun, 2011. **414**(3): p. 456-61.
89. Singer, D., et al., *Orphan transporter SLC6A18 is renal neutral amino acid transporter B0AT3.* J Biol Chem, 2009. **284**(30): p. 19953-60.
90. Jiang, F., et al., *Angiotensin-converting enzyme 2 and angiotensin 1-7: novel therapeutic targets.* Nat Rev Cardiol, 2014. **11**(7): p. 413-26.
91. Hernandez Prada, J.A., et al., *Structure-based identification of small-molecule angiotensin-converting enzyme 2 activators as novel antihypertensive agents.* Hypertension, 2008. **51**(5): p. 1312-7.
92. Shoemaker, R., et al., *ACE2 deficiency reduces beta-cell mass and impairs beta-cell proliferation in obese C57BL/6 mice.* Am J Physiol Endocrinol Metab, 2015. **309**(7): p. E621-31.
93. Bernardi, S., et al., *ACE2 deficiency shifts energy metabolism towards glucose utilization.* Metabolism, 2015. **64**(3): p. 406-15.

94. Singer, D., et al., *Defective intestinal amino acid absorption in Ace2 null mice.* Am J Physiol Gastrointest Liver Physiol, 2012. **303**(6): p. G686-95.
95. Kuba, K., Y. Imai, and J.M. Penninger, *Multiple functions of angiotensin-converting enzyme 2 and its relevance in cardiovascular diseases.* Circ J, 2013. **77**(2): p. 301-8.
96. Camargo, S.M., et al., *Tissue-specific amino acid transporter partners ACE2 and collectrin differentially interact with hartnup mutations.* Gastroenterology, 2009. **136**(3): p. 872-82.
97. Singer, D., et al., *Defective intestinal amino acid absorption in Ace2 null mice.* American Journal of Physiology-Gastrointestinal and Liver Physiology, 2012. **303**(6): p. G686-G695.
98. Perlot, T. and J.M. Penninger, *ACE2 - from the renin-angiotensin system to gut microbiota and malnutrition.* Microbes Infect, 2013. **15**(13): p. 866-73.
99. Vuille-dit-Bille, R.N., et al., *Human intestine luminal ACE2 and amino acid transporter expression increased by ACE-inhibitors.* Amino Acids, 2015. **47**(4): p. 693-705.
100. Zhang, H., et al., *Collectrin, a collecting duct-specific transmembrane glycoprotein, is a novel homolog of ACE2 and is developmentally regulated in embryonic kidneys.* J Biol Chem, 2001. **276**(20): p. 17132-9.
101. Turner, A.J. and N.M. Hooper, *The angiotensin-converting enzyme gene family: genomics and pharmacology.* Trends Pharmacol Sci, 2002. **23**(4): p. 177-83.
102. Cechova, S., et al., *Loss of collectrin, an angiotensin-converting enzyme 2 homolog, uncouples endothelial nitric oxide synthase and causes hypertension and vascular dysfunction.* Circulation, 2013. **128**(16): p. 1770-80.
103. Rechsteiner, M.P., et al., *Automated assessment of beta-cell area and density per islet and patient using TMEM27 and BACE2 immunofluorescence staining in human pancreatic beta-cells.* PLoS One, 2014. **9**(6): p. e98932.
104. Malakauskas, S.M., et al., *Increased insulin sensitivity in mice lacking collectrin, a downstream target of HNF-1alpha.* Mol Endocrinol, 2009. **23**(6): p. 881-92.
105. Jiang, Y., et al., *Mice lacking neutral amino acid transporter B(0)AT1 (Slc6a19) have elevated levels of FGF21 and GLP-1 and improved glycaemic control.* Molecular Metabolism, 2015. **4**(5): p. 406-417.
106. Palacin, M., J. Bertran, and A. Zorzano, *Heteromeric amino acid transporters explain inherited aminoacidurias.* Curr Opin Nephrol Hypertens, 2000. **9**(5): p. 547-53.
107. Broer, S., et al., *Iminoglycinuria and hyperglycinuria are discrete human phenotypes resulting from complex mutations in proline and glycine transporters.* J Clin Invest, 2008. **118**(12): p. 3881-92.
108. Auray-Blais, C., R. Giguere, and B. Lemieux, *Newborn urine screening programme in the province of Quebec: an update of 30 years' experience.* J Inherit Metab Dis, 2003. **26**(4): p. 393-402.
109. Broer, S., *Apical transporters for neutral amino acids: physiology and pathophysiology.* Physiology (Bethesda), 2008. **23**: p. 95-103.
110. Baron, D.N., et al., *Hereditary pellagra-like skin rash with temporary cerebellar ataxia, constant renal amino-aciduria, and other bizarre biochemical features.* Lancet, 1956. **271**(6940): p. 421-8.
111. Broer, S., *The role of the neutral amino acid transporter B0AT1 (SLC6A19) in Hartnup disorder and protein nutrition.* IUBMB Life, 2009. **61**(6): p. 591-9.
112. Wilcken, B., J.S. Yu, and D.A. Brown, *Natural history of Hartnup disease.* Arch Dis Child, 1977. **52**(1): p. 38-40.
113. Azmanov, D.N., et al., *Further evidence for allelic heterogeneity in Hartnup disorder.* Hum Mutat, 2008. **29**(10): p. 1217-21.
114. Broer, A., et al., *The molecular basis of neutral aminoacidurias.* Pflugers Arch, 2006. **451**(4): p. 511-7.
115. Jonas, A.J. and I.J. Butler, *Circumvention of Defective Neutral Amino-Acid Transport in Hartnup Disease Using Tryptophan Ethyl-Ester.* Journal of Clinical Investigation, 1989. **84**(1): p. 200-204.

116. Asatoor, A.M., et al., *Intestinal absorption of two dipeptides in Hartnup disease.* Gut, 1970. **11**(5): p. 380-7.
117. Frias, J.P., et al., *The Sustained Effects of a Dual GIP/GLP-1 Receptor Agonist, NNC0090-2746, in Patients with Type 2 Diabetes.* Cell Metab, 2017. **26**(2): p. 343-352 e2.
118. Orgeron, M.L., et al., *The impact of dietary methionine restriction on biomarkers of metabolic health.* Prog Mol Biol Transl Sci, 2014. **121**: p. 351-76.
119. De Sousa-Coelho, A.L., et al., *FGF21 mediates the lipid metabolism response to amino acid starvation.* J Lipid Res, 2013. **54**(7): p. 1786-97.
120. Reitman, M.L., *FGF21 mimetic shows therapeutic promise.* Cell Metab, 2013. **18**(3): p. 307-9.
121. Allen, D.D., et al., *Cell lines as in vitro models for drug screening and toxicity studies.* Drug Dev Ind Pharm, 2005. **31**(8): p. 757-68.
122. Pavlopoulou, A., D.A. Spandidos, and I. Michalopoulos, *Human cancer databases (review).* Oncol Rep, 2015. **33**(1): p. 3-18.
123. Yanagi, T., et al., *Melanoma antigen A12 regulates cell cycle via tumor suppressor p21 expression.* Oncotarget, 2017.
124. Chen, L., et al., *Functional characterization of lysine-specific demethylase 2 (LSD2/KDM1B) in breast cancer progression.* Oncotarget, 2017.
125. Zhou, J., et al., *A potential prognostic biomarker SPC24 promotes tumorigenesis and metastasis in lung cancer.* Oncotarget, 2017.
126. Chen, Y.H., et al., *Next-generation sequencing of circulating tumor DNA to predict recurrence in triple-negative breast cancer patients with residual disease after neoadjuvant chemotherapy.* NPJ Breast Cancer, 2017. **3**: p. 24.
127. Crea, F., et al., *Pharmacologic disruption of Polycomb Repressive Complex 2 inhibits tumorigenicity and tumor progression in prostate cancer.* Mol Cancer, 2011. **10**: p. 40.
128. Xu, B., et al., *hsa-miR-135a-1 inhibits prostate cancer cell growth and migration by targeting EGFR.* Tumour Biol, 2016. **37**(10): p. 14141-14151.
129. Wang, Q., et al., *Targeting amino acid transport in metastatic castration-resistant prostate cancer: effects on cell cycle, cell growth, and tumor development.* J Natl Cancer Inst, 2013. **105**(19): p. 1463-73.
130. Pedraz-Cuesta, E., et al., *The glutamate transport inhibitor DL-Threo-beta-Benzyloxyaspartic acid (DL-TBOA) differentially affects SN38- and oxaliplatin-induced death of drug-resistant colorectal cancer cells.* BMC Cancer, 2015. **15**: p. 411.
131. Kim, T.K. and J.H. Eberwine, *Mammalian cell transfection: the present and the future.* Anal Bioanal Chem, 2010. **397**(8): p. 3173-8.
132. O'Gorman, S., D.T. Fox, and G.M. Wahl, *Recombinase-mediated gene activation and site-specific integration in mammalian cells.* Science, 1991. **251**(4999): p. 1351-5.
133. Waldner, C., et al., *Double conditional human embryonic kidney cell line based on FLP and PhiC31 mediated transgene integration.* BMC Res Notes, 2011. **4**: p. 420.
134. Preston, C.M. and M.J. Nicholl, *Role of the cellular protein hDaxx in human cytomegalovirus immediate-early gene expression.* J Gen Virol, 2006. **87**(Pt 5): p. 1113-21.
135. Kim, J.Y., Y.G. Kim, and G.M. Lee, *CHO cells in biotechnology for production of recombinant proteins: current state and further potential.* Appl Microbiol Biotechnol, 2012. **93**(3): p. 917-30.
136. Ellaiah, P., et al., *Site specific integration of FLP recombinase in BHK-21 cell line.* Indian J Exp Biol, 2003. **41**(6): p. 570-3.
137. Kiselev, Y., et al., *3T3 cell lines stably expressing Pax6 or Pax6(5a)--a new tool used for identification of common and isoform specific target genes.* PLoS One, 2012. **7**(2): p. e31915.
138. Xia, Z.B., et al., *The MLL fusion gene, MLL-AF4, regulates cyclin-dependent kinase inhibitor CDKN1B (p27kip1) expression.* Proc Natl Acad Sci U S A, 2005. **102**(39): p. 14028-33.
139. Hacker, D.L., M. De Jesus, and F.M. Wurm, *25 years of recombinant proteins from reactor-grown cells - where do we go from here?* Biotechnol Adv, 2009. **27**(6): p. 1023-7.

140. Puck, T.T., S.J. Cieciura, and A. Robinson, *Genetics of somatic mammalian cells. III. Long-term cultivation of euploid cells from human and animal subjects.* J Exp Med, 1958. **108**(6): p. 945-56.
141. Kao, F.T. and T.T. Puck, *Genetics of somatic mammalian cells, VII. Induction and isolation of nutritional mutants in Chinese hamster cells.* Proc Natl Acad Sci U S A, 1968. **60**(4): p. 1275-81.
142. Fischer, S., R. Handrick, and K. Otte, *The art of CHO cell engineering: A comprehensive retrospect and future perspectives.* Biotechnol Adv, 2015. **33**(8): p. 1878-96.
143. Xu, X., et al., *The genomic sequence of the Chinese hamster ovary (CHO)-K1 cell line.* Nat Biotechnol, 2011. **29**(8): p. 735-41.
144. Gamper, N., J.D. Stockand, and M.S. Shapiro, *The use of Chinese hamster ovary (CHO) cells in the study of ion channels.* J Pharmacol Toxicol Methods, 2005. **51**(3): p. 177-85.
145. Sen, S., et al., *Functional expression and direct visualization of the human alpha 2B -adrenergic receptor and alpha 2B -AR-green fluorescent fusion protein in mammalian cell using Semliki Forest virus vectors.* Protein Expr Purif, 2003. **32**(2): p. 265-75.
146. Lohse, M.J., *Stable overexpression of human beta 2-adrenergic receptors in mammalian cells.* Naunyn Schmiedebergs Arch Pharmacol, 1992. **345**(4): p. 444-51.
147. Su, T.Z., et al., *Transport of gabapentin, a gamma-amino acid drug, by system l alpha-amino acid transporters: a comparative study in astrocytes, synaptosomes, and CHO cells.* J Neurochem, 1995. **64**(5): p. 2125-31.
148. Su, T.Z., M.R. Feng, and M.L. Weber, *Mediation of highly concentrative uptake of pregabalin by L-type amino acid transport in Chinese hamster ovary and Caco-2 cells.* J Pharmacol Exp Ther, 2005. **313**(3): p. 1406-15.
149. Rajan, D.P., et al., *Cloning and functional characterization of a Na(+)-independent, broad-specific neutral amino acid transporter from mammalian intestine.* Biochim Biophys Acta, 2000. **1463**(1): p. 6-14.
150. Shikano, N., et al., *Stimulation of 125I-3-iodo-alpha-methyl-L-tyrosine uptake in Chinese hamster ovary (CHO-K1) cells by tyrosine esters.* Nucl Med Biol, 2010. **37**(2): p. 189-96.
151. Wolff, C., B. Fuks, and P. Chatelain, *Comparative study of membrane potential-sensitive fluorescent probes and their use in ion channel screening assays.* J Biomol Screen, 2003. **8**(5): p. 533-43.
152. Schroeder, K.S. and B.D. Neagle, *FLIPR: A New Instrument for Accurate, High Throughput Optical Screening.* Journal of Biomolecular Screening, 1996. **1**(2): p. 75-80.
153. Arkin, M.R., et al., *FLIPR Assays for GPCR and Ion Channel Targets*, in *Assay Guidance Manual*, G.S. Sittampalam, et al., Editors. 2004: Bethesda (MD).
154. McNeish, J., et al., *High-throughput screening in embryonic stem cell-derived neurons identifies potentiators of alpha-amino-3-hydroxyl-5-methyl-4-isoxazolepropionate-type glutamate receptors.* J Biol Chem, 2010. **285**(22): p. 17209-17.
155. Douhan, J., 3rd, et al., *A FLIPR-based assay to assess potency and selectivity of inhibitors of the TEC family kinases Btk and Itk.* Assay Drug Dev Technol, 2007. **5**(6): p. 751-8.
156. Broad, L.M., et al., *Identification and pharmacological profile of a new class of selective nicotinic acetylcholine receptor potentiators.* J Pharmacol Exp Ther, 2006. **318**(3): p. 1108-17.
157. Whiteaker, K.L., J.P. Sullivan, and M. Gopalakrishnan, *Cell-based assays using the fluorometric imaging plate reader (FLIPR).* Curr Protoc Pharmacol, 2001. **Chapter 9**: p. Unit 9 2.
158. Liu, C.J., et al., *A high-capacity membrane potential FRET-based assay for NaV1.8 channels.* Assay Drug Dev Technol, 2006. **4**(1): p. 37-48.
159. Solly, K., et al., *Miniaturization and HTS of a FRET-based membrane potential assay for K(ir) channel inhibitors.* Assay Drug Dev Technol, 2008. **6**(2): p. 225-34.
160. Vanoaica, L., et al., *Real-time functional characterization of cationic amino acid transporters using a new FRET sensor.* Pflugers Archiv-European Journal of Physiology, 2016. **468**(4): p. 563-572.

161. Whitfield, J.H., et al., *Construction of a robust and sensitive arginine biosensor through ancestral protein reconstruction.* Protein Science, 2015. **24**(9): p. 1412-1422.
162. Gonzalez, J.E., et al., *Cell-based assays and instrumentation for screening ion-channel targets.* Drug Discov Today, 1999. **4**(9): p. 431-439.
163. Zhang, J.H., T.D. Chung, and K.R. Oldenburg, *A Simple Statistical Parameter for Use in Evaluation and Validation of High Throughput Screening Assays.* J Biomol Screen, 1999. **4**(2): p. 67-73.
164. Minta, A. and R.Y. Tsien, *Fluorescent indicators for cytosolic sodium.* J Biol Chem, 1989. **264**(32): p. 19449-57.
165. Harootunian, A.T., et al., *Fluorescence ratio imaging of cytosolic free Na+ in individual fibroblasts and lymphocytes.* J Biol Chem, 1989. **264**(32): p. 19458-67.
166. Despa, S., P. Steels, and M. Ameloot, *Fluorescence lifetime microscopy of the sodium indicator sodium-binding benzofuran isophthalate in HeLa cells.* Anal Biochem, 2000. **280**(2): p. 227-41.
167. Katoh, D., et al., *A technique for quantifying intracellular free sodium ion using a microplate reader in combination with sodium-binding benzofuran isophthalate and probenecid in cultured neonatal rat cardiomyocytes.* BMC Res Notes, 2013. **6**: p. 556.
168. Szmacinski, H. and J.R. Lakowicz, *Sodium Green as a potential probe for intracellular sodium imaging based on fluorescence lifetime.* Analytical Biochemistry, 1997. **250**(2): p. 131-138.
169. Baron, S., et al., *Role of mitochondrial Na+ concentration, measured by CoroNa red, in the protection of metabolically inhibited MDCK cells.* J Am Soc Nephrol, 2005. **16**(12): p. 3490-7.
170. Poburko, D., et al., *Transient receptor potential channel 6-mediated, localized cytosolic [Na+] transients drive Na+/Ca2+ exchanger-mediated Ca2+ entry in purinergically stimulated aorta smooth muscle cells.* Circ Res, 2007. **101**(10): p. 1030-8.
171. Despa, S., et al., *Fluorescence lifetime microscopy of the Na+ indicator Sodium Green in HeLa cells.* Anal Biochem, 2000. **281**(2): p. 159-75.
172. Iamshanova, O., et al., *Comparison of fluorescence probes for intracellular sodium imaging in prostate cancer cell lines.* Eur Biophys J, 2016. **45**(7): p. 765-777.
173. Meier, S.D., Y. Kovalchuk, and C.R. Rose, *Properties of the new fluorescent Na+ indicator CoroNa Green: comparison with SBFI and confocal Na+ imaging.* J Neurosci Methods, 2006. **155**(2): p. 251-9.
174. Lamy, C.M. and J.Y. Chatton, *Optical probing of sodium dynamics in neurons and astrocytes.* Neuroimage, 2011. **58**(2): p. 572-8.
175. Maruyama, I., et al., *Effects of pluronic F-127 on loading of fura 2/AM into single smooth muscle cells isolated from guinea pig taenia coli.* J Toxicol Sci, 1989. **14**(3): p. 153-63.
176. Hamad, M.I., M. Krause, and P. Wahle, *Improving AM ester calcium dye loading efficiency.* J Neurosci Methods, 2015. **240**: p. 48-60.
177. Gregory T. O'Donnell, K.S., Carissa Quinn, Brian Squadroni, Eric Johnson, Jeffrey Hermes, and Michael Finley. *Evaluation of the Sodium Sensing Dye Asante Natrium Green 2 in a Voltage-gated Sodium Channel Assay in 1536-well Format*. in *the Society for Laboratory Automation and Screening (SLAS)*. 2012.
178. Gregory T. O'Donnell, e.a. *ANG-2 (AM) Loading Protocol*. 2011.
179. Kao, J. *Figure 2.7 Response of intracellular ANG-2 to Na+ influx*.
180. Knight, K.K., D.M. Wentzlaff, and P.M. Snyder, *Intracellular sodium regulates proteolytic activation of the epithelial sodium channel.* J Biol Chem, 2008. **283**(41): p. 27477-82.
181. Carvalho, A.F., et al., *Control of osmotic pressure to improve cell viability in cell-laden tissue engineering constructs.* J Tissue Eng Regen Med, 2018. **12**(2): p. e1063-e1067.
182. Camargo, S.M., et al., *Steady-state kinetic characterization of the mouse B(0)AT1 sodium-dependent neutral amino acid transporter.* Pflugers Arch, 2005. **451**(2): p. 338-48.
183. Rhodes, D.R., et al., *ONCOMINE: a cancer microarray database and integrated data-mining platform.* Neoplasia, 2004. **6**(1): p. 1-6.

184. Tumer, E., et al., *Enterocyte-specific regulation of the apical nutrient transporter SLC6A19 (B(0)AT1) by transcriptional and epigenetic networks.* J Biol Chem, 2013. **288**(47): p. 33813-23.
185. Zhang, Y. and J. Wada, *Collectrin, a homologue of ACE2, its transcriptional control and functional perspectives.* Biochem Biophys Res Commun, 2007. **363**(1): p. 1-5.
186. Liang, X., et al., *Rapid and highly efficient mammalian cell engineering via Cas9 protein transfection.* J Biotechnol, 2015. **208**: p. 44-53.
187. Torrente, M., et al., *Amino acids regulate transgene expression in MDCK cells.* PLoS One, 2014. **9**(5): p. e96823.
188. Codamo, J., et al., *Efficient mAb production in CHO cells incorporating PEI-mediated transfection, mild hypothermia and the co-expression of XBP-1.* Journal of Chemical Technology and Biotechnology, 2011. **86**(7): p. 923-934.
189. Wulhfard, S., et al., *Mild hypothermia improves transient gene expression yields several fold in Chinese hamster ovary cells.* Biotechnol Prog, 2008. **24**(2): p. 458-65.
190. Timm, M., et al., *Considerations regarding use of solvents in in vitro cell based assays.* Cytotechnology, 2013. **65**(5): p. 887-94.
191. Zarogiannis, S., et al., *Effect of sodium-potassium pump inhibition by ouabain on the permeability of isolated visceral sheep peritoneum.* Adv Perit Dial, 2007. **23**: p. 43-7.
192. Kyriakopoulos, S., K.M. Polizzi, and C. Kontoravdi, *Comparative analysis of amino acid metabolism and transport in CHO variants with different levels of productivity.* J Biotechnol, 2013. **168**(4): p. 543-51.
193. Palmisano, I., et al., *Amino acid starvation induces reactivation of silenced transgenes and latent HIV-1 provirus via down-regulation of histone deacetylase 4 (HDAC4).* Proc Natl Acad Sci U S A, 2012. **109**(34): p. E2284-93.
194. Bjork, S., M. Vainio, and M. Scheinin, *Uneven cellular expression of recombinant alpha2A-adrenoceptors in transfected CHO cells results in loss of response in adenylyl cyclase inhibition.* Biochim Biophys Acta, 2005. **1744**(1): p. 38-46.
195. Levy, L.M., et al., *Inducible expression of the GLT-1 glutamate transporter in a CHO cell line selected for low endogenous glutamate uptake.* FEBS Lett, 1998. **422**(3): p. 339-42.
196. Maier, T., M. Guell, and L. Serrano, *Correlation of mRNA and protein in complex biological samples.* FEBS Lett, 2009. **583**(24): p. 3966-73.
197. Fotiadis, D., Y. Kanai, and M. Palacin, *The SLC3 and SLC7 families of amino acid transporters.* Mol Aspects Med, 2013. **34**(2-3): p. 139-58.
198. Wagner, C.A., F. Lang, and S. Broer, *Function and structure of heterodimeric amino acid transporters.* Am J Physiol Cell Physiol, 2001. **281**(4): p. C1077-93.
199. Broer, A., et al., *The heterodimeric amino acid transporter 4F2hc/y+LAT2 mediates arginine efflux in exchange with glutamine.* Biochem J, 2000. **349 Pt 3**: p. 787-95.
200. Broer, S. and C.A. Wagner, *Structure-function relationships of heterodimeric amino acid transporters.* Cell Biochem Biophys, 2002. **36**(2-3): p. 155-68.
201. Broer, A., et al., *Association of 4F2hc with light chains LAT1, LAT2 or y+LAT2 requires different domains.* Biochem J, 2001. **355**(Pt 3): p. 725-31.
202. Cao, Y., et al., *Crystal structure of a potassium ion transporter, TrkH.* Nature, 2011. **471**(7338): p. 336-40.
203. Shimizu, H., et al., *Parallel homodimer structures of the extracellular domains of the voltage-gated sodium channel beta4 subunit explain its role in cell-cell adhesion.* J Biol Chem, 2017. **292**(32): p. 13428-13440.
204. Eriksen, J., T.N. Jorgensen, and U. Gether, *Regulation of dopamine transporter function by protein-protein interactions: new discoveries and methodological challenges.* J Neurochem, 2010. **113**(1): p. 27-41.
205. Tulumello, D.V. and C.M. Deber, *SDS micelles as a membrane-mimetic environment for transmembrane segments.* Biochemistry, 2009. **48**(51): p. 12096-103.

206. Daulat, A.M., et al., *Purification and identification of G protein-coupled receptor protein complexes under native conditions.* Mol Cell Proteomics, 2007. **6**(5): p. 835-44.
207. Stuchbury, G. and G. Munch, *Optimizing the generation of stable neuronal cell lines via pre-transfection restriction enzyme digestion of plasmid DNA.* Cytotechnology, 2010. **62**(3): p. 189-94.
208. Merkle, F.T., et al., *Efficient CRISPR-Cas9-Mediated Generation of Knockin Human Pluripotent Stem Cells Lacking Undesired Mutations at the Targeted Locus.* Cell Reports, 2015. **11**(6): p. 875-883.
209. Roy, A., et al., *Generation of WNK1 knockout cell lines by CRISPR/Cas-mediated genome editing.* Am J Physiol Renal Physiol, 2015. **308**(4): p. F366-76.
210. Li, K., et al., *Optimization of genome engineering approaches with the CRISPR/Cas9 system.* PLoS One, 2014. **9**(8): p. e105779.
211. Smurnyy, Y., et al., *DNA sequencing and CRISPR-Cas9 gene editing for target validation in mammalian cells.* Nat Chem Biol, 2014. **10**(8): p. 623-5.
212. Kriz, A., et al., *A plasmid-based multigene expression system for mammalian cells.* Nat Commun, 2010. **1**: p. 120.
213. Baser, B., et al., *A method for specifically targeting two independent genomic integration sites for co-expression of genes in CHO cells.* Methods, 2016. **95**: p. 3-12.
214. Assur, Z., W.A. Hendrickson, and F. Mancia, *Tools for coproducing multiple proteins in mammalian cells.* Methods Mol Biol, 2012. **801**: p. 173-87.
215. Miyazaki, K. and W.N. Ross, *Simultaneous Sodium and Calcium Imaging from Dendrites and Axons.* eNeuro, 2015. **2**(5).
216. Yu, H.B., et al., *High throughput screening technologies for ion channels.* Acta Pharmacologica Sinica, 2016. **37**(1): p. 34-43.
217. Irwin, J.J. and B.K. Shoichet, *ZINC--a free database of commercially available compounds for virtual screening.* J Chem Inf Model, 2005. **45**(1): p. 177-82.
218. Jones, L.H. and M.E. Bunnage, *Applications of chemogenomic library screening in drug discovery.* Nat Rev Drug Discov, 2017. **16**(4): p. 285-296.
219. Shoichet, B.K., *Virtual screening of chemical libraries.* Nature, 2004. **432**(7019): p. 862-5.
220. Doman, T.N., et al., *Molecular docking and high-throughput screening for novel inhibitors of protein tyrosine phosphatase-1B.* J Med Chem, 2002. **45**(11): p. 2213-21.
221. Paiva, A.M., et al., *Inhibitors of dihydrodipicolinate reductase, a key enzyme of the diaminopimelate pathway of Mycobacterium tuberculosis.* Biochim Biophys Acta, 2001. **1545**(1-2): p. 67-77.
222. Broer, S. and U. Gether, *The solute carrier 6 family of transporters.* Br J Pharmacol, 2012. **167**(2): p. 256-78.
223. Penmatsa, A. and E. Gouaux, *How LeuT shapes our understanding of the mechanisms of sodium-coupled neurotransmitter transporters.* J Physiol, 2014. **592**(5): p. 863-9.
224. O'Mara, M., A. Oakley, and S. Broer, *Mechanism and putative structure of B(0)-like neutral amino acid transporters.* J Membr Biol, 2006. **213**(2): p. 111-8.
225. Singh, S.K., et al., *A competitive inhibitor traps LeuT in an open-to-out conformation.* Science, 2008. **322**(5908): p. 1655-61.
226. Pochini, L., et al., *Membrane transporters for the special amino acid glutamine: structure/function relationships and relevance to human health.* Front Chem, 2014. **2**: p. 61.
227. Du, G., Q. Fang, and J.M. den Toonder, *Microfluidics for cell-based high throughput screening platforms - A review.* Anal Chim Acta, 2016. **903**: p. 36-50.
228. Hu, G., et al., *New fluorescent substrate enables quantitative and high-throughput examination of vesicular monoamine transporter 2 (VMAT2).* ACS Chem Biol, 2013. **8**(9): p. 1947-54.

229. Dong, H. and M.G. Wade, *Application of a nonradioactive assay for high throughput screening for inhibition of thyroid hormone uptake via the transmembrane transporter MCT8.* Toxicol In Vitro, 2017. **40**: p. 234-242.
230. de Jong, L.A., et al., *Receptor-ligand binding assays: technologies and applications.* J Chromatogr B Analyt Technol Biomed Life Sci, 2005. **829**(1-2): p. 1-25.
231. Park, Y.W., et al., *Homogeneous proximity tyrosine kinase assays: scintillation proximity assay versus homogeneous time-resolved fluorescence.* Anal Biochem, 1999. **269**(1): p. 94-104.
232. Kutchukian, P.S., et al., *Iterative Focused Screening with Biological Fingerprints Identifies Selective Asc-1 Inhibitors Distinct from Traditional High Throughput Screening.* ACS Chem Biol, 2017. **12**(2): p. 519-527.
233. Ma, H., S. Deacon, and K. Horiuchi, *The challenge of selecting protein kinase assays for lead discovery optimization.* Expert Opin Drug Discov, 2008. **3**(6): p. 607-621.
234. Michael, S., et al., *A robotic platform for quantitative high-throughput screening.* Assay Drug Dev Technol, 2008. **6**(5): p. 637-57.
235. Benjamin, E.R., et al., *Validation of a fluorescent imaging plate reader membrane potential assay for high-throughput screening of glycine transporter modulators.* J Biomol Screen, 2005. **10**(4): p. 365-73.
236. Miller, M., et al., *Identification of ML204, a novel potent antagonist that selectively modulates native TRPC4/C5 ion channels.* J Biol Chem, 2011. **286**(38): p. 33436-46.
237. Thorne, N., D.S. Auld, and J. Inglese, *Apparent activity in high-throughput screening: origins of compound-dependent assay interference.* Curr Opin Chem Biol, 2010. **14**(3): p. 315-24.
238. Feng, B.Y., et al., *A high-throughput screen for aggregation-based inhibition in a large compound library.* J Med Chem, 2007. **50**(10): p. 2385-90.
239. Jadhav, A., et al., *Quantitative analyses of aggregation, autofluorescence, and reactivity artifacts in a screen for inhibitors of a thiol protease.* J Med Chem, 2010. **53**(1): p. 37-51.
240. Ilouga, P.E. and T. Hesterkamp, *On the prediction of statistical parameters in high-throughput screening using resampling techniques.* J Biomol Screen, 2012. **17**(6): p. 705-12.
241. Hughes, J.P., et al., *Principles of early drug discovery.* British Journal of Pharmacology, 2011. **162**(6): p. 1239-1249.
242. Kvist, T., K.B. Hansen, and H. Brauner-Osborne, *The use of Xenopus oocytes in drug screening.* Expert Opinion on Drug Discovery, 2011. **6**(2): p. 141-153.
243. Witchel, H.J., et al., *Troubleshooting problems with in vitro screening of drugs for QT interval prolongation using HERG K+ channels expressed in mammalian cell lines and Xenopus oocytes.* J Pharmacol Toxicol Methods, 2002. **48**(2): p. 65-80.
244. Markovich, D., *Expression cloning and radiotracer uptakes in Xenopus laevis oocytes.* Nat Protoc, 2008. **3**(12): p. 1975-80.
245. Hamilton, K.L. and A.G. Butt, *Glucose transport into everted sacs of the small intestine of mice.* Adv Physiol Educ, 2013. **37**(4): p. 415-26.
246. Van Dam, D. and P.P. De Deyn, *Animal models in the drug discovery pipeline for Alzheimer's disease.* Br J Pharmacol, 2011. **164**(4): p. 1285-300.
247. Frank, R. and R. Hargreaves, *Clinical biomarkers in drug discovery and development.* Nat Rev Drug Discov, 2003. **2**(7): p. 566-80.
248. Ross, J.S., et al., *Pharmacogenomics and clinical biomarkers in drug discovery and development.* Am J Clin Pathol, 2005. **124 Suppl**: p. S29-41.
249. Pochini, L., et al., *Nimesulide binding site in the B0AT1 (SLC6A19) amino acid transporter. Mechanism of inhibition revealed by proteoliposome transport assay and molecular modelling.* Biochem Pharmacol, 2014. **89**(3): p. 422-30.
250. Norgan, A.P., et al., *Multilevel Parallelization of AutoDock 4.2.* J Cheminform, 2011. **3**(1): p. 12.
251. Cheng, Q., et al., *Identification of novel inhibitors of the amino acid transporter B0 AT1 (SLC6A19), a potential target to induce protein restriction and to treat type 2 diabetes.* Br J Pharmacol, 2017. **174**(6): p. 468-482.

252. Broer, S., *Xenopus laevis Oocytes.* Methods Mol Biol, 2010. **637**: p. 295-310.
253. Bachmanov, A.A., et al., *Food intake, water intake, and drinking spout side preference of 28 mouse strains.* Behav Genet, 2002. **32**(6): p. 435-43.
254. Dulloo, A.G. and D.S. Miller, *The effect of parasympathetic drugs on energy expenditure: relevance to the autonomic hypothesis.* Can J Physiol Pharmacol, 1986. **64**(5): p. 586-91.
255. Cuboni, S., et al., *Loratadine and analogues: discovery and preliminary structure-activity relationship of inhibitors of the amino acid transporter B(0)AT2.* J Med Chem, 2014. **57**(22): p. 9473-9.
256. Eckle, V.S. and B. Antkowiak, *ALX 1393 inhibits spontaneous network activity by inducing glycinergic tonic currents in the spinal ventral horn.* Neuroscience, 2013. **253**: p. 165-71.
257. Khunweeraphong, N., et al., *Establishment of Stable Cell Lines With High Expression of Heterodimers of Human 4F2hc and Human Amino Acid Transporter LAT1 or LAT2 and Delineation of Their Differential Interaction With alpha-Alkyl Moieties.* Journal of Pharmacological Sciences, 2012. **119**(4): p. 368-380.
258. Whiteaker, K.L., et al., *Validation of FLIPR membrane potential dye for high throughput screening of potassium channel modulators.* Journal of Biomolecular Screening, 2001. **6**(5): p. 305-312.
259. Joesch, C., et al., *Use of FLIPR membrane potential dyes for validation of high-throughput screening with the FLIPR and mu ARCS technologies: Identification of ion channel modulators acting on the GABA(A) receptor.* Journal of Biomolecular Screening, 2008. **13**(3): p. 218-228.
260. Ruggiero, A.M., et al., *Nonoisotopic Assay for the Presynaptic Choline Transporter Reveals Capacity for Allosteric Modulation of Choline Uptake.* Acs Chemical Neuroscience, 2012. **3**(10): p. 767-781.
261. Wang, Q. and J. Holst, *L-type amino acid transport and cancer: targeting the mTORC1 pathway to inhibit neoplasia.* American Journal of Cancer Research, 2015. **5**(4): p. 1281-1294.
262. Freeman, T.L., H.Q. Ngo, and M.E. Mailliard, *Inhibition of system A amino acid transport and hepatocyte proliferation following partial hepatectomy in the rat.* Hepatology, 1999. **30**(2): p. 437-444.
263. Karunakaran, S., et al., *Interaction of tryptophan derivatives with SLC6A14 (ATB0,+) reveals the potential of the transporter as a drug target for cancer chemotherapy.* Biochem J, 2008. **414**(3): p. 343-55.
264. McDonald, K.K., et al., *Inhibition of endothelial cell amino acid transport system y(+) by arginine analogs that inhibit nitric oxide synthase.* Biochimica Et Biophysica Acta-Biomembranes, 1997. **1324**(1): p. 133-141.
265. Lehmann, A., et al., *(R)-(3-Amino-2-fluoropropyl) Phosphinic Acid (AZD3355), a Novel GABA(B) Receptor Agonist, Inhibits Transient Lower Esophageal Sphincter Relaxation through a Peripheral Mode of Action.* Journal of Pharmacology and Experimental Therapeutics, 2009. **331**(2): p. 504-512.
266. Moitessier, N., et al., *Towards the development of universal, fast and highly accurate docking/scoring methods: a long way to go.* Br J Pharmacol, 2008. **153 Suppl 1**: p. S7-26.
267. Lionta, E., et al., *Structure-based virtual screening for drug discovery: principles, applications and recent advances.* Curr Top Med Chem, 2014. **14**(16): p. 1923-38.
268. Ogrizek, M., et al., *Molecular dynamics to enhance structure-based virtual screening on cathepsin B.* J Comput Aided Mol Des, 2015. **29**(8): p. 707-12.
269. Marschall, M., et al., *Assessment of drug candidates for broad-spectrum antiviral therapy targeting cellular pyrimidine biosynthesis.* Antiviral Res, 2013. **100**(3): p. 640-8.
270. Remsberg, J.R., et al., *Structural analogues of smoothened intracellular loops as potent inhibitors of Hedgehog pathway and cancer cell growth.* J Med Chem, 2007. **50**(18): p. 4534-8.
271. Yu, S.P. and G.A. Kerchner, *Endogenous voltage-gated potassium channels in human embryonic kidney (HEK293) cells.* J Neurosci Res, 1998. **52**(5): p. 612-7.

272. Seo, M., et al., *Structure-based development of small molecule PFKFB3 inhibitors: a framework for potential cancer therapeutic agents targeting the Warburg effect.* PLoS One, 2011. **6**(9): p. e24179.
273. Tan, A., et al., *Chemical modification of the glucosidase inhibitor 1-deoxynojirimycin. Structure-activity relationships.* J Biol Chem, 1991. **266**(22): p. 14504-10.
274. Miyoshi, H., *Structure-activity relationships of some complex I inhibitors.* Biochim Biophys Acta, 1998. **1364**(2): p. 236-44.
275. Lin, L., et al., *SLC transporters as therapeutic targets: emerging opportunities.* Nat Rev Drug Discov, 2015. **14**(8): p. 543-60.
276. Yang, S.Y., *Pharmacophore modeling and applications in drug discovery: challenges and recent advances.* Drug Discov Today, 2010. **15**(11-12): p. 444-50.
277. Taylor, P.M., et al., *Amino-acid-dependent modulation of amino acid transport in Xenopus laevis oocytes.* J Exp Biol, 1996. **199**(Pt 4): p. 923-31.
278. Wang, Q., et al., *Monoterpene glycoside ESK246 from Pittosporum targets LAT3 amino acid transport and prostate cancer cell growth.* ACS Chem Biol, 2014. **9**(6): p. 1369-76.
279. Wright, S.H. and W.H. Dantzler, *Molecular and cellular physiology of renal organic cation and anion transport.* Physiol Rev, 2004. **84**(3): p. 987-1049.
280. Kiehn, J., et al., *Molecular physiology and pharmacology of HERG. Single-channel currents and block by dofetilide.* Circulation, 1996. **94**(10): p. 2572-9.
281. Ovens, M.J., et al., *AR-C155858 is a potent inhibitor of monocarboxylate transporters MCT1 and MCT2 that binds to an intracellular site involving transmembrane helices 7-10.* Biochemical Journal, 2010. **425**: p. 523-530.
282. Uitdehaag, J.C.M. and G.J.R. Zaman, *A theoretical entropy score as a single value to express inhibitor selectivity.* Bmc Bioinformatics, 2011. **12**.
283. Gupta, N., et al., *Upregulation of the amino acid transporter ATB0,+ (SLC6A14) in colorectal cancer and metastasis in humans.* Biochim Biophys Acta, 2005. **1741**(1-2): p. 215-23.
284. Gupta, N., et al., *Up-regulation of the amino acid transporter ATB(0,+) (SLC6A14) in carcinoma of the cervix.* Gynecol Oncol, 2006. **100**(1): p. 8-13.
285. Yu, X.C., et al., *Discovery and characterization of potent small molecule inhibitors of the high affinity proline transporter.* Neurosci Lett, 2009. **451**(3): p. 212-6.
286. Tourtellotte, W.W., et al., *Parkinson's disease: Cogentin with Sinemet, a better response.* Prog Neuropsychopharmacol Biol Psychiatry, 1982. **6**(1): p. 51-5.
287. Wekerle, H. and E. Meinl, *MULTIPLE SCLEROSIS An old drug plays a new trick.* Nature, 2013. **502**(7471): p. 314-315.
288. White, P.J., et al., *Branched-chain amino acid restriction in Zucker-fatty rats improves muscle insulin sensitivity by enhancing efficiency of fatty acid oxidation and acyl-glycine export.* Mol Metab, 2016. **5**(7): p. 538-551.
289. Hasbini, D.A., M.A. Mikati, and Z.M. Habbal, *Isolated adipic aciduria.* Pediatr Neurol, 2001. **24**(1): p. 77-8.
290. Javed, K., et al., *Development of Biomarkers for Inhibition of SLC6A19 (B(0)AT1)-A Potential Target to Treat Metabolic Disorders.* Int J Mol Sci, 2018. **19**(11).

Appendix: sequence of primers used in this study

Primer Name	**sense primer (5'-3')**	**antisense primer (5'-3')**
hB^0AT1	TACGGTGTGGACAGGTTCAA	GTACTTCAGGTCCCCGTTCA
hcollectrin	CGAATTCCACCATGTTGTGGCTGCTCT	AGAATTCAACAGCCCTTCAGAGAGG
hLAT1	CTTTGCCTATGGAGGATGGA	AGAGCAGCGTCATCACACAC
hLAT2	GCCTCAATGCATCCATCTTT	GGGACTCTGGCAGGTAAACA
4F2hc	GAGCCGAGAAGAATGGTCTG	AGCCGATTGCAAGAGACTGT
$hATB^{0,+}$	AGAGGCTCTAGCCCAACTCC	AGCTCTCCACCATAGCCAGA
hASCT2	TCCTGGATCTTGCGAGAAAT	GGGCAAAGAGTAAACCCACA
Actin	GCTCACCATGGATGATGATATCGC	GGAGGAGCAATGATCTTGATCTTC
Clathrin	GACAGTGCCATCATGAATCC	TTTGTGCTTCTGGAGGAAAGAA